1965

Ultimate strength of stiffened plate panels subjected to combined axial and lateral loading, Ph.D. Dissertation, June 1965

J. Kondo

CORRECTIONS in FRITZ ENGINEERING LABORATORY REPORT NO. 248.13 -

"ULTIMATE STRENGTH OF LONGITUDINALLY STIFFENED PLATE PANELS SUBJECTED TO COMBINED AXIAL AND LATERAL LOADING"

by JUN KONDO
AUGUST, 1965

Note: "SHOULD READ" will be abbreviated as "S. R."

Page	Correction
18	eqn 2.7 S.R. $\frac{dM}{ds} = -H\sin\Theta - V\cos\Theta$
48	eqn 4.1 S.R. $\Phi = \Phi_{j-1} + \frac{\Phi_j - \Phi_{j-1}}{\Delta s_j}\Delta$
49	eqn 4.5 S.R. $= V_{j-1} - q b d_1 (\sin\Theta - \sin\Theta_{j-1}) + q b \int_0^{\Delta} dz_j$
	eqn 4.6 S.R. $= M_{j-1} - H_{j-1}\Delta z - V_{j-1}\Delta y - q b \left[\frac{(\Delta y)^2}{2} + \frac{(\Delta z)^2}{2} + d_1 \Delta y \cos\Theta_{j-1} - d_1 \Delta z \sin\Theta_{j-1}\right]$
	eqn 4.7 S.R. $\Delta z = \int_0^{\Delta} \cos\Theta\, ds_j \approx \cos\Theta_{j-1}(\Delta) - \left(\frac{\Phi_{j-1}}{3} + \frac{\Phi_{j0}}{6}\right)\sin\Theta_{j-1}(\Delta)^2$
	Note: capital "S" (i.e. S) is for the non-dimensionalized form of segment length while lower case "s" (i.e. Δ) refers to the dimensional form.
	eqn 4.8 S.R. $\Delta y = \int_0^{\Delta} \sin\Theta\, ds_j \approx \sin\Theta_{j-1}(\Delta) + \left(\frac{\Phi_{j-1}}{3} + \frac{\Phi_{j0}}{6}\right)\cos\Theta_{j-1}(\Delta)^2$
	eqn 4.10 S.R. $\Delta Y = \sin\Theta_{j-1}\Delta S \frac{1}{\sqrt{\epsilon_{yp}}} + \left(\frac{\Sigma_{j-1}}{3} + \frac{\Sigma_{j0}}{6}\right)\cos\Theta_{j-1}(\Delta S)^2 \frac{1}{d_2}$
50	eqn 4.11 S.R. $m = m_{j-1} - h_{j-1}\Delta Y \frac{d_2}{r} - v_{j-1}\Delta Z - Q\left[\frac{1}{2}(\Delta Y)^2 \epsilon_{yp} + \frac{1}{2}(\Delta Z)^2 + \cos\Theta_{j-1}\Delta Y \frac{d_1}{r}\epsilon_{yp} - \sin\Theta_{j-1}\Delta Z \frac{d_1}{r}\sqrt{\epsilon_{yp}}\right]$
	eqn 4.12 etc, S.R. $Q = \frac{E b d_2}{\sigma_{yp}^2 A}$, $v = \frac{d_2 V}{A r}\sqrt{\frac{E}{\sigma_{yp}^3}}$, $h = \frac{H}{\sigma_{yp} A}$
	$\Sigma = \frac{\Phi}{\Phi_y}$, $m = \frac{M}{M_y}$
	$\Delta S = \frac{\Delta s}{r}\sqrt{\frac{\sigma_{yp}}{E}}$, $Z = \frac{\Delta z}{r}\sqrt{\frac{\sigma_{yp}}{E}}$, $\Delta Y = \frac{\Delta y}{r}$

Page	Correction
50 (cont'd)	Note: capital "S", "Z", "Y", "Q" are non-dimensional lower case " " " " " are dimensional capital "V", "N", "M" are dimensional lower case " " " " are non-dimensional 9th line from bottom reads: —— showed a deviation of less —— but it S.R. —— showed a deviation of less ——
51	eqn. 4.15 S.R. $\Theta_j = \Theta_{j-1} + \frac{1}{2}(\bar{E}_{j-1} + \bar{E}_j)\sqrt{\epsilon_{yp}}\frac{L}{d_2}\Delta S$ eqn 4.16 S.R. $h_j = h_{j-1} + Q\cdot\epsilon_{yp}\left[\Delta Y\cdot\frac{L}{d_2} + (\cos\Theta_j - \cos\Theta_{j-1})\cdot\frac{d_1}{d_2}\right]$ eqn 4.17 S.R. $N_j = N_{j-1} + Q\left[\Delta Z - \sqrt{\epsilon_{yp}}(\sin\Theta_j - \sin\Theta_{j-1})\cdot\frac{d_1}{2}\right]$ eqn 4.20 S.R. $L_j = L_{j-1} + \frac{2\Delta S}{2 - \epsilon_{yp}\left[G_{j-1} + G_j - (\bar{E}_{j-1} + \bar{E}_j)\cdot\frac{d_1}{d_2}\right]}$
81	in eqn 6.7, the web thickness eqn S.R. Web thickness : $w = \frac{\alpha(1-\beta)}{\gamma}\beta$
82	1st line reads: ——— in this anaylsis, but it S.R. ——— in this analysis
99	change "H" to "R" change $H = \frac{R}{\sigma_{yp} A}$ to read $R = \frac{H}{\sigma_{yp} A}$
105	eqn 10.3 S.R. $d_2 = \left[\frac{\frac{1}{2} + \gamma + \frac{1}{2}\alpha(1-\beta)\gamma}{1+\alpha}\right]t$ eqn 10.3 (cont'd) S.R. $d_1 = \left[1 + \gamma - \frac{\gamma + \frac{1}{2} + \frac{1}{2}\alpha(1-\beta)\gamma}{1+\alpha}\right]t$

Page	Correction
105 (cont'd)	the last two lines of eqn 10.6 s.r. $Q_x = \frac{\alpha_1}{\varepsilon} = \lambda + \gamma - \frac{1}{2}\alpha\gamma - \frac{1}{2}\alpha(1-\beta)\gamma$ (with $\lambda \to \alpha$) $Q_z = \frac{\alpha_2}{\varepsilon} = \frac{\frac{1}{2}\gamma + \frac{1}{2}\alpha(1-\beta)\gamma}{1+\alpha}$
108	11th line from top change :- limits that it is, for Σ —— to read :- limits that is, for Σ ——
113	eqn 10.25 s.r. $m_1 = m_0 - h_0 \Delta y \frac{Q}{R} - N_0 \Delta z$ $- Q\left[\frac{1}{2}(\Delta y)^2 \varepsilon_{yy} + \frac{1}{2}(\Delta z)^2 + \cos\theta_0 \Delta y \frac{Q}{R}\varepsilon_{yy} - \sin\theta_0 \Delta z \frac{Q}{R}\varepsilon_{yy}\right]$
104	last paragraph: change "areas" to read "areas".
116	eqn. 10.34 s.r. $((m_j - m_{j-1})\Delta s_{j-1} + (m_{j-2} - m_{j-1})\Delta s_j)(\Delta s)^2$ $-((m_{j-2} - m_{j-1})(\Delta s_j)^2 - (m_j - m_{j-1})(\Delta s_{j-1})^2)(\Delta s)$ $+ m_{j-1}\Delta s_j \Delta s_{j-1}(\Delta s_j + \Delta s_{j-1}) = 0$ 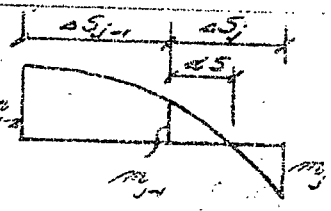
117	eqn 10.35 s.r. $L_x^p = \frac{(L_j - L_{j-1})\Delta s_{j-1} + (L_{j-2} - L_{j-1})\Delta s_j}{\Delta s_j \Delta s_{j-1}(\Delta s_j + \Delta s_{j-1})}(\Delta s)^2$ $+ \frac{(L_j - L_{j-1})(\Delta s_{j-1})^2 - (L_{j-2} - L_{j-1})(\Delta s_j)^2}{\Delta s_j \Delta s_{j-1}(\Delta s_j + \Delta s_{j-1})}(\Delta s) + L_{j-1}$ eqn 10.36 s.r. $[(\theta_j - \theta_{j-1})\Delta s_{j-1} + (\theta_{j-2} - \theta_{j-1})\Delta s_j](\Delta s)^2$ $-[(\theta_{j-2} - \theta_{j-1})(\Delta s_j)^2 - (\theta_j - \theta_{j-1})(\Delta s_{j-1})^2](\Delta s)$ $+ \Delta s_j \Delta s_{j-1}(\Delta s_j + \Delta s_{j-1})\theta_{j-1} = 0$

Page	Corrections
118	eqn 10.38 S.R. $L^P = L^P_{K-1} - \frac{1}{\beta} \frac{(L^P_K - L^P_{K-2})^2}{L^P_{K-2} - 2L^P_{K-1} + L^P_K}$ eqn 10.39 S.R. $\Sigma^P = \Sigma^P_K + \frac{1}{2} \frac{L^P_{K-2} - L^P_K}{L^P_{K-2} - 2L^P_{K-1} + L^P_K} \Sigma_{inc}$
119	eqn 10.40 S.R. $Y^P = \frac{Y^P_K - 2Y^P_{K-1} + Y^P_{K-2}}{2\Sigma^2_{inc}} (K\Sigma)^2$ $+ \frac{Y^P_K - Y^P_{K-2}}{2\Sigma_{inc}} (K\Sigma) + Y^P_{K-1}$ Where, $K\Sigma = \frac{1}{2} \frac{L^P_{K-2} - L^P_K}{L^P_{K-2} - 2L^P_{K-1} + L^P_K} \Sigma_{inc}$
161	Fig. 2.2 (a) change $d\Theta = \Phi \times ds$ to read "$d\Theta = \Phi ds$"

Built-up Members in Plastic Design

ULTIMATE STRENGTH OF LONGITUDINALLY STIFFENED PLATE PANELS, SUBJECTED TO COMBINED AXIAL AND LATERAL LOADING

by

Jun Kondo

This work has been carried out as a part of an investigation sponsored by the Department of the Navy with funds furnished by the Bureau of Ships Contract Nobs-90041.

Fritz Engineering Laboratory
Department of Civil Engineering
Lehigh University
Bethlehem, Pennsylvania

August 1965

Fritz Engineering Laboratory Report No. 248.13

TABLE OF CONTENTS

A B S T R A C T

This dissertation presents results of an analytical investigation of the ultimate strength of longitudinally stiffened plate panels. The load considered were the axial load applied to the ends and the hydrostatic pressure acting on the plate surface. Under these external loads, longitudinally stiffened plate panels fail due to excessive bending and can be treated as beam-columns if local buckling of the plate components is prevented.

The analysis was performed by solving the equilibrium equations numerically. Consideration was given to the non-linear effects of both the inelastic action and deformation.

The factors which have an effect on the ultimate strength were found to be:

a) Yield stress of material,

b) Residual stresses in both magnitude and distribution,

c) Ratio of stiffener cross-sectional area to plate area,

d) Ratio of stiffener flange area to stiffener area,

e) Ratio of stiffener depth to plate thickness,

f) Intensity of hydrostatic pressure.

In the non-dimensionalized Ultimate Axial-Load--Lateral Load--Panel Length relationship, the interelation between these geometric ratios was found to be practically negligible.

By organizing the information supplied by the numerical analysis, a chart was constructed for the design of longitudinally stiffened plate panels having low plate slenderness ratios ($b/t \leq 44$ for a steel with yield stress of 33 ksi). With this design chart, the most advantageous combination of a plate and stiffeners can be selected without conducting a numerical analysis.

1. INTRODUCTION

1.1 IMPORTANCE OF THE ELASTIC-PLASTIC ANALYSIS FOR STIFFENED PLATE PANEL DESIGN

A ship hull is essentially a hollow box girder, composed of plates stiffened by a grid of longitudinal and transverse frames (Fig. 1.1). The principal function of the deck and bottom plating constituting the flanges of this girder is to resist longitudinal forces arising from the bending of the ship under the action of waves. The longitudinally arranged frames have an important function of not only aiding in resisting longitudinal bending of the hull girder directly, but also of greatly increasing the buckling strength of the plating to which they are attached. Hence, except for cargo vessels in which the deep transverses required to support longitudinals interfere with cargo space, longitudinal framing is generally adopted for most of the other types of vessels, such as naval vessels, oil tankers and ore carriers.

The conventional design method used by naval architects is based on elastic considerations. An allowable or working stress is chosen at some fraction of the lower yield stress of material. Stresses computed for a given load are restricted to be less than the specified working stress and also to be well below the buckling stress. The safety of a structure thus depends upon the selection of the working stress, as well as on the accuracy of stress calculations.

Although the procedure described above is mathematically straightforward and there is much to recommend it, certain fundamental objections to such an approach exist. First, in an actual structure, initial stresses produced in the fabrication of the structure and the stress concentration due to discontinuities of the structure are inevitably present. A combination of the initial stress and a stress concentration may result in the occurrence of plastic flow long before the working load is reached. Thus the stress state obtained by elastic calculation may be considerably different from the actual stress state under the working load. Secondly, and far more importantly, the calculated first yield load has no direct relation to the ultimate failure load of the structure. The amount of reserve strength varies from one structure to another according to the sectional properties of members and according to the degree of indeterminateness of the structure. This, together with an insufficient knowledge in load prediction, is the cause of the necessity of varying the factor of safety for different members and different structures in the conventional design method.

To achieve a rational design of a structure, it is necessary to use a factor of safety based on the ultimate failure strength of the structure. An exact plastic analysis of the structure would, in general, be a formidable task. However, by neglecting the strain hardening and assuming an initially elastic--perfectly plastic stress-strain relationship, a simple method of the plastic analysis has been developed for steel structures failing due to unrestricted plastic flow.(1)*

* The numbers in parentheses refer to the list of references, Chapter 8 .

The solution thus obtained is not only a very good approximation to the true failure load, but by using methods of limit analysis, one can obtain it much more easily than by the elastic analysis. Many steel building frames have been designed according to the simple plastic theory. As a successful example of the application of the plastic design methods to ship structural design, the reinforcement of the flight deck of World War II aircraft carriers can be mentioned.[2]

In the application of simple plastic design to ship structures, however, Drucker points out that limitations due to instability, fatigue, and brittle fracture should be carefully observed.[3]

In this dissertation, the first of the three problems, instability, is investigated.

1.2 APPROACH TO THE INSTABILITY PROBLEM

Under service conditions, longitudinally stiffened plate panels which compose the top and bottom flanges of a box hull girder experience compression, tension, shear and bending, in varying proportions and directions. One of the most severe types of loading is a combined action of axial compression due to bending of the hull girder and a uniformly distributed lateral loading due to water pressure or deck load (Fig. 1.1).

Under such loading, stiffened plate panels become unstable due to the presence of axial compression before the unrestricted plastic flow can take place. To predict the ultimate load-carrying capacity of a

structure failing by instability, the analysis must be more complete than a simple plastic analysis.

The mode of failure of stiffened plate panels can be divided into two types: failure preceded by the buckling of plate components and failure of the stiffened plate panel as a whole without premature buckling of plate components. As early as 1891, Bryan presented the analysis of a rectangular plate which was simply supported on all its edges, and which was acted upon on two opposite sides by a uniformly distributed compressive load in the plane of the plate.[4] Since then, the theories of elastic plate buckling have been developed from an accumulation of many researchers' efforts. A review of the historical development can be found in Refs. 5 and 6.

Attempts to formulate a rational theory of stability of plates beyond the elastic limit were made by Bijlaard[7], Ilyushin[8], and Handelman and Prager[9] using modern theories of plasticity, (Hencky's deformation theory and Prandtl-Reuss' incremental theory). Being spurred by the requirement of the aircraft industry, these theories were further advanced mainly for aluminum plates by Stowell[10,11], and Pearson.[12] In 1956, Thurlimann and Haaijer proposed a plastic buckling theory of steel plates.[13,14]

The effect of residual stress on the elastic buckling strength of a steel plate was studied by Yoshiki and others.[15] The study was extended into the inelastic range by Ueda[16] and Nishino.[17]

When a plate is reinforced by longitudinal stiffeners, these stiffeners carry not only a portion of the compressive load, but subdivide the plate into smaller panels, thus increasing considerably the critical stress at which the plate will buckle. The effect of the bending rigidity of stiffeners on the elastic buckling strength of the plate was first investigated by Timoshenko using the energy method.[18] The concept of the required minimum bending rigidity of the stiffener was also considered first by Timoshenko.[18] The effect of the torsional rigidity of the supporting elastic stiffeners was discussed first by Chwalla, who showed the considerable influence of the torsional rigidity of supporting stiffeners on the critical stress of the plate.[19] At present, a considerable number of references are available on the elastic buckling strength of stiffened plates.[20] An attempt to extend the theory beyond the elastic limit was made by Kusuda, who obtained a solution for longitudinally or transversely stiffened plates in the strain-hardening range.[21]

When a stiffened plate is subjected to a lateral load in addition to an axial load, as in the bottom plating of a ship, the question arises whether normal pressure applied to a plate supported on all four edges reduces the critical load of the plate. Levy and others made theoretical[22,23] and experimental investigations[24] on the problem for a plate of length-width ratio 4 to 1. Their conclusion was that the buckling load of a rectangular plate increased considerably when sufficiently large normal loads were present. However, normal loads in the case of bottom plating are not large enough to have any significant effect on the elastic plate buckling.

Unlike columns, in which buckling is often synonymous with failure, plates may be able to sustain ultimate loads noticeably exceeding the buckling loads. The difference between buckling and ultimate loads becomes important for thin plates (high b/t ratio) and for materials with low modulus of elasticity. In some fields of structural design, such as the design of aircraft and light gage cold-formed steel structures, it is often advantageous to use thin plates that buckle locally under loads that are much smaller than the loads which will cause failure of the whole structure. Most of the work on post-buckling behavior of thin plates has been associated with the design of either aircraft structures, ship plate structures, or building construction. Summaries of the work done in each of these fields are available in literature.[25,5,26] These theoretical studies are supplemented by numerous experimental studies.[5,6,25 to 30] The post-buckling behavior of a stiffened plate is somewhat similar to that of a single plate supported along its four edges, except that the question of the stability of the stiffeners enters into the picture. Vasta conducted a series of tests in order to determine the required rigidity of the stiffeners which will enable the plate to develop full post-buckling strength.[31.32] The elastic post-buckling behavior of a rectangular plate under edge compression and hydrostatic pressure was investigated by Bengston.[33] A limited study in the inelastic range was made by T. Lee.[34]

As for the ultimate strength of stiffened plate panels subjected to combined axial and lateral loads, only a few experimental studies have been made. Results of several full scale ship structural tests, in which plate slenderness of bottom plating varied from 62 to 89, showed

that the ultimate failure was caused by the instability of the compression flange of the hull and that the compressive stresses in the bottom plate at the ultimate failure were fairly close to the ultimate strength of single plates under edge compression determined by experiment.[35] In the scale model tests conducted at Fritz Engineering Laboratory, Lehigh University, a stiffened plate panel with medium plate slenderness, $b/t = 60$, could withstand a 5 to 10 per cent increase of axial load after plate buckling when loading edges were fixed, but did not show any significant post-buckling strength when loading edges were simply supported.[36,37,38] In the specimens with small plate slenderness, $b/t = 40$, the failure was due to general column instability of the entire panel, and the plate itself buckled only after the panel reached the ultimate load.

When the cross-sectional dimensions of a stiffened plate panel are chosen in such a manner that the premature local buckling of component elements is prevented until the ultimate load is reached, the stiffened plate panel fails as a unit. The load deformation response of longitudinally stiffened plate panels varies according to the cross-sectional shape of the stiffeners. When a stiffener has an unsymmetrical cross section about its own web, the stiffener starts twisting at the first application of lateral load. Investigation of the behavior of plate panels with unsymmetric stiffeners is an involved step-by-step analysis based on the biaxial bending theory in the inelastic range. So far, no attempt has been made to solve this problem, except for an elastic analysis made by Terazawa and others.[39] Present knowledge is not as yet enough to give an inelastic solution to this problem.

When the cross section is symmetric about the web of the stiffener, the stiffened plate panel deflects in the plane of the external moment upon the application of lateral load. This deformation increases elastically with the axial load. The analysis of elastic beam-column behavior can be made without difficulty. Many such solutions are summarized by Timoshenko.(6)

Design curves based on the assumption that the failure load is the load which produces the beginning of yielding in the highest stressed fiber were developed by Young.(40)

However, beam-columns can carry a load larger than the first yield load without collapsing. As the load is further increased beyond the first yield load, yielding progresses across and along the member, thereby reducing its resistance to further loading. Finally, a point is reached at which an increase in load is impossible and the member deflects as the load remains constant or reduces. At this point equilibrium passes from stable to unstable equilibrium.

The ultimate strength of a beam-column was first considered by von Kármán(41) in terms of the stability concept outlined above. All later solutions of the inelastic beam-column instability problem have been based on the work of von Kármán. In general, the starting point of the analysis is the evaluation of the relationship between the bending moment, the thrust, and the resulting curvature in the cross section. The moment- curvature-thrust relationship is dependent on the cross-sectional dimensions, the stress-strain relationship of the material, and the magnitude of the axial thrust. Based on the established moment-

curvature-thrust relationship, the equilibruim configuration of the beam-column is determined. The ultimate strength of the beam-column is defined as the load at which the equilibrium changes from stable to unstable.

Starting from von Kármán's concept, Chwalla rigorously investigated the stability of eccentrically loaded columns with various shapes of cross section.(42) He based all his computations on one stress-strain diagram adopted as typical for structural steel.

One of the difficulties involved in the analysis is the non-linearity of the moment-curvature relationship. For a simple rectangular or circular section, and a simplified stress-strain diagram, the moment-curvature-thrust relationship can be expressed analytically. For other conventional types of cross section, the moment-curvature-thrust relationship should be expressed either graphically or numerically. The analytical expressions of the moment-curvature-thrust relationship for a rectangular cross section with an idealized stress-strain diagram can be found in the paper of Baker, Horm and Roderick.(43) Ježek found that when applied to unrestrained beam-column problems a simplified stress-strain diagram consisting of two straight lines gave substantially the same results as those obtained with the use of an exact stress-strain diagram of a typical structural steel.(44) Ježek further introduced in his approximate solution a "shape factor" the purpose of which was to relate the relative stiffness of the section in question to that of the rectangle.(45)

The effect of residual stresses which may reduce the effective yield strain of the material and thereby the ultimate strength of beam-

columns, was first investigated by Ketter, Kaminsky and Beedle,[46] and it has been taken into account in more recent studies.[49,54,55,56]

In an exact analysis, the deflected configuration of a beam-column is determined by graphically or numerically integrating the curvature which in the inelastic range depends on both the magnitudes of the axial thrust and the bending moment in the cross section. The bending moments, however, depend on the deflections; therefore a trial-and-error procedure is usually required. Although this general approach considers the true problem, solutions by this method are time consuming. Approximate solutions based on the assumption that the deflection of the member will conform to a certain analytical curve, simplify the procedure substantially. A "full cosine" curve was assumed as a deflection curve by Roš and Brunner[47] Ježek[48] Timoshenko[6] and Ketter.[49] Westergaard and Osgood suggested a "part of cosine curve" as an assumed deflection curve.[50] The magnitude of error introduced by assuming the various deflection curves was discussed by Clark[51] and Ketter.[49] It was noted that the difference between the ultimate loads obtained by the varuous methods were comparatively small and that the accuracy obtained by using the more complicated deflection expression did not warrant the added work required to obtain a solution.

The exact analysis of beam-columns subjected to an axial force and end moments can be considerably simplified by the use of the column deflection curve (C.D.C.) concept, which was proposed by Chwalla.[52] The column deflection curve is the shape that a column would take if it is held in a bent configuration by an axial load applied to the ends. Any given beam-column in equilibrium, with the end moments and axial

thrust applied to it, can be regarded as a segment of a column deflection curve. There are an infinite number of possible CDC's for any beam-column with a given axial load and cross section. These CDC's allow the development of an end-moment versus end-rotation curve. Then the ultimate strength is obtained by applying the von Kármán concept of stability to the established end-moment versus end-rotation curve. The CDC method was successfully used by Chwalla[53], Ojalvo[54], Levi and Driscoll[55], and Ojalvo and Fukumoto.[56]

The studies briefly reviewed above have been mainly advanced for structural sections used in columns of building frames and are not directly applicable to stiffened plate panels. While the primary bending is applied on the beam-column by the end moments in building frames, the primary bending in the stiffened plate panel is caused by the lateral hydrostatic pressure. Beam-columns under lateral hydrostatic pressure not only defy the application of the CDC concept, but the effect of hydrostatic pressure on the ultimate strength may differ from the effect of eccentricity of axial load, both quantitatively and qualitatively.

The second difference is in the shape of the cross section. While the cross sections of most of structural sections are symmetric about the bending axis(rectangle, I-and WF- shapes), the cross section of a stiffened plate panel, in which a large plate area and a small stiffener flange area are connected by the web of the stiffener, is unsymmetric about the bending axis. Due to the unsymmetry in geometry and the residual stress distribution, stiffened plate panels have moment-curvature-thrust relationships which are considerably different from symmetric sections. Only a few approximate solutions are available for

beam-columns with lateral loads.[49] However, none of them consider members with unsymmetric cross sections.

The objectives of this dissertation can be summarized as follows:

(1) To develop a method of theoretical elastic-plastic analysis for the beam-column instability of longitudinally stiffened plate panels subjected to an axial thrust and uniformly distributed lateral loading.

(2) To investigate the parameters governing the ultimate strength.

(3) To present the computed data in a form suitable for a convenient determination of a most advantageous proportion of a stiffener-plate combination.

Basic assumptions and equilibrium equations are presented in Chapter 2. The procedure to establish the moment-curvature-thrust relationship is described in Chapter 3. From the established moment-curvature-thrust relationship, a method for determining the ultimate strength of a stiffened plate panel is developed in Chapter 4 through the application of the von Kármán criterion. Chapter 5 gives discussion of parameters which influence the ultimate strength of stiffened plate panels. Based on this information, a design chart is constructed in Chapter 6 and an illustrative design example is given in Appendix 10.3. Numerical calculations needed for this dissertion were carried out on a digital computer(G.E. 225).

2. BASIC ASSUMPTIONS AND EQUATIONS

2.1 BASIC ASSUMPTIONS

Present study is concerned with the development of a theory and procedures for the determination of the ultimate strength of longitudinally stiffened plate panels which fail by excessive bending in the direction of the applied lateral load.

A longitudinally stiffened plate panel is composed of a plate and equally spaced tee stiffeners which are welded on one side of the plate. The cross-sectional dimensions of the stiffened plate panel do not vary over its length.

The loads applied are an axial thrust and a hydrostatic lateral load. The axial thrust acts along the original centroidal plane of the stiffened plate panel. The hydrostatic pressure is applied on the surface of the plate opposite to the stiffeners.

The analysis was made on the bases of the following assumptions:

(1) The stiffened plate panels are initially straight and free of any imperfections.

(2) The stress-strain relationship of the material is ideally elastic-plastic. The yield stress of the stiffeners may differ from that of the plate.

(3) Cooling and welding residual stresses are present in the member.

(4) Strain reversal in the material which is stressed beyond the elastic limit is not considered in the analysis.

(5) Deflections due to shear strain are neglected.

(6) No local instability takes place prior to the ultimate failure.

(7) Width of the plate panel is large, so that the effect of the support at the side edges of the panel is negligible. Therefore all atiffeners may be considered to behave identically.

(8) The plate action between stiffeners is neglected, and the plate is assumed to remain flat. Under lateral load, the plate between neighboring stiffeners deflects changing the cross-sectional shape of the panel. While the resultant cross section is weaker than the original cross section, the restraint to the transverse strain provided by adjacent plates gives an additional stiffness to the stiffened plate panel. However, an analysis of the deflection, and strains in the plate from the experimental data[37,38] showed that the magnitudes of the deflection and lateral contraction of the plate were too small to have any significant effect on the strength of the stiffened plate panel.

(9) The entire cross section of the stiffened plate panel remains plane and normal to the centroidal axis after deformation.

(10) The effective width of the plate is assumed to be equal to the stiffener spacing. For the loading under consideration, unsymmetric stress distribution in the plate is caused both by out-of-plane deformation of the plate and by the shear lag. No solution considering both these causes is available at present. However, for the practical range of side ratios of the plate subpanel, 3 or more, all the elastic

and inelastic solutions available give an effective width which is very close to the full width of the plate subpanel.[21,33]

Assumptions (7), (8), and (10) lead to the conclusion that the cross section of stiffened plate panel can be represented by a simplified cross section which consists of a single stiffener and a plate having a width equal to the stiffener spacing.

2.2 BASIC EQUATIONS

In Fig. 2.1 is shown the simplified cross section used in the analysis. All the equations are derived from the equilibrium of a deformed stiffened plate panel and the stress-strain relationship.

The coordinate axes are taken as shown in Fig. 2.1.a, with the origin O on the centroidal axis of the section in the deflected position at the point of maximum deflection. The z-axis is parallel to the original centroidal axis, and tangential to the deflected centroidal axis at the origin. The s-axis measures the distance along the deflected centroidal axis from origin O.

The sign covention used is:

Stress and strain are positive if in compression.

Bending moment M and curvature ϕ are positive if they cause compression in the plate.

Components of resultant forces in the direction of the y- and z-axes, V and H, are positive if in the direction shown in Fig. 2.2.a.

Taking the equilibrium of the element with length ds (Fig. 2.2),

the relations among qb, H, V, and M are obtained as :

$$H + qbds_p \sin\theta - (H + dH) = 0 \tag{2.1}$$

$$V + qbds_p \cos\theta - (V + dV) = 0 \tag{2.2}$$

$$M - Hds \sin\theta - Vds \cos\theta - qbds_p \frac{ds}{2} - (M + dM) = 0 \tag{2.3}$$

where ds_p is the length of the plate surface subjected to hydrostatic pressure q.

The length ds_p can be evaluated from ds, ϕ, and the distance from the centroid to the plate surface d_1.

$$ds_p = (1 - \phi d_1) ds \tag{2.4}$$

If terms of second order are neglected, and if Eq. 2.4 is used for ds_p, Eqs. 2.1, 2.2 and 2.3 become:

$$\frac{dH}{ds} = (1-\phi d_1) qb \sin\theta \tag{2.5}$$

$$\frac{dV}{ds} = (1-\phi d_1) qb \cos\theta \tag{2.6}$$

$$dM = -H \sin\theta - V \cos\theta \tag{2.7}$$

The exact expression for the curvature ϕ is,

$$\phi = \frac{d\theta}{ds} \tag{2.8}$$

If the variation of the curvature ϕ along the s-axis were known, the bending moment M would be obtained by integrating Eqs. 2.5, 2.6 and 2.7 together with Eq. 2.8.

Another moment-curvature relationship is obtained independently from the equilibrium of the stresses over the cross section. This relationship is defined as the moment-curvature-thrust relationship of the cross section.

$$M = F(\phi, N) \tag{2.9}$$

where N is the axial thrust acting on the cross section.
The axial thrust N is related to H and V as follows:

$$N = H \cos \theta - V \sin \theta \tag{2.10}$$

To maintain equilibrium in the member, both moment-curvature relations should be satisfied over the entire length of the member. Thus the problem of the determination of the deflected configuration becomes a problem of finding the curvature ϕ which yields identical moments from both moment-curvature relationships. Once the curvature ϕ is determined over the entire length of the member, the deflected configuration of the panel can be obtained using the following equations:

$$\frac{dy}{ds} = \sin \theta \tag{2.11}$$

$$\frac{dz}{ds} = \cos \theta \tag{2.12}$$

Shortening of the member is caused not only by the axial thrust, but also by the strain at the centroid of the cross section ϵ_c.

$$\frac{d\theta}{ds} = \frac{1}{1-\epsilon_c(\phi, N)} \tag{2.13}$$

Differential Equation in the Elastic Range

When it is assumed that the behavior is elastic and the deflection is small, the two sets of moment-curvature relationships can be combined into a linear ordinary differential equation.

For small deflections,

$$\theta = \frac{dy}{dz}$$

$$\phi = \frac{d\theta}{dz} = \frac{d^2y}{dz^2}$$

$$\sin\theta = \theta = \frac{dy}{dz} \qquad (2.14)$$

$$\cos\theta = 1$$

$$1 - \phi d_1 = 1$$

Substituting Eqs. 2.14, Eqs. 2.5 through 2.7 are simplified to,

$$\frac{dH}{dz} = 0$$

$$\frac{dV}{dz} = qb \qquad (2.15)$$

$$\frac{dM}{dz} = -H\frac{dy}{dz} - V$$

For the elastic range and small deflection, Eq. 2.9 becomes,

$$M = -EI\frac{d^2y}{dz^2} \qquad (2.16)$$

Combining Eqs. 2.15 and 2.16, one obtains the following differential equation:

$$EI\frac{d^4y}{dz^4} + H\frac{d^2y}{dz^2} = qb \qquad (2.17)$$

This differential equation is identical to that given in texts books.[6]

2.3 ULTIMATE STRENGTH

The ultimate strength of excessively bent columns was considered as an instability problem by von Kármán.[41] In the buckling of columns, the column changes its deflected shape from one stable configuration to another stable configuration. This is called a bifurcation problem. At the ultimate failure of excessively bent columns, however, the transition from a stable state to an unstable state takes place in the same deformed configuration.

The instability of excessively bent columns can be explained in terms of the load-deflection characteristics of the loading system and the structure. The load-deflection characteristic of the structure depends on the material properties, the cross-sectional dimensions, the length of the structure, and the eccentricity (or lateral load). When the material properties and cross-sectional dimensions of the structure, and the eccentricity (or lateral load) are specified, the internal forces are defined as a function of the deflection and the length of the structure. Representing the deflection by the maximum curvature in the structure ϕ^o,

$$P = f(\ell, \phi^o) \tag{2.18}$$

The load-deformation characteristics of the loading system depends on the type of loading, whether it be a gravity loading, a deformation loading or some other type of loading. The simplest load-deformation characteristic is the one independent of deformation and it is represented by a series of straight lines parallel to the deformation axis on the load-deformation plot as shown in Fig. 2.3. In this paper the load-deformation characteristic of the loading system is assumed to be the

one described above.

For a given length ℓ, the load-deformation characteristic of a structure becomes a curve on the load-deformation plot, which rises to the maximum point, then falls off with the weakening of the section due to yielding. In Fig. 2.3, a typical load-deflection curve of the structure is shown.

Intersections of the loading system and structure load-deflection curves, A_1 and A_2, represent equilibrium conditions. If the external force is further increased, a new series of equilibrium points A_1',A_2' ... is obtained. All the points A_1, A_1' ..... represent conditions of static equilibrium, but not necessarily of stable equilibrium. The stability of the structure can be checked by comparing the gradients of loading system and structure curves. For the structure to be stable, the gradient of structure curve S_s must be greater than the gradient of loading system curve S_f. The criterion for stability is:

$$S_s > S_f$$

For the assumed load-deflection characteristic of the loading system,

$$S_f = 0$$

and then the criterion becomes,

$$S_s > 0 \qquad (2.19)$$

Thus by this inequality, Eq. 2.19, points A_1, A_1' .... are seen to be stable. The external force will be increased through a series of stable points, until a point C is reached, where $S_s = 0$. Beyond point C, the system becomes unstable. Thus, the ultimate condition can be expressed as the zero gradient of the load-deflection curve of the structure.

$$S_s = 0 \tag{2.20}$$

Since, $$S_s = \frac{dP}{d\phi^o}$$

the ultimate strength of the structure defined above coincides with the maximum axial load the structure can carry.

In the discussion above, the length of the structure ℓ is kept constant and the ultimate condition is expressed in terms of P and ϕ^o. However, sometimes it is found convenient to keep P constant and express the ultimate condition in terms of ℓ and ϕ^o. Differentiating Eq. 2.18, one obtains:

$$\frac{dP}{d\phi^o} = f_\ell \frac{d\ell}{d\phi^o} + f_{\phi^o} \tag{2.21}$$

Referring to Eq. 2.20,

$$\left(\frac{dP}{d\phi^o}\right)_{\ell = \text{const.}} = f_{\phi^o} = 0$$

Thus the ultimate condition can be defined as,

$$f_{\phi^o} = 0 \tag{2.22}$$

If P is kept constant, substitution of Eq. 2.22 and $\frac{dP}{d\phi^o} = 0$ into Eq. 2.21 leads to the ultimate condition in terms of ℓ and ϕ^o.

The ultimate condition defined by Eq. 2.22 can be expressed in terms of ϕ^o and either P or ℓ as follows:

$$\left(\frac{dP}{d\phi^o}\right)_{\ell = \text{const.}} = 0 \tag{2.23}$$

or

$$\left(\frac{d\ell}{d\phi^o} \right)_{P = \text{const.}} = 0 \qquad (2.24)$$

The relationships of Eqs. 2.23 and 2.24 are graphically shown in the three-dimensional sketch of Fig. 2.5. The surface in the figure represents the equilibrium points, and the space curve U defines the ultimate condition at which both Eq. 2.23 and Eq. 2.24 are satisfied.

When the structure is in equilibrium in the deformed configuration, the axial thrust in the structure varies along the centroidal axis. The axial thrust can be represented by an axial thrust at a specified location in the structure instead of the axial thrust at the loading ends. If the origin of the coordinate axis 0 is chosen as the specified location, the relation between the axial thrust N^o at the origin and P is:

$$N^o + qby^o = P \qquad (2.25)$$

where y^o is the deflection of the structure at the origin of the s-axis. On the $N^o - \phi^o$ plot (Fig. 2.4), the shape of the structure curve is slightly changed from that shown in Fig. 2.3. Also, the load curves are no longer straight lines parallel to the deformation axis, but they become a series of curves with negative gradient. Consequently, the limit of stable equilibrium does not coincide with the maximum N^o, but becomes point C, where the tangent of the structure curve coincides with the tangent of the load curve passing through the point. The gradient of the load deflection curve at point C is,

$$\left(\frac{dN^o}{d\phi^o} \right)_{\ell = \text{const.}} = - qb \frac{dy^o}{d\phi^o} \qquad (2.26)$$

When the magnitudes of lateral loading q and the differential of y^o with respect to $\emptyset^o$ are small, Eq. 2.26 can be approximated by

$$\left(\frac{dN^o}{d\emptyset^o} \right)_{\ell = \text{const.}} = 0 \qquad (2.27)$$

Equation 2.27 is satisfied at the apex of the $N^o - \emptyset^o$ curve, point B, as shown in Fig. 2.5. The external load in equilibrium at point B, P_3, is slightly lower than the true ultimate load. For the range of q and the dimensions of the structures under consideration in this analysis, however, the error introduced by the approximate equation 2.27 was found to be less than 0.1%, and the approximate solution is without exception on the safe side.

In a manner similar to that used in approximating Eq. 2.23 by Eq. 2.24, the approximate ultimate condition can be expressed in terms of ℓ and $\emptyset^o$ as follows,

$$\left(\frac{d\ell}{d\emptyset^o} \right)_{N^o = \text{const.}} = 0 \qquad (2.28)$$

Equation 2.28 was used throughout the analysis as the ultimate condition, except where otherwise noted.

3. MOMENT - CURVATURE - THRUST RELATIONSHIP

3.1 INTRODUCTION

All methods of solving the basic equations given in Art. 2.2 require that the moment-curvature-thrust relationship be known. This relationship depends on the shape of the cross sections, the axial thrust, the residual stresses, and the material properties.

The deformation which occurs when a cross section is subjected to axisl thrust and bending moment is shown in Fig. 3.1 where N is the axial thrust and M is the bending moment. N and M are obtained by integrating stresses over the cross section.

$$N = \int_A \sigma dA \qquad (3.1)$$

$$M = \int_A \sigma \eta dA \qquad (3.2)$$

Assuming that the strain distribution is linear in the elastic-plastic range as well as in the elastic range, one can express the curvature ϕ in terms of strains.

$$\phi = \frac{\epsilon_1 - \epsilon_2}{d + t}$$

where: ϵ_1, ϵ_2 = the strains at the extreme fibers in the cross section

d = the depth of the stiffener

t = the thickness of the plate

The problem is to determine M for the given values of N and ϕ. It is solved by relating strains ϵ to stresses σ by the specified stress - strain relationship of the given material.

An analytical solution using an elastic-plastic stress-strain relationship like the one in Fig. 3.2 was given by Baker, Horne and Roderick for a rectangular cross-section.[43] However, if one considers other cross-sections or the presence of residual stresses, an analytical solution is much more difficult to obtain. To overcome these difficulties a semi-graphical method was introduced by Ketter and others.[46] In their method the integrations in Eqs. 3.1 and 3.2 are carried out for a certain number of well chosen strain distribution in order to construct a set of moment-curvature and thrust-curvature diagrams. Then, proceeding graphically, one can determine the moment-curvature-thrust relationships for specified cross sections.

The availability of high speed computers has brought a new approach to the problem. Fukumoto has produced solutions and computer programs for wide-flange shapes containing residual strains of simplified distribution.[57] In his approach, algebraic relationships are established between moment, thrust, curvature, and extent of yielding. Then, these equations are solved analytically in terms of the given parameters as a preparation for the calculation by the digital computer. This preparatory work of setting up algebraic equations is required for every possible yielding configuration. For the unsymmetric cross sections under consideration in this study, the number of possible yielding configurations is much larger than for symmetric sections of wide-flange shapes, and even the development of the algebraic statement of the problem becomes a considerable task. The number of possible yielding configurations may further increase with the variation in the cross-sectional dimensions and the intensity of residual strains.

Recently, Birnstiel and Michalos developed a method using a totally numerical approach.[58] In this method, the section is divided into a number of sub-areas, and the integration is carried out as a machine summation. Thus, the solution can be obtained without modification of a computer program for any residual stress pattern, yield stress variation in the cross-section, and change of cross-sectional dimensions. The difficulty is that the subdivision size must be sufficiently small to give the required accuracy.

For the work described in this report a new semi-analytical and semi-numerical method was devised by dividing the cross section into a few sub-areas so that in each sub-area the analytical integration could be done easily. A detailed procedure for computing the moment-curvature-thrust relationships is described in the following articles.

3.2 MATERIAL PROPERTIES AND RESIDUAL STRESSES

MATERIAL PROPERTIES

The stress-strain relationship of the material is assumed to be elastic--perfectly plastic as shown in Fig. 3.2. The idealized stress-strain diagram of Fig. 3.2 closely approximates the experimental stress-strain diagrams of mild structural steels until the beginning of strain hardening. Stress and strain are proportional in the range between the tensile yield strain ε_{yt} and the compressive yield strain ε_{yc}. Beyond these elastic limits, the stress is maintained constant at the yield stress level and the material flows plastically. In this simplified relationship strain hardening is neglected. If strain reversal does not take place, a strain defines a corresponding stress uniquely. Ježek found that for problems of unrestrained beam-columns, the idealized stress-strain diagram gave substantially the same results as those obtained with the use of an exact stress-strain diagram of a typical structural steel.[44]

The material properties in compression are assumed to be identical to those in tension. Several experimental studies on the compressive material properties of structural material showed that the moduli of elasticity were essentially the same for compression and tension.[59,60,61] Yield stresses, however, were from 1.8% to 9% higher in compression. A consistent relationship between yield stresses in compression and tension has not yet been established. In the present analysis the same yield stress was used for both tension and compression(σ_{yp} for the plate and σ_{st} for the stiffeners)

Residual Stresses

The importance of the effect of residual stresses on column strength is well known. For beam columns failing in excessive bending, residual stresses have the effect of reducing the magnitude of strain at which yielding starts.

Residual stresses are formed as a result of plastic deformations which may be caused by cooling after welding or after hot-rolling, or by fabricating operations such as cold-bending or cambering.

The bottom plating of the ship's hull experiences several welding processes before the completion of the ship. These include seam and butt welding of the plates, welding of the stiffeners to the plate, and welding of subassemblies.

The measurement of residual stresses due to welding has been pursued almost since the beginning of modern welding. Experimental and analytical studies have been made on residual stresses in a simple plate by many researchers.[62,63,64,65]

Studies on residual stresses encountered in welded ships were made by the National Defense Research Committee[66] and others. A brief account of these studies can be found in Ref. 67.

The measurement of residual stresses caused by welding of stiffeners to a plate was performed on scale models of stiffened plate panels in Fritz Engineering Laboratory, Lehigh University.[37,38] A typical residual stress distribution is shown in Fig. 3.3. At the weld, tensile residual stresses, whose magnitueds are usually greater then the yield stress of the base plate, form narrow peaks.

The tensile stresses are balanced by broad bands of comparatively smaller and approximately uniform compressive stresses lying in the body of the plate. When weld lines are long, the variation of residual stresses along the weld line becomes negligible.

Residual stresses caused by girth welding differ considerably from those described above. The fore-and-aft stresses* vary gradually from compression in the vicinity of the start of weld to tension at the location of the completion of the weld. The variation of fore-and-aft stresses in the fore-and-aft direction is of negligible magnitude, since the nature of these residual stresses is closer to that of reaction stresses than that of residual welding stresses. The athwartship residual stresses were neglected in the analysis so that the uniaxial stress-strain law would be applicable.

Unfortunately the final fore-and-aft residual stresses cannot be obtained by a simple summation of residual stresses due to several causes, as they are dependent on building sequence. Except for the welding of stiffeners to the plate, however, the welds produce approximately uniform residual stresses over the individual stiffener and plate-subpanel combination. Therefore, their final contribution can be expected as uniform residual stresses. Such residual stresses can be taken into account by modifying the analyzed results. On the other hand, residual stresses caused by welding of stiffeners to the plate are not uniform, and should be included in the analysis.

---

*Fore-and-aft stresses in a complete ship are longitudinal stresses in the longitudinally stiffened plate panel. Athwartship stresses are transverse stresses in the same panel.

Consistent with the measured residual stress distribution as shown in Fig. 3.3, the residual stress pattern is further idealized for convenience of mathematical treatment. In the plate, the rectangular distribution shown in Fig. 3.4 is assumed. The magnitude of the tensile residual stresses is taken to be equal to the yield stress of the base plate, and the change of the yield stress of the plate in the vicinity of the weld is neglected.

The distribution pattern of measured residual stresses in the stiffeners did not show any consistent trend, because cambering and preheating of the stiffeners was needed in order to fabricate the scale models as straight as possible.[37,38] Although a considerable number of residual stress measurements have been made for rolled sections, none of the results can be directly applicable to the structure under consideration.[68,69] Since the residual stress distribution in the flange could not be established, a triangular residual stress distribution, similar to those found in rolled WF shapes, is arbitrarily assumed in the flange. A comparison of numerical results for sections with a triangular and a uniform residual stress distribution in the flange showed only a negligible difference in the moment-curvature-thrust relationships.

Residual stresses in the web of the stiffener will be considerably different from those in the webs of rolled shapes. In the analysis, however, residual stresses in the web are neglected since the contribution of the web to the bending rigidity of the cross section is small.

The simplified residual stress distribution is shown in Fig. 3.4. The magnitudes and the distribution of residual stresses are fully defined by four parameters: compressive residual stress in the plate

σ_{rc}, residual stress at the flange tip σ_{fc}, residual stress at the junction of the flange and the web σ_{ft}, and the breadth of the tensile residual stress zone in the plate b_{rt}.

These four parameters are assumed to be constant along the length of a longitudinally stiffened plate panel.

In the idealized cross section shown in Fig. 35, the variation of the flange thickness of the stiffener and the fillet at the flange-to-web junction (see Fig. 2.1) are neglected. Thus, the cross section is composed of three rectangles. The difference in the material properties between the base plate and the weld metal within these rectangles, as found in case of bevelled fillet welds, is not included in the analysis.

3.2 DETERMINATION OF MOMENT-CURVATURE-THRUST RELATIONSHIP

From the assumption that the strains in the cross section vary linearly, the strain at any location is defined by the strain at a specified location and the curvature ϕ. Taking the strain at the outer surface of the plate ϵ_1 as a reference, the strain on the cross section at distance η_1 from the outer surface of the plate is given by

$$\epsilon = \epsilon_1 - \phi \eta \tag{3.4}$$

The effective yield strain can be represented by the yield strain of material ϵ_y and the residual strain ϵ_r as follows:

$$\begin{aligned} &\text{in compression:} \quad \bar{\epsilon}_{yc} = \epsilon_{yc} - \epsilon_r = \epsilon_y - \epsilon_r \\ &\text{in tension:} \quad \bar{\epsilon}_{yt} = \epsilon_{yt} - \epsilon_r = -\epsilon_y - \epsilon_r \end{aligned} \tag{3.5}$$

For the idealized stress-strain relationship the stress is given by the following equation:

$$\begin{aligned} &\text{if} \quad \bar{\epsilon}_{yc} < \epsilon \qquad \sigma = E\,\bar{\epsilon}_{yc} \\ &\text{if} \quad \bar{\epsilon}_{yt} < \epsilon < \bar{\epsilon}_{yc} \qquad \sigma = E\,\epsilon \\ &\text{if} \quad \epsilon < \bar{\epsilon}_{yt} \qquad \sigma = E\,\bar{\epsilon}_{yt} \end{aligned} \tag{3.6}$$

where E is Young's Modulus

Substituting Eq. 3.6 into Eqs. 3.1 and 3.2 one obtains the integrals for axial thrust and bending moment about the elastic neutral axis as follows:

$$N = \int_{A_e} E\epsilon \, dA_e + \int_{A_{pc}} E\bar{\epsilon}_{yc} \, dA_{pc} + \int_{A_{pt}} E\bar{\epsilon}_{yt} dA_{pt} \tag{3.7}$$

$$M = \int_{Ae} E\epsilon\eta dA_e + \int_{A_{pc}} E\bar{\epsilon}_{yc}\eta dA_{pc} + \int_{A_{pt}} E\bar{\epsilon}_{yt}\eta dA_{pt} \tag{3.8}$$

where the three integrals are to be taken over the elastic core A_e, the yielded zone in compression A_{pc}, and the yielded zone in tension A_{pt}, respectively.

Using Eq. 3.4 and relationships

$$\bar{\epsilon}_{yc} = \epsilon - (\epsilon - \bar{\epsilon}_{yc})$$

$$\bar{\epsilon}_{yt} = \epsilon - (\epsilon - \bar{\epsilon}_{yt})$$

Eqs. 3.7 and 3.8 can be rewritten as:

$$N = E(\epsilon_1 - \phi d_1)A - E\left[\int_{A_{pc}}(\epsilon_1 - \phi\eta_1 - \bar{\epsilon}_{yc})dA_{pc} + \int_{A_{pt}}(\epsilon_1 - \phi\eta_1 - \bar{\epsilon}_{yt})dA_{pt}\right] \tag{3.9}$$

$$M = E\phi I - E\left[\int_{A_{pc}}(\epsilon_1 - \phi\eta_1 - \bar{\epsilon}_{yc})\eta dA_{pc} + \int_{A_{pt}}(\epsilon_1 - \phi\eta_1 - \bar{\epsilon}_{yt})\eta dA_{pt}\right] \tag{3.10}$$

A is the total area and I is the moment of inertia of the cross section.

In terms of a distance η_2 from the stiffener flange instead of η Eq. 3.10 becomes

$$M = E\phi I + E(\epsilon_1 - \phi d_1)Ad_2 - Nd_2 - E\left[\int_{A_{pc}}(\epsilon_1 - \phi\eta_1 - \bar{\epsilon}_{yc})\eta_2 dA_{pc} + \int_{A_{pt}}(\epsilon_1 - \phi\eta_1 - \bar{\epsilon}_{yt})\eta_2 dA_{pt}\right] \tag{3.11}$$

Thus, the necessary integrations are reduced to integrations over the yielded zones.

$$\bar{N} = -E[\int_{A_{pc}}(\epsilon_1 - \emptyset\eta_1 - \bar{\epsilon}_{yc})dA_{pc} + \int_{A_{pt}}(\epsilon_1 - \emptyset\eta_1 - \bar{\epsilon}_{yt})dA_{pt}] \quad (3.12)$$

$$\bar{M} = -E[\int_{A_{pc}}(\epsilon_1 - \emptyset\eta_1 - \bar{\epsilon}_{yc})\eta_2 dA_{pc} + \int_{A_{pt}}(\epsilon_1 - \emptyset\eta_1 - \bar{\epsilon}_{yt})\eta_2 dA_{pt}] \quad (3.13)$$

$$N = E(\epsilon_1 - \emptyset d_1)A + \bar{N} \quad (3.14)$$

$$M = EI\emptyset + E(\epsilon_1 - \emptyset d_1)Ad_2 - Nd_2 + \bar{M} \quad (3.15)$$

These integrations can be considerably simplified by dividing the cross section into four rectangular sub-areas as follows:

Sub-area 1: part of the plate where the tensile residual stress exists

Sub-area 2: part of the plate where the compressive residual stress exists

Sub-area 3: stiffener web

Sub-area 4: stiffener flange

The effective yield strains on each sub-area are given in Table 3.1.

In sub-area 1 through sub-area 3, the effective yield strains are constant over the whole sub-area, while in sub-area 4, the effective strains vary linearly from the flange tip to the centerline. Various yield configurations for the first three sub-areas are shown in Fig. 3.6. The plastic strains are shown as shaded areas. Generally these shaded areas are given as combinations of two triangular prisms, the

bases of which are the plastic strains at the lowest and the uppermost fibers of the sub-area. The plastic strains are determined by the strain at the outer surface of the plate ϵ_1, the curvature $\emptyset$, the distance from the plate surface to the extreme fibers η_{1i1}, η_{1i2}, and the effective yield strain $\bar{\epsilon}_{yi}$.

$$\epsilon_{pi1} = \epsilon_1 - \emptyset\, \eta_{1i1} - \bar{\epsilon}_{yi}$$
$$\epsilon_{pi2} = \epsilon_1 - \emptyset\, \eta_{1i2} - \bar{\epsilon}_{yi} \qquad (3.16)$$

Consequently the integrations in Eqs. 3.12 and 3.13 over the sub-area are evaluated as quadratic and cubic functions of ϵ_1.

$$\bar{N}_i = \frac{E}{2\emptyset}\left[c_{i11}(\epsilon_1 + c_{i12})^2 + c_{i21}(\epsilon_1 + c_{i22})^2\right] \qquad (3.17)$$

$$\bar{M}_i = \frac{E}{2\emptyset}\left[c_{i11}(\epsilon_1+c_{i12})^2\left(\eta_{2i1} - \frac{\epsilon_1 + c_{i12}}{3\emptyset}\right) + c_{i21}(\epsilon_1 + c_{i22})^2\left(\eta_{2i2} - \frac{\epsilon_1 + c_{i22}}{3\emptyset}\right)\right] \qquad (3.18)$$

where η_{2i1} and η_{2i2} are distances from stiffener flange to the lowest and the uppermost fibers in the sub-area i. Coefficients c_i are tabulated in Table 3.2.

In sub-area 4(the stiffener flange) the effective yield strains vary linearly. Therefore, plastic strains are represented by a combination of four triangular pyramids instead of two triangular prisms as shown in Fig. 3.7. The integrations in Eqs. 3.12 and 3.13 over sub-area 4 are expressed as cubic and 4-th power functions of ϵ_1, respectively.

In a stiffened plate panel, however, sub-area 4 occupies a

very small portion of the cross-sectional area; thus the thickness of the flange can be neglected without introducing any significant errors in the moment-curvature-thrust relationship. If we neglect the thickness of the flange, the integrations over sub-area 4 become:

$$\bar{N}_4 = \frac{E}{2\bar{\phi}} [c_{411}(\epsilon_1 + c_{412})^2 + c_{421}(\epsilon_1 + c_{422})^2] \tag{3.19}$$

$$\bar{M}_4 = 0 \tag{3.20}$$

where coefficients c are given in Table 3.3.

Equation 3.19 is identical in form to Eq. 3.17. According to Eq. 3.17 through Eq. 3.20, Eqs. 3.14 and 3.15 are expressed as quadratic and cubic functions of ϵ_1.

$$N = E(\epsilon_1 - \phi d_1)A + \frac{E}{2\bar{\phi}} \sum_{i=1}^{4} [c_{i11}(\epsilon_1 + c_{i12})^2 + c_{i12}(\epsilon_1 + c_{i22})^2] \tag{3.21}$$

$$M = EI\phi + [EA(\epsilon_1 - \phi d_1) - N]d_2 + \frac{E}{2\phi} \sum_{i=1}^{3} [c_{i11}(\epsilon_1 + c_{i12})^2 (\eta_{2i1} - \frac{\epsilon_1 + c_{i12}}{3\phi}) + c_{i21}(\epsilon_1 + c_{i12})^2 (\eta_{2i2} - \frac{\epsilon_1 + c_{122}}{3\phi})] \tag{3.22}$$

Equations 3.21 and 3.22 together with Tables 3.2 and 3.3, are valid not only for positive bending as shown in Fig. 3.6, but also for negative bending.

Equations 3.21 and 3.22 are nondimensionalized for further use. Using nondimensionalized moment, thrust and curvature:

$$m = \frac{M}{M_y} = \frac{M}{\sigma_{yp} S}$$

$$n = \frac{N}{N_y} = \frac{N}{\sigma_{yp} A} \qquad (3.23)$$

$$\Phi = \frac{\phi}{\phi_y} = \frac{\phi d_2}{\epsilon_{yp}}$$

where S is the section modulus with respect to the stiffener flange.

Equations 3.21 and 3.22 become:

$$n = (G_1 - \frac{\Phi d_1}{d_2}) + \frac{bd_2}{2\Phi A} \sum_{j=1}^{8} [\, C_{j1}(G_1 + C_{j2})^2] \qquad (3.24)$$

$$m = \Phi + [G_1 - \frac{\Phi d_1}{d_2} - N]\frac{Ad_2}{S} + \frac{bd_2 t}{2\Phi S} \sum_{j=1}^{6} [C_{j1}(G_1 + C_{j2})^2 (C_{j3} - \frac{G_1 + C_{j2}}{3\Phi} \frac{d_2}{t})] \qquad (3.25)$$

where

$$G_1 = \frac{\epsilon_1}{\epsilon_{yp}}$$

Coefficients C are summarized in Table 3.4 in nondimensionalized form. Geometric constants, $\frac{d_1}{d_2}$, $\frac{bd_2}{A}$, $\frac{Ad_2}{S}$, $\frac{bd_2 t}{S}$, and $\frac{d_2}{t}$ vary according to the relative dimensions of the cross section. However, as shown in the detailed discussion given in Appendix 10.1, these geometric coefficients can be defined by only three relative nondimensional parameters, namely:

$\alpha = \frac{A_{st}}{bt}$; ratio of stiffener area to plate area.

$\beta = \frac{A_f}{A_{st}}$; ratio of stiffener flange area to whole stiffener area

$\gamma = \frac{d}{t}$; ratio of stiffener depth to plate thickness

It should be noted here that the plate slenderness ratio $\frac{b}{t}$ is not included in the determination of the moment-curvature-thrust relationship.

The material properties and the residual stress distribution can be defined by nondimensional parameters.

$$G_{st} = \frac{\sigma_{st}}{\sigma_{yp}}$$

$$G_{fc} = \frac{\sigma_{fc}}{\sigma_{yp}}$$

$$G_{ft} = \frac{\sigma_{ft}}{\sigma_{yp}}$$

For the specified geometric parameters α , β , γ , and the specified residual stress distribution, coefficients C are easily selected with the aid of Table 3.4 for given values of Φ and G_1. Then the corresponding thrust and moment can be evaluated using Eqs. 3.24 and 3.25. In the numerical integration described in Chapter 4, it is desirable to have the moment-curvature relationships for a specified thrust, n. Accordingly, the procedure is reversed to first obtaining G_1 by solving Eq. 3.24 for a given n and Φ. Then the corresponding moment is evaluated from Eq. 3.25. The difficulty in this procedure arises from the fact that coefficients C are functions of the yield configurations of the cross section, and consequently are dependent on G_1. Thus the procedure is further revised as follows:

(1) Assume an appropriate G_1.

(2) Select coefficients C for an assumed G_1 and a given Φ.

(3) Determine true G_1 by solving Eq. 3.24.

(4) Evaluate M fro Eq. 3.25 for the true G_1 and the given Φ, and n.

One of the advantages of this approach is that the assumed G_1 must give the correct yield configuration, but needs not to be a close approximation of the true value of G_1. The selection of the assumed G_1 is discussed in Appendix 10.1 in detail.

Numerical computations were carried out using a high speed digital computer, GE-225. The flow diagram is shown in Fig. 10.1. For each given n, 200 sets of Φ - G_1 - m values were computed and stored in computer memory for future use. The increment of Φ was so chosen that the moment-curvature relationship between computed points could be approximated by linear interpolation with an error of less than 0.1% (Appendix 10.1).

3.4 CHARACTERISTICS OF MOMENT-CURVATURE-THRUST RELATIONSHIP OF LONGITUDINALLY STIFFENED PLATE PANELS

In Fig. 3.9 are shown typical nondimensionalized moment-curvature curves of a longitudinally stiffened plate panel. The cross-sectional and material properties of the panel are:

$$\alpha = 0.3$$
$$\beta = 0.45$$
$$\gamma = 10$$
$$G_{st} = 1$$

The effect of residual stresses is also shown in Fig. 3.9. The residual stress parameters used are,

$$G_{rc} = 0,\ 0.125,\ \text{and}\ 0.25$$

$$B_{rt} = \frac{G_{rc}}{1+G_{rc}}$$

$$G_{fc} = -G_{ft} = 0.3$$

Due to the unsymmetry of the cross section and the residual stress distribution, m-Φ curves of a longitudinally stiffened plate panel differ considerably from those of symmetric sections. The main differences are as follows:

For a longitudinally stiffened plate panel in the presence of the axial thrust,

(1) m-Φ curves in positive and negative bending are not identical.

(2) in positive bending, a low axial thrust may have a reinforcing effect on the bending rigidity of the cross section,

(3) a zero curvature does not necessarily correspond to a zero moment.

The first two aspects are clearly represented in the plot of the ultimate bending moment carrying capacity of the cross section (Fig. 3.10) The effect of axial thrust on the moment carrying capacity of a longitudinally stiffened plate panel is explained with the aid of Fig. 3.10. The stress distribution at full plastification of the cross section is given by the stress blocks. Since the cross section is unsymmetric, the neutral axis(the line of zero strain) does not coincide with the centroidal axis, but it is distant from the centroidal axis by $\bar{\eta}$. The full plastic moment about the centroidal axis, ξ - axis, is expressed by:

$$\text{positive bending, } M_{np}=\sigma_{yp}\left[\int_{\eta=\bar{\eta}_{np}}^{\eta=d_1}\eta dA - \int_{\eta=-d_2}^{\eta=\bar{\eta}_{np}}\eta dA\right] \qquad (3.26)$$

$$\text{negative bending, } M_{nn}=\sigma_{yp}\left[\int_{\eta=\bar{\eta}_{nn}}^{\eta=d_1}\eta dA - \int_{\eta=-d_2}^{\eta=\bar{\eta}_{nn}}\eta dA\right] \qquad (3.27)$$

When axial thrust is not present, $\bar{\eta}_{op}$ is equal to $\bar{\eta}_{on}$ (Fig. 3.11 (a) and (b)). From Eqs. 3.26 and 3.27, the full plastic moment is:

$$\text{With zero axial thrust: } M_{op}=|M_{on}| \qquad (3.28)$$

With the increase of axial thrust, $\bar{\eta}_{np}$ for positive bending decreases, while $\bar{\eta}_{nn}$ for negative bending increases. Comparing Eqs. 3.26 and 3.27 one can see that under low axial thrust, $M_{np}>|M_{nn}|$ (3.29)

For a high axial thrust which causes negative $\bar{\eta}_{np}$ (Fig. 3.11(e), the inequality between M_{np} and $|M_{nn}|$ becomes dependent on the cross-sectional dimensions, and the generalization as given by Eq. 3.29 is impossible.

The reinforcing effect of axial thrust can be investigated by comparing Fig. 3.11 (b), (d) and (e). As shown in Fig. 3.11, $\bar{\eta}_{np}$ for

positive bending decreases with an increase of axial thrust.

Equation 3.26 results in an increase of M_{np} for a decrease of $\bar{\eta}_{np}$. Therefore, the positive bending moment M_{np} increases with an increase of axial thrust until $\bar{\eta}_{np}$ becomes zero.

The magnitude of the axial thrust which gives the maximum full plastic moment is given by:

$$N = \sigma_{yp}\left[\int_{\eta=0}^{\eta=d_1} dA - \int_{\eta=-d_2}^{\eta=0} dA\right] \tag{3.30}$$

The third aspect of the characteristics of M-Φ curves of longitudinally stiffened plate panels is caused by the unsymmetric distribution of residual stresses. Under high centroidal compression, the cross section is plastified unsymmetrically and the M-Φ curves deviate from the straight line at the origin. An enlarged plot of M-Φ curves in the vicinity of the origin is given in Fig. 3.12. For the given residual stress parameters ($G_{rc}<G_{fc}$) the cross section remains elastic for zero curvature until the axial thrust reaches $n = 1 - G_{fc} = 0.7$. Thereafter with an increase of axial thrust, yielding in the stiffener flange progresses, and the bending moment about the centroidal axia for zero curvature assumes not a zero, but a positive value. When the axial thrust reaches $n = 1 - G_{rc} - \frac{(G_{fc} - G_{rc})^2\,\alpha\beta}{2(G_{fc} - G_{ft})(1+\alpha)}$ a part of the plate starts to yield. Since the compressive residual stress zone in the plate has a much larger cross-sectional area than the stiffener flange the effect of yielding in the plate becomes predominant after a certain increase of the axial thrust, and the bending moment for zero curvature becomes negative. The direction and the amount of deviation from the origin is dependent on the residual stress parameters, the

cross-sectional dimensions, and the magnitude of the axial thrust. When G_{rc} is larger than G_{fc}, only a deviation in the direction of negative moment takes place.

These deviations due to unsymmetrically distributed residual stresses are very important for stiffened plate panels under a centrally applied axial thrust. Stiffened plate panels, whose elastic buckling strain is larger than the minimum effective yield strain, will start bending before the buckling load is reached, and the ultimate strength may be reduced considerably.

4. ULTIMATE STRENGTH OF LONGITUDINALLY STIFFENED PLATE PANELS

4.1 INTRODUCTION

The ultimate strength of a longitudinally stiffened plate panel is determined by applying a stability criterion to an established load-deflection curve (or panel length--deflection curve) of the stiffened plate panel, as described in Art. 2.3. The load-deflection relationship (or panel length--deflection relationship) is evaluated from the equilibrium equations and the moment-curvature relationships of the cross section.

Non-linearity of the moment-curvature relationship and basic equilibrium equations, however, does not permit the use of an analytical procedure. In the numerical procedure, the panel length--deflection relationship is more easily evaluated than the load-deflection relationship, since only one moment-curvature curve is needed for a given axial thrust. The available numerical methods for the evaluation of a panel length--deflection relationship can be divided into two groups. The first group, such as Newmark's numerical integration procedure, computes the deflections for given lengths.[70] On the other hand, the second group, such as a stepwise integration procedure, can compute the length of the panel in equilibrium for given deflection.

Although Newmark's numerical integration procedure is widely used in beam-column analysis, it furnished only the stable branch of the panel length-deflection curve and has the inconvenience of defining the ultimate failure of the structure by the divergence of the numerical integraion. A stepwise integration procedure evaluated the unstable branch of the panel length--deflection curve as well as the stable

branch without modification of the procedure. The main difficulty encountered in the stepwise integration procedure is that it requires a considerable amount of repetitive computation. This difficulty, however, is easily overcome by the use of high speed digital computers.

With a stepwise integration procedure, a numerical procedure for exact analysis was developed and programmed for a digital computer as described in Art. 4.2. In Art. 4.3 numerical results are compared with test results.

The developed procedure can also be used in an ultimate strength analysis of columns subjected only to an axial thrust. In Art. 4.4, it is shown that the behavior of longitudinally stiffened plate panels under axial thrust differs considerably from the behavior of columns with doubly symmetric section.

4.2 PROCEDURE OF NUMERICAL ANALYSIS

The panel length--deflection relationship of a longitudinally stiffened plate panel is obtained by the stepwise integration of basic equilibrium equations along using the true moment-curvature relationship of the cross section.

The j-th segment of the integration is shown in Fig. 4.1. Over the length of the segment Δs along the centroidal axis, curvature ϕ is no longer constant. To assume ϕ to be constant, the segment length should be very small. If the variation of ϕ is assumed to approximate closely the true variation of ϕ over the segment, the segment length can be increased without reducing the accuracy. However, since the

true variation of $\emptyset$ is unknown, the assumption of a too elaborate variation of $\emptyset$ is not worth the increased amount of computation required by such an assumption. In this analysis, the linear variation of $\emptyset$ is assumed over each segment. Then the magnitude of $\emptyset$ at any point A in the j-th segment is given by:

$$\emptyset = \emptyset_{j-1} + \frac{\emptyset_j - \emptyset_{j-1}}{\Delta s} s_j \qquad (4.1)$$

where subscripts j-1 and j designate the values at the initial and final points of the segment, respectively and s_j is the distance from the point j-1 to point A along the centroidal axis. The magnitudes of the unknown variables at point j are obtained by integrating Eqs. 2.5 through 2.13 with Eq. 4.1 starting from the known variables at point j-1.

First, $\emptyset$ at point j is assumed to be $\emptyset_{ja}$. Then the assumed $\emptyset$ in the segment is given by:

$$\emptyset = \emptyset_{j-1} + \frac{\emptyset_{ja} - \emptyset_{j-1}}{\Delta s} s_j \qquad (4.2)$$

From Eqs. 2.8, 2.5 and 2.6, θ, H and V in the segment become,

$$\theta = \theta_{j-1} + \int_o^{s_j} \emptyset \, d\bar{s}_j$$
$$= \theta_{j-1} + \emptyset_{j-1} s_j + \frac{\emptyset_{ja} - \emptyset_{j-1}}{2\Delta s} s_j^2 \qquad (4.3)$$

$$H = H_{j-1} + \int_o^{s_j} (1-\emptyset\, d_1) qb \sin\theta \, d\bar{s}_j$$
$$= H_{j-1} + qbd_1(\cos\theta - \cos\theta_{j-1}) + qb\int_o^{s_j} dy \qquad (4.4)$$

$$V = V_{j-1} + \int_o^{s_j} (1-\emptyset\, d_1) qb \cos\theta \, d\bar{s}_j$$

$$= V_{j-1} - qbd_1(\sin \theta_{j-1}) + qb\int_o^{s_j} dz \qquad (4.5)$$

Substituting Eqs. 4.4 and 4.5 into Eq 2.7 and integrating over the length of the segment, one gets:

$$M_j = M_{j-1} - \int_o^{\Delta s}[H_{j-1} + qbd_1(\cos \theta_{j-1}) + qb\int_o^{s_j} dz] \sin \theta \, d\bar{s}_1$$
$$- \int_o^{\Delta s}[V_{j-1} - qbd_1(\sin \theta_{j-1}) + qb\int_o^{s_j} dy]\cos \theta \, d\bar{s}_i$$
$$= M_{j-1} - H_{j-1}\Delta z$$
$$- qb\left[\frac{(\Delta y)^2}{2} + \frac{(\Delta z)^2}{2} - d_1\Delta y \cos \theta_{j-1} + d_1\Delta z \sin \theta_{j-1}\right] \qquad (4.6)$$

where Δz and Δy are obtained from Eqs. 2.11 and 2.12.

$$\Delta z = \int_o^{\Delta s} \cos \theta \, d\bar{s}_j \approx \cos \theta_{j-1}(\Delta s) - \left(\frac{\phi_{j-1}}{3} + \frac{\phi_{ja}}{6}\right) \sin \theta_{j-1}(\Delta S)^2 \qquad (4.7)$$

$$\Delta y = \int_o^{\Delta s} \sin \theta \, d\bar{s}_j \approx \sin \theta_{j-1}(\Delta s) + \left(\frac{\phi_{j-1}}{3} + \frac{\phi_{ja}}{6}\right) \cos \theta_{j-1}(\Delta S)^2 \qquad (4.8)$$

The bending moment at point j is thus evaluated by Eqs. 4.6, 4.7 and 4.8 for the assumed curvature ϕ_{ja}. These equations are nondimensionlized with the following results:

$$\Delta Z = \cos \theta_{j-1} \, \Delta S - \left(\frac{\Phi_{j-1}}{3} + \frac{\Phi_{ja}}{6}\right) \sin \theta_{j-1}(\Delta S)^2 \sqrt{\epsilon_{yp}} \frac{r}{d_2} \qquad (4.9)$$

$$\Delta Y = \sin \theta_{j-1} \, \Delta S \, \frac{1}{\sqrt{\epsilon_{yp}}} + \left(\frac{\Phi_{j-1}}{3} + \frac{\Phi_{ja}}{6}\right) \cos \theta_{j-1}(\Delta S)^2 \qquad (4.10)$$

$$m = m_{j-1} - H_{j-1}\,\Delta Y\,\frac{d_2}{r} - V_{j-1}\,\Delta Z - Q\left[\tfrac{1}{2}(\Delta Y)^2 \epsilon_{yp} + \tfrac{1}{2}(\Delta Z)^2 - \cos\theta_{j-1}\Delta Y\frac{d_1}{r}\epsilon_{yp} + \sin\theta_{j-1}\,\Delta Z\frac{d_1}{r}\sqrt{\epsilon_{yp}}\right] \qquad (4.11)$$

where

$$Q=\frac{qEbd_2}{\sigma_{yp}^2 A}\,,\quad v = \frac{d_2}{Ar}\sqrt{\frac{E}{\sigma_{yp}}}3,\quad h = \frac{H}{\sigma_{yp}A}$$

$$\Phi = \frac{\phi}{\phi_y}\,,\quad M = \frac{M}{M_y} \qquad (4.12)$$

$$\Delta S = \frac{\Delta s}{r}\sqrt{\frac{E}{\sigma_{yp}}}\,,\quad Z = \frac{\Delta z}{r}\sqrt{\frac{E}{\sigma_{yp}}}\,,\quad \Delta Y = \frac{\Delta y}{r}$$

The curvature corresponding to m_j is obtained by the moment-curvature-thrust relationship of the cross section. The axial thrust at point j is given by

$$n_j = h_j \cos\theta - v_j \frac{r}{d_2}\sqrt{\epsilon_{yp}}\sin\theta_j \qquad (4.13)$$

Since the variation of axial thrust along the centroidal axis is small (numerical results showed a devistion of less than 0.05%), the moment-curvature relationship for an axial thrust n^o can be used for the entire length of the structure.

Curvature Φ_{jc} thus obtained from the moment- curvature relationship does not generally coincide with the assumed curvature Φ_{ja}. If Φ_{jc} differs from Φ_{ja}, a new Φ_{ja} is assumed to be equal to Φ_{jc} and a new Φ_{jc} is computed. The same procedure is repeated until Φ_{ja} and Φ_{jc} converge. When the difference between Φ_{ja} and Φ_{jc} become negligible, the variation of curvature over the j-th segment is es-

tablished and variables at point j are evaluated.

$$\Phi_j = \Phi_{jc} = \Phi_{ja} \tag{4.14}$$

$$\theta_j = \theta_{j-1} + \tfrac{1}{2}(\Phi_{j-1} + \Phi_j)\sqrt{\epsilon_{yp}} \cdot \frac{r}{d_2} \Delta s \tag{4.15}$$

$$h_j\, h_{j-1} + Q \cdot \epsilon_{yp}[\Delta Y \cdot \frac{r}{d_2} + (\cos \theta_j - \cos \theta_{j-1}) \cdot \frac{d_1}{d_2}] \tag{4.16}$$

$$v_j = v_{j-1} + Q\,[\Delta Z - \sqrt{\epsilon_{yp}}(\sin \theta_j - \sin \theta_{j-1}) \cdot \frac{d_1}{d_2}\,] \tag{4.17}$$

$$Y_j = Y_{j-1} + \Delta Y \tag{4.18}$$

$$Z_j = Z_{j-1} + \Delta Z \tag{4.19}$$

The length of the centroidal axis ℓ is given by Eq. 2.13 and expressed non-dimensionally at point j by:

$$L_j = L_{j-1} + \frac{2\,\Delta S}{2 - \epsilon_{yp}[G_{j-1} + G_j - (\Phi_{j-1} + \Phi_j) - \frac{d_1}{d_2}]} \tag{4.20}$$

where $L = \frac{\ell}{r}\sqrt{\epsilon_{yp}}$

and $G_{j-1} = \frac{\epsilon_{1j-1}}{\epsilon_{yp}}$; $G_j = \frac{\epsilon_{1j}}{\epsilon_{yp}}$

Using the variables evaluated in Eq. 4.11 and Eqs. 4.14 through 4.20, the integration over the (j+1)-st segment is carried out by the same procedure. Repeating this procedure the integration is continued until the end conditions are reached.

Initial Values. To commence the stepwise integration, the initial values of the variables in the first segment should be known. For each

integration, specified values of n^o and Φ^o are assumed. Moment m^o corresponding to n^o and Φ^o is obtained by the moment-curvature - thrust relationship of the cross section. At origin O,

$$Y_o = 0; \quad Z_o = 0; \quad L_o = 0 \tag{4.21}$$

According to the orientation of the coordinate axis,

$$\theta_o = 0 \qquad \text{and } h_o = n^o \tag{4.22}$$

For a structure whose loading edges have different end conditions, the shearing force at origin v_o is unknown and should be determined by trial. But when both end conditions are the same, v_o becomes zero due to the symmetry of the structure and loading.

$$v_o = 0 \tag{4.23}$$

Furthermore, for such symmetric structure integration over only one half the length of the structure is needed to represent the entire length.

Boundary Conditions. In the numerical computations used in this report, only two boundary conditions are considered; pinned- end and fixed-end conditions. The pinned-end condition is defined by a zero moment,*

$$m = 0 \tag{4.24}$$

while the fixed-end condition is defined by

$$\theta = 0 \tag{4.25}$$

---

* In longitudinally stiffened plate panels, the location of zero moment does not necessarily coincide with the location of zero curvature. This is shown in Fig. 3.11.

As shown in Fig. 4.2, the integration for the pinned-end condition is a part of the integration for the fixed-end condition. Similarly by performing the integration for the fixed-end condition, the equilibrium configuration of the structure with any elastically restrained end can be obtained as a part of the integration process.

Ultimate Condition. The ultimate condition is given by the point of zero slope on the panel length--deflection curve.

$$\left(\frac{d\ell}{d\phi^o}\right)_{N^o = \text{const.}} = 0 \tag{2.28}$$

Non- dimensionalizing the equation, one obtains,

$$\left(\frac{dL}{d\Phi^o}\right)_{n^o = \text{const.}} = 0 \tag{4.26}$$

To find the combination of $(L - \Phi^o)$ which satisfies Eq. 4.26 the integration is repeated by increasing the magnitude of Φ^o by small increments $\Delta\Phi^o$ as Φ^o_1, Φ^o_2, ... $\Phi^o_{(k-2)}$, $\Phi^o_{(k-1)}$ and Φ^o_k, and corresponding lengths L are evaluated. If three successive lengths L satisfy the following inqualiities,

$$L_{k-2} < L_{k-1}$$
$$L_{k-1} > L_k \tag{4.27}$$

The value of Φ^o which satisfies Eq. 4.26 lies between $\Phi^o_{(k-2)}$ and Φ^o_k. The ultimate values of L and Φ^o are then determined by assuming L to be a quadratic function of Φ^o in the range between $\Phi^o_{(k-2)}$ and Φ^o_k.

Error in Stepwise Integration. As previously discussed, the accuracy of the stepwise integration depends on the length of the segments. In Fig. 4.3 a typical relationship between the error and the segmental length is shown. Specific parameters of the longitudinally stiffened plate panel investigated are as follows:

$$\alpha = 0.3$$

$$\beta = 0.45$$

$$\gamma = 10$$

$$G_{rc} = 0.125$$

$$G_{fc} = -G_{ft} = 0.3$$

$$P = 0.7\ P_y$$

$$Q = 2$$

The general trend is that the shorter the segmental length, the smaller the error becomes. The pinned-end condition led to considerably smaller error than the fixed- end condition. For the plate panel with pinned-ends, $\Delta S = 0.18$ gave an error less than 0.1%, while the same segmental length resulted in the errors of more than 0.7% for the panel with the fixed-ends. Since the integration for the pinned-end panel is carried out as a part of the integration for the panel with fixed-ends, the difference in the errors is considered to be accumulated after the pinned-end condition is reached. By reducing the segmental length after reaching the pinned-end condition, the error could be kept to the same order of magnitude for both pinned-end and fixed-end panels without an excessive increase in the number of segments, as shown in Fig. 4.3. In numerical computations, whose results are compiled in this paper, $\Delta S = 0.18$

is used until the pinned-end condition is reached. Thereafter ΔS is reduced to 0.036 and even smaller where required. In Art. 10.2 a step-by-step account of the numerical integration procedure is given together with the flow diagram for the computer program.

4.3 COMPARISON WITH TEST RESULTS

A number of longitudinally stiffened plate panels have been tested at Lehigh University.[36,37,38] Of these, two tests(Test No. T-5 and T-6), which failed in column instability[36,37], are chosen for comparison with the theoretical results. Specimens were tested under pinned-end conditions. Lateral loading was applied by means of a compressed air system. The nominal dimensions of the specimens are given in Figs. 4.4 and 4.5. Table 4.1 gives the actual dimensions and material properties obtained from coupon tests. Values of the non-dimensional parameters used in the numerical computation are given in Table 4.2. These parameters were computed from the dimensions of simplified cross sections composed of a single stiffener and a plate with a width equal to the stiffener spacing.

Unfortunately, residual stresses were not measured in the specimens. Compressive residual stresses in the plate were estimated from the measured deflection and the observation of first yielding during the tests.

The test results are compared with the theoretical ultimate strength curve in Fig. 4.6. The ultimate axial load of Specimen T-5

obtained by testing slightly exceeds the theoretical prediction.

The test result of T-6 is located somewhat below the predicted curve (95% of predicted value). The cause for this disagreement seems to be initial deflection of the specimen. Specimen T-6 had a positive initial deflection (positive meaning concave on the plate side.) Since the initial deflection was in the direction of the lateral load, Specimen T-6 could not carry the axial load predicted on the assumption of an initially perfectly straight stiffened plate panel. The initial deflection in Specimen T-5 was slight and in the opposite direction.

Considering a possible error involved in the estimation of the magnitude of residual stresses, good correlation is indicated between the test results and the theoretical predictions.

4.4 ULTIMATE STRENGTH OF LONGITUDINALLY STIFFENED PLATE PANELS SUBJECTED TO A CENTRALLY APPLIED AXIAL LOAD

The behavior of longitudinally stiffened plate panels under a centrally applied axial load depends on the slenderness of the structure, the yield stress of the material, and the residual stresses. When elastic flexural buckling takes place, the yield stress of the material and residual stresses have no effect on the buckling strength. With a further increase of axial load, the deflection increases and the stiffened plate panel fails by excessive bending due to yielding of the cross section. If yielding starts in the cross section prior to buckling, the stress distribution in the cross section is no longer uniform. Due to the unsymmetry of the cross section and the residual stress distribution, non-uniformly distributed stresses produce a resultant bending moment

about the elastic neutral axis (ξ - axis), as discussed in Art. 3.4. Such a bending moment is indicated as a shift of the moment-curvature curve from the origin on the moment axis in Fig. 3.11. To maintain equilibrium with the internal moment, a longitudinally stiffened plate panel with pinned-ends deflects in the y-direction, and fails by excessive bending without buckling after a further increase of axial load. When the stiffened plate panel has fixed-ends, fixed-end moments cancel out the internal bending moment, and the stiffened plate panel remains straight until the axial load reaches the inelastic buckling load.

Since the stiffened plate panels fail by excessive bending either with or without buckling, the ultimate strength of centrally loaded stiffened plate panels can be obtained by the numerical procedure described in Art. 4.2 if the lateral load parameter Q is taken equal to zero. The ultimate strength curve of longitudinally stiffened plate panels with a typical cross section is shown in Fig. 4.7. Cross-sectional dimensions and material properties used in the numerical computation are;

$$\alpha = 0.3$$

$$\beta = 0.45$$

$$\gamma = 10$$

$$G_{st} = 1.0$$

$$G_{rc} = 0.125$$

$$G_{fc} = -G_{ft} = 0.3$$

In Fig. 4.8 the panel length--deflection curves for the cross section under consideration are shown. When the elastic buckling takes place before first yielding ($P_{cr} < 0.7\ P_y$ in this stiffened panel), the

stiffened plate panel may deflect in either the positive or negative direction. If the first yielding load is smaller than the elastic buckling load, the direction of deflection is dictated by the yield configuration in the cross section and the deflected configuration of the stiffened plate panel is uniquely determined.

Taking the non-dimensional length L as a parameter, the numerical results can be shown by conventional load-deflection curves (Fig. 4.9). For slender plate panels (L = 4.0 and 5.0) in which elastic buckling takes place, the post-buckling strength is of neglibile magnitudes. All the shorter stiffened plate panels with L smaller than 3.8 start to deflect at $P = 0.7\ P_y$, where the stiffener flange starts yielding.

The elastic buckling load P_{cr} and inelastic buckling load $\bar{P}_{cr}$ are also shown in Fig. 4.7. The inelastic buckling load $\bar{P}_{cr}$ was computed by neglecting the eccentricity induced by partial yielding of the cross section.

$$\text{Elastic buckling} \quad : \quad P_{cr} = \left(\frac{\pi}{L}\right)^2 P_y \tag{4.28}$$

$$\text{Inelastic buckling} \quad : \quad \bar{P}_{cr} = \left(\frac{\pi}{L}\right)^2 \frac{I_e}{I} P_y \tag{4.29}$$

where I_e is the moment of inertia of the elastic core of the cross section.

When the stiffened plate panel fails after elastic buckling ($P_{cr} < 0.7P_y$), the elastic buckling load P_{cr} gives a good approximation of the ultimate load. When the plate panel fails without buckling ($P_{cr} > 0.7P_y$), however, the ultimate load and the inelastic buckling load do not show any correlation. Nevertheless, this seeming inconsistency can be explained with the aid of Fig. 4.10.

The buckling loads P_{cr}, $\bar{P}_{cr}$ are computed on the basis of the bending rigidity of the cross section, which corresponds to the slope of m - Φ curve at C on the m-axis. On the other hand, the bending rigidity of a stiffened plate panel at the ultimate condition is represented by the range of slopes of the section AB of the m-Φ curve. If the m - Φ curve passes through the origin, points A and C coincide and a close relationship between the ultimate load and the buckling load can be expected. If the m - Φ curve shifts from the origin, the slope at point C could be considerably different from any slope occurring on AB, and consequently, the ultimate strength may differ from the inelastic buckling load considerably. Since the slope of m - Φ curve depends on the cross-sectional dimensions, the residual stress distribution, and the magnitude of axial load, the slope at point C could be larger than the slope on AB. This, in turn, leads to an ultimate load considerably smaller than the computed inelastic buckling load.

From the above discussion on the ultimate strength of a centrally loaded, longitudinally stiffened plate panel, the following conclusions can be drawn.

(1) For longitudinally stiffened plate panels with fixed-ends, the ultimate load can be approximated by an elastic (or inelastic) buckling load.

(2) For longitudinally stiffened plate panels with pinned-ends, in which elastic flexural buckling takes place, the elastic buckling load gives a good approximation of the ultimate load.

(3) When yielding takes place prior to elastic buckling

in a longitudinally stiffened plate with pinned-ends, the computed inelastic buckling load does not approximate the ultimate load, although the eccentricity at the loading ends induced by the partial yielding in the cross section is small. The ultimate load of the plate panel should be predicted by an ultimate strength analysis.

4.5 SUMMARY: ON THE DEVELOPED METHOD OF ULTIMATE STRENGTH ANALYSIS

A numerical method of ultimate strength analysis was developed for longitudianlly stiffened plate panels having low b/t ratios, and programmed for a digital computer (G.E. 225). The procedure consists of two steps: (1) evaluation of moment-curvature-thrust relationship and (2) determination of the relationship between the ultimate axial load, lateral load, and panel length.

Although the procedure for the evaluation of the moment-curvature-thrust relationship is developed for plate panels with tee stiffeners, it is applicable to other cross sections provided that the cross section is composed of rectangular sub-areas, and that material properties and residual stresses are constant or vary linearly in each sub-area.

After the moment-curvature-thrust relationship is established the panel length-deflection relationship is evaluated by a stepwise integration, and the ultimate strength is determined according to the instability criterion. Thus, if a moment-curvature-thrust relationship in which the post-buckling behavior of plate components are taken into

account, is established for a longitudinally stiffened plate panel having a high b/t ratio, it can be analyzed by the same procedure.

The external loads considered in the computer program were a centrally applied axial load and a lateral hydrostatic pressure. A centrally loaded column was analyzed by taking lateral load to be equal to zero. End moments (or eccentrically applied load) generally encountered in the beam-column problem can be taken into account by changing the end condition in the stepwise integration.

One of the advantages of a procedure using a stepwise integration is that the column length--deflection relationships can be evaluated simultaneously for various end conditions.

5. NUMERICAL RESULTS AND PARAMETERS INFLUENCING ULTIMATE STRENGTH

The parameters influencing the ultimate strength of longitudinally stiffened plate panels were investigated by numerical computation. A discussion on the effect of each parameter is given in this chapter. The findings can be summarized as follows:

1. Residual stresses in the plate have a considerable effect on the ultimate strength, while the effect of residual stresses in the stiffener flange is negligible.
2. Lateral load has a pronounced influence on the ultimate axial load.
3. Cross-sectional dimensions can be fully defined by $\frac{A_{st}}{bt}$, $\frac{A_f}{A_{st}}$, and $\frac{d}{t}$. Plate slenderness ratio b/t has no effect on the ultimate strength since the plate panels are expected to fail because of excessive bending.
4. The optimum $\frac{A_{st}}{bt}$ value is a function of $\frac{P}{P_y}$. For a high $\frac{P}{P_y}$, a low $\frac{A_{st}}{bt}$ is advantageous while for a low $\frac{P}{P_y}$ a high $\frac{A_{st}}{bt}$ is advantageous.
5. The parameter $\frac{d}{t}$ does not have any influence detectable on non-dimensionalized ultimate strength curves.
6. The ratio of the stiffener flange area to the stiffener area $\frac{A_f}{A_{st}}$ has a small effect on the ultimate strength.
7. The loading sequence of the axial and lateral loads may influence the ultimate strength.

8. A stiffener whose yield stress is higher than that in the plate could be used to increase the ultimate strength without increasing the cross-sectional area.

5.1 NUMERICAL RESULTS

To investigate the effect of various parameters, their magnitudes were systemtically varied. The ranges of variation of parameters were chosen to cover the most practical cross sections. They are the following:

$$\alpha = \frac{A_{st}}{bt} = 0.1 \text{ to } 0.5$$

$$\beta = \frac{A_f}{A_{st}} = 0.15 \text{ t0 } o.45$$

$$\gamma = \frac{d}{t} = 5 \text{ to } 15$$

$$G_{rc} = \frac{\sigma_{rc}}{\sigma_{yp}} = 0 \text{ to } 0.25$$

$$q = \frac{q E b d_2}{\sigma_{yp} {}^2 A} = 0.5 \text{ to } 5.0$$

Minor parameters, G_{fc} and G_{ft}, which have little influence on the ultimate strength, were kept constant throughout the study ($G_{fc} = -G_{ft} = 0.3$). The material properties of the plate and stiffeners were assumed to be the same ($G_{st} = 1$). The ultimate strength of plate panels reinforced by stiffeners with higher yield stress ($G_{st} = 1$) is discussed separately in Art. 5.6. Only stiffened panels with pinned-ends and fixed-ends were analyzed. The data of the anlayzed cross sections are listed in Table 5.1.

By performing the numerical analysis described in Chapters 3 and 4, not only the ultimate axial load--lateral load--panel length relationship (p-Q-L) but also the longitudinal deflection, the lateral deflection, the curvature at mid-span, the slope at pinned-end, and the fixed-end moment were obtained at the ultimate condition. All this information is given in Table 5.2 for some of typical cross sections, the ultimate axial load--lateral load--panel length relationship is given in Table 5.3.

All the major parameters except for the lateral load parameter Q influence the moment-curvature-thrust relationship. Furthermore, since the geometric properties d_1/r and d_2/r, belong only to the higher order, and almost negligible terms in the stepwise integration, parameters α, β, γ and G_{rc} reflect on the ultimate strength mainly through moment-curvature-thrust relationships. In the following articles, all parameters are discussed in terms of the ultimate axial load--lateral load--panel length relationships.

Results of the ultimate strength calculations are represented in the form of the ultimate strength curves which show the relationship between the non-dimensionalized ultimate axial load ($p=\frac{P}{P_y}$) and the slenderness ratio modified by the yield strain ($L = \frac{\ell}{r}\sqrt{\frac{\sigma_{yp}}{E}}$) for a given lateral load ($Q = \frac{qEbd_2}{\sigma_{yp} A}$). The ultimate strength curves of cross sections 1-A, -B and -C (Table 5.1) are shown in Fig. 5.1 and 5.2, for pinned-end and fixed-ends, respectively. The lateral load parameter Q and the residual stress parameter $G_{rc} = \frac{\sigma_{rc}}{\sigma_{yp}}$ are shown as parameters pertinent to each curve.

When p = 0, the stiffened plate panel behaves as a beam, and the ultimate strength curve intersects the L-axis.

at $$L = \sqrt{\frac{8m_{np}}{Q}} \quad \text{for pinned end} \tag{5.1}$$

and $$L = \sqrt{\frac{8(m_{np}-m_{nn})}{Q}} \quad \text{for fixed end} \tag{5.2}$$

When L approaches zero, bending due to Q vanishes and the structure can carry the axial load equal to $P_y = \sigma_{yp}A$. Thus all the ultimate strength curves intersect the p-axis at p = 1. The conditions at p = 0 and L = 0 are extreme cases. Between these two extremes, the beam-column action takes place.

An ultimate strength curve can be divided into two portions, the upper and lower branches. The transition from the upper to the lower branch is located roughly at the axial load at which the positive full plastic moment of the cross section is maximum. The transition is sometimes indicated by the sharp bend in the ultimate strength curve as shown in Fig. 5.1 for Q = 4 and Q = 5. In the upper branch of the ultimate strength curve, the ultimate strength decreases gradually with the increase of L, while in the lower branch, the ultimate strength curve is almost vertical under a high lateral load. The effect of various parameters on the ultimate strength is gradual in the upper branch, but the lower branch rapidly changes its shape with a change of the magnitudes of the parameters. Furthermore, the loading sequence can play an important role in the range of the lower branch. The discussion on the effect of the loading sequence is given in Art. 5.5.

5.2 EFFECT OF RESIDUAL STRESSES

To investigate the effect of residual stresses, several cross sections were numerically analyzed assuming $G_{rc} = \frac{\sigma_{rc}}{\sigma_{yp}} = 1$, 1.125 and 0.25. Since residual stresses in the stiffener flange have no detectable influence on the moment-curvature- thrust relationship, residual stresses in the flange were kept constant. Ultimate strength curves for a cross section having three different residual stresses can be compared in Fig. 5.1 for pinned ends and in Fig. 5.2 for fixed ends.

Residual stresses in the plate reduce the ultimate strength considerably. For an assumed residual stress distribution, the larger the compressive residual stress, the greater is the reduction of the ultimate strength. The trend in the amount of the reduction in the upper branch is quite different from that in the lower branches of the ultimate strength curves. In the upper branch, the effect of residual stresses is more pronounced under a low lateral load than under a high lateral load. In the lower branch, a high lateral load results in a greater reduction of the ultimate strength that a low lateral load.

Another effect of the compressive residual stresses in the plate is the reduction of the maximum length of the stiffened plate panel which can carry a given lateral load. This is shown in the ultimate strength curves for $Q \geq 2$ in Fig. 5.1

Quantitatively, the amount of the reduction of the ultimate axial load due to the residual stresses depends on the magnitude of the

lateral load Q and the length for L. For a given section, the ultimate strength of the stiffened plate panel with residual stresses can be obtained by multiplying the ultimate strength of the panel free of residual stresses by modification factor K_r.

$$(p)_{G_{rc} \neq 0} = K_r \, (p)_{G_{rc}} = 0 \qquad (5.3)$$

where K_r is a function of G_{rc}, Q, and $(p)G_{rc} = 0$

Computation of K_r from the numerical results shows that for the upper branch of the ultimate strength curves, the modification factor K_r depends mainly on G_{rc}, Q, and $(p)_{G_{rc}=0}$, and that the effect of geometric parameters is negligible. Thus, once the K_r function is established, the upper branch of the ultimate strength curves for cross sections with residual stresses can be easily constructed from the exact ultimate strength curves for cross sections with zero residual stress. The graphical presentation of the K_r function is given in Fig. 5.8.

5.3 GEOMETRIC PARAMETERS

Relative dimensions of a cross section are defined by three geometric parameters: stiffener area ratio α, stiffener flange area ratio β, and stiffener depth ratio γ. In this article the effect of these geometric parameters on the ultimate strength of stiffened plate panels is discussed.

Stiffener Area Ratio α

Figures 5.3a and 5.3b show the ultimate strength curves for three cross sections with different stiffeners area ratios, α = 0.1, 0.3 and 0.5. Regardless of the other parameters, the cross sections with the smaller α can sustain higher P/P_y than those with the larger α. The difference in the shape of the ultimate strength curves is due to the difference in the reinforcing effect of the axial thrust on the moment-curvature relationship of the cross sections.

The study of the numerical results showed that the modification factor for α (Fig. 5.9) is mainly dependent on α, Q, and $(p)_{\alpha=0.3}$.

$$(p)_{\alpha = 0.3} = K_{\alpha} (p)_{\alpha = 0.3} \qquad (5.4)$$

The variation of K_{α} due to the variation of the other parameters is less than 1%.

To find the most favorable magnitude of α, it is necessary to make a comparison of the ultimate strength of stiffened plate panels having the same cross-sectional area A, length ℓ, and lateral load q. Since geometric properties r and $\frac{bd_2}{A}$ vary with α, the change in α results in L and Q of different magnitudes for a given set of A, ℓ, and q. Therefore, L-p curves are not appropriate for a direct comparison. The numerical results are replotted in Fig. 5.4 using a new abscissa $\frac{\ell}{A_b}\sqrt{\frac{\sigma_{yp}}{E}}$ and lateral load parameter $\frac{qE}{\sigma_{yp}}{}^2$. A_b is the cross-sectional area per unit width.

$$A_b = \frac{A}{b} \qquad (5.5)$$

In this figure, it is seen that the most favorable magnitude of α varies according to the magnitude of the axial load. For high P/P_y, a small α is advantageous, while a large α is advantageous for low P/P_y.

Stiffener Flange Area Ratio β

In Fig. 5.5 are shown the ultimate strength curves of three cross sections with different stiffener flange area ratios, $\beta = 0.15$, 0.30 and 0.45, respectively. The change of the shape of the ultimate strength curve due to the variation of β is considerably smaller than that due to the variation of α. The modification factor for the stiffener flange area ratio, K_β, is found to be dependent on the magnitude of β and on the non-dimensionalized axial thrust P/P_y.

$$(p)_{\beta \neq 0.45} = K_\beta \, (p)_{\beta = 0.45} \tag{5.6}$$

The effect of other parameters on the modification factor K_β is practically negligible. The modification factor curves are shown in Fig. 5.10.

To find the optimum magnitude of β, a P/P_y vs. $\frac{\ell}{A_b}\sqrt{\frac{\sigma_{yp}}{E}}$ plot is made for the same sections discussed above (Fig. 5.6). In the range of β ivestigated numerically, the larger the magnitude of β, the stronger the stiffened plate panel becomes. However, the largest permissible stiffener flange area ratio is limited by the plate slenderness of the stiffener web needed to present local buckling. The plate slenderness of the stiffener web is given by

$$\frac{d}{w} = \frac{\gamma^2}{\frac{b}{t} \cdot \alpha (1-\beta)} \qquad (5.7)$$

Since β is less than 1, the plate slenderness of the web d/w increases with an increase in β. When d/w is larger than a certain value, local buckling of the stiffener web would take place prior to the ultimate failure of the stiffened plate panel. The buckling load of the stiffener web depends on the stress distribution in the structure. The precise prediction of the buckling load of the stiffener web requires an involved analysis and is beyond the scope of this paper. However, a safe value can be taken as that given by the AISC specification for plastic design.(73)

$$\frac{d}{w} \leq 43\sqrt{\frac{33}{\sigma_{yp}}} \qquad (5.8)$$

where σ_{yp} is in ksi.

Stiffener Depth Ratio γ

The stiffener depth ratio, $\gamma = \frac{d}{t}$, does not give a detectable difference in the $\frac{P}{P_y} - \frac{\ell}{r}\sqrt{\frac{\sigma_{yp}}{E}} - \frac{qEbd_2^t}{\sigma_{yp}^2 A}$ relationship, except in the vicinity of $P/P_y = 0$. This is easily understood because the variation of γ hardly affects the non-dimensionlized moment-curvature-thrust relationship. If the plate thickness is neglected in the calculation of moment-curvature-thrust relationship, cross sections with various γ values produce identical moment-curvature-thrust relationships.

The absolute value of the ultimate axial load, however, varies with the magnitude of γ. As shown in Fig. 5.7, a higher γ gives a greater ultimate strength. Since the plate slenderness of the stiffener web is proportional to the square of γ (Eq. 5.7) the maximum permissible magnitude of γ is again determined by a limiting value of the plate slenderness of the stiffener web d/w.

5.4 EFFECT OF LATERAL LOAD

The ultimate strength curves of a cross section (Section 1) are shown in Fig. 5.1 and 5.2 for several magnitudes of lateral load. The effect of lateral load is seen in the reduction of ultimate axial load. Another interesting effect of lateral load is the change of shape of the ultimate strength curve of pin-ended stiffened plate panels (Fig. 5.1). Although the upper branches of the ultimate strength curves are more or less of the same shape, the lower branches change their shape according to the magnitude of the lateral load. Under a high lateral load, the slope of the ultimate strength curve on L-axis is positive showing the reinforcing effect of the axial thrust.

Since the maximum length of the stiffened plate panels which can carry the given high lateral load is found at a certain axial load other than zero, for the panels shorter than the maximum length and longer than the panel which fails as a beam, two ultimate axial loads exist. For such panels the ultimate axial load is dependent on the loading sequence.

A quantitative study of the effect of lateral load was

made by rearranging numerical results in the following form:

$$J_q(\tfrac{1}{2}L/\sqrt{\bar{p}}, \frac{Q_2}{Q_1}) = \frac{(L)_{Q=Q_2}}{(L)_{Q=Q_1}} \qquad (5.9)$$

A plot of these results (Fig. 5.11) showed that the modification factor J_q can be approximated by the following equation.

$$(J_q)\ \text{approx.} = \frac{1}{u_1}\ \sec^{-1}\left(1 + \frac{\sec u_1 - 1}{\frac{Q_2}{Q_1}}\right) \qquad (5.10)$$

where $$u_1 = \tfrac{1}{2}L\sqrt{\left(\frac{P}{P_y}\right)_{Q = Q_1}}$$

Equation 5.10 is derived from an approximate solution. The detailed derivation is given in Appendix 10.4.

5.5 END RESTRAINT AND LOADING SEQUENCE

End Restraint

Only two end conditions, pinned-end and fixed-end, were numerically analyzed. In the upper branch of the ultimate strength curve, stiffened plate panels with fixed-ends showed up to about 25% greater ultimate axial load than panels with pinned ends. The increase of the strength due to the end restraint becomes noticeable for small lateral load and high stiffener area ratio.

Because of its consistency, an expression of the effect of end restraint in terms of the length of the stiffened plate panels which fail at a given combination of axial and lateral load is preferred over an expression of this effect in terms of ultimate axial load. The length conversion curve derived from the approximate analysis (Fig. 5.12)

gives good correlation with numerical results. The deriviation of the length conversion curve is described in Appendix 10.4. Using Fig. 5.12 one can predict the ultimate strength curve of stiffened plate panels with fixed ends from the established ultimate strength curves of pin ended stiffened plate panels without numerical analysis.

Loading Sequence

As described in Art. 5.4, under high lateral load the reinforcing effect of axial thrust appears in the ultimate strength curve. In such cases, the loading sequence controls the combination of axial and lateral load at collapse. To illustrate this, a p-Q-L interaction curve for Section 1-B is given in Fig. 5.13. The curve shows the relationship between p and Q at collapse for L = 1.5. The domain enclosed by the curve and the two axes corresponds to the combinations of p and Q under which the stiffened plate panel is stable.

When p = 0, the stiffened plate panel acts as a beam and can carry lateral load Q_o determined by simple plastic theory. Due to the reinforcing action of axial thrust, the maximum lateral load Q_{max} that the stiffened plate can sustain is realized under axial load $p_1 = 0.48$. To achieve the ultimate condition $p = p_1$ and $Q = Q_{max}$, the load must be applied in such a manner that the combination of axial and lateral loads always stays inside the interaction curve until the ultimate condition is reached.

If lateral load is increased to its maximum before the application of the axial load, the stiffened plate panel fails at $p = 0$ and $Q = Q_o$, and it cannot realize the combination, $p=p_1$ and $Q=Q_{max}$.

When L is large, the reinforcing effect of the axial thrust disappears as shown by a curve for L = 3 in Fig. 5.8. For such stiffened plate panels, the loading sequence has no effect on the ultimate strength unless significant strain reversal is produced.

5.6 HYBRID SECTION

To achieve the most economical design of the structure, hybrid construction is successfully adopted in many cases. A plate panel reinforced by stiffeners with high yield stress was numerically analyzed to investigate the feasibility of hybrid construction in stiffened plate panels. The cross section analyzed is identical to the Section 1-B except that the yield stress of the stiffener is twice as great as the yield stress of the plate ($G_{st} = 2$)

The ultimate strength curves for this hybrid section are compared with those for the uniform section (Section 1-B) in Fig. 5.14a(pinned ends) and 5.14b (fixed ends). For the stiffened plate panels with fixed ends the use of stiffeners with high yield stress increases the ultimate strength considerably. This is the result of the delay of plastification of the stiffener flange at the ends. For the stiffened plate panel with pinned ends, the difference between ultimate strength curves for a hybrid and a uniform section is relatively small for the intermediate values of $\frac{P}{P_y}$.

Although there are not enough numerical data to draw definite conclusion, the use of hybrid construction in longitudinally stiffened plate panels with fixed ends appears to be promising. A more extensive study of hybrid stiffened plate panels with pinned ends is desirable.

6. ULTIMATE STRENGTH CHARTS FOR ANALYSIS AND DESIGN

The method of ultimate strength analysis of longitudinally stiffened plate panels is described in the preceeding chapters. In practice an exact numerical analysis may prove to be too time consuming and therefore impractical. If the compiled numerical results are available in proper chart forms, the ultimate strength analysis of a plate-stiffener combination or the selection of the most advantageous combination for design can be made without conducting a numerical analysis. Since the known and unknown quantities are different for analysis and for design, the analysis and design by charts are discussed, separately in this chapter.

6.1 STANDARD CROSS SECTION

In this chapter, a standard cross section is introduced as a basis for the analysis and design of stiffened plate panels. The "Standard Cross Section" refers to a specific, numerically analyzed section. An estimate of the ultimate axial load for a given plate panel is obtained by modifying the ultimate load for the Standard Cross Section.

Since the geometric parameters of Section 1(see Table 5.1) are the approximate mean values of the cross-sectional dimensions of practical plate panels, Section 1-A was selected as the Standard Cross Section in order to avoid excessive differences in the geometric parameters between a given plate panel and the Standard Cross Section.

The Standard Cross Section is free of residual stresses.

6.2 ANALYSIS OF LONGITUDINALLY STIFFENED PLATE PANELS

When a longitudinally stiffened plate panel is to be analyzed, panel length, cross-sectional dimensions, material properties and residual stresses in the panel are known. From this information parameters α, β, γ, G_{rc} and L can be computed. An estimate of the ultimate axial load that the panel can sustain under a given lateral load can be obtained by modifying the ultimate axial load for the Standard Section(see Art. 6.1) with modification factors K_r, K_α, K_β, consecutively.

The modification is illustrated by the following example.

EXAMPLES OF ANALYSIS

The stiffened panel used in example is Specimen T-5 described in Art. 4.3. Values of parameters for this specimen are given in Table 4.1.

1) Non-dimensionalized length L is

$$L = \frac{\ell}{r}\sqrt{\frac{\sigma_{yp}}{E}} = \frac{60.875}{1.135}\sqrt{\frac{39.7}{29.6\text{x}10^3}} = 1.96$$

2) For L = 1.96 and Q = 0.689, the Standard Section gives (Fig. 5.1)

$$p = 0.889$$

3) For p = 0.889, Q = 0.689 and $G_{rc} = 0.234$, modification factor K_r is read from Fig. 5.8 .

$$K_r = 0.939$$

p is then modified by K_r.

$$p_r = K_r\, p = 0.939 \times 0.889 = 0.834$$

4) Modification factor K_α is found in Fig. 5.9 for $p_r = 0,834$, $Q = 0.689$ and $\alpha = 0.519$.

$$K_\alpha = 0.918$$

$$p_\alpha = K_\alpha p_r = 0.918 \times 0.834 = 0.765$$

5) Modification for β is carried out in a similar manner using Fig. 5.10.

$$K_\beta = 1.028 \text{ (for } p_\alpha = 0.765, \beta = 0.392)$$

$$p_\beta = K_\beta p_\alpha = 1.028 \times 0.765 = 0.786$$

6) The ultimate axial load is then evaluated as follows:

$$P = p_\beta P_y = p_\beta \sigma_{yp} A = 0.786 \times 39.7 \times 21.43 = 670 \text{ kips}$$

This value of P = 670 kips obtained by the use of the modification factors compares very favorably with the results obtained by an experiment and by an exact analysis as shown in the following tabulation.

	Ultimate Axial Load (ksi)	Error
Test Result	684	----
Exact Analysis	676	-1.2%
Estimation using Modification Factors	670	-2.1%

6.3 DESIGN OF LONGITUDINALLY STIFFENED PLATE PANELS

A ship at sea is subjected to a longitudinal bending moment produced by the non-uniformly distributed weight of the ship and its contents, and by the supporting bouyancy. The ship's hull behaves as a

beam in bending, provided all the component parts of the structure maintain the configuration of the tubular hull girder.[71,72] The bottom plate panel must withstand the imposed loads without excessive deformation or instability until the hull develops its ultimate strength.

The loads to which the whole bottom plate panel is subjected at failure of the hull are as follows:

$$\text{Axial Tension: } P_t = \frac{M_{sag}}{K} \frac{L.F.}{D_h} \qquad (6.1)$$

or

$$\text{Axial Compression: } P_c = \frac{M_{hog}}{K} \frac{L.F.}{D_h}$$

where M_{sag} = maximum sagging moment at service

M_{hog} = maximum hogging moment at service

$L.F.$ = load factor

D_h = depth of hull

K = coefficient, dependent on the type of hull structure

In addition to the axial load, the bottom plating is subjected to a lateral load due to the water pressure and the weight of the cargo stored on top of the bottom plate panel. When the cargo is a liquid as in tankers, the lateral load becomes hydrostatic, and the intensity of lateral hydrostatic pressure is given by,

$$q = (\gamma_w d_s - \gamma_c H_s) L.F. \qquad (6.2)$$

where γ_w = unit weight of water

γ_c = unit weight of cargo

d_s = draft

H_s = depth of fluid cargo in the tank

The appropriate values of the load factor are not yet well established at present. Furthermore, the proper load factor for axial loads may differ from the load factor for the lateral load. However, the determination of the load factors is beyond the scope of this study.

Once the principal dimensions, the form, the general arrangement of the ship are decided upon, the longitudinal bending moments encountered in service can be estimated on the basis of an assumed distribution of bouyancy. Using an adequate load factor, one can compute the ultimate loads acting on the bottom plate panel from Eqs. 6.1 and 6.2. The unsupported length of the plate panel ℓ will be determined by the requirement for the transverse strength of the hull. The design of the bottom plate panels thus becomes a problem of determining the lightest combination of a plate and stiffeners for a given combination of axial and lateral loads and a given length ℓ.

$\bar{P} - \bar{Q} - \bar{L}$ Curve

The relative dimensions of the cross section α, β, γ and the plate thickness t are the unknown quantities to be determined. The ultimate strength curve (p-Q-L curve) used in the analysis of the plate panel is not adequate for the design procedure, since the principal parameters p, Q and L include the unknown quantities α, β γ , and t.

A new set of non-dimensionalized parameters is introduced for the axial and lateral loads and the length of the plate panel.

$$\bar{p} = p\,(1 + \alpha) = \frac{P_c}{\sigma_{yp} Bt}$$

$$\bar{Q} = Q \frac{1+\alpha}{D_2} = \frac{qE}{2\sigma_{yp}}$$

$$\bar{L} = L R = \frac{\ell}{t}\sqrt{\frac{\sigma_{yp}}{E}} \qquad (6.3)$$

where B is the breadth of the ship.

As seen in the right hand terms of Eq. 6.3, once the yield stress of the plate is decided upon, new parameters are defined by known quantities except for the plate thickness t. The results of the numerical analysis are rearranged in terms of $\bar{p}$, $\bar{Q}$, and $\bar{L}$. Some of the $\bar{p}$, $\bar{Q}$, $\bar{L}$ curves are shown in Fig. 6.1. Each curve represents a specified set of α, β, and γ values, and one of design conditions $\bar{Q}$. Neither $\bar{p}$ nor $\bar{L}$ are defined by design conditions unless plate thickness t is assumed. However, ratio of $\bar{p}$ to $\bar{L}$ is independent of the plate thickness and can be determined from the design conditions.

$$a = \frac{\bar{p}}{\bar{L}} = \frac{P_c}{B\ell}\sqrt{\frac{E}{\sigma_{yp}}}^3 \qquad (6.4)$$

The relation given by Eq. 6.4 is expressed in Figure 6.1 by a straight line which passes through the origin of the $\bar{L}$ - and $\bar{p}$ - axes and whose slope is $a = \frac{P_c}{B\ell}\sqrt{\frac{E}{\sigma_{yp}}}^3$. Any coordinate $(\bar{L}, \bar{P})$ on the straight line satisfies all the design conditions except for the lateral load. Since the lateral load is represented by the parameter $\bar{Q}$, which is pertinent to a $\bar{p}$ - $\bar{Q}$ - $\bar{L}$ curve, the intersection of the straight line and a $\bar{p}$ - $\bar{Q}$- $\bar{L}$ curve gives the coordinate $(\bar{L}, \bar{p})$ for the given lateral load and

a set of α, β, and γ. The required plate thickness is given from the coordinate $(\bar{L}, \bar{p})$ as:

$$t = \frac{P_c}{\sigma_{yp} B \bar{p}}$$

or (6.5)

$$t = \frac{\ell}{L} \sqrt{\frac{\sigma_{yp}}{E}}$$

Since a $\bar{p}$, $\bar{Q}$, $\bar{L}$ curve extends from $\bar{p}$- axis to $\bar{L}$-axis the straight line intersects the $\bar{p}$ - $\bar{Q}$ - $\bar{L}$ curve for any combination of α, β, and γ. However, the coordinate $(\bar{L}, \bar{p})$ and consequently the required plate thickness vary according to the magnitudes of α, β, and γ. The total cross-sectional area of the plate and stiffeners is given by

$$A = (1 + \alpha) B t \tag{6.6}$$

Comparing the total cross sectional areas for various sets of α, β, γ in the practical range, one can select α, β, γ, and the plate thickness so that the total cross sectional area becomes a minimum. Once α,β,γ, and t are selected the actual size of the stiffeners can be determined from the definitions of α, β, and γ as follows:

Stiffener depth: $d = \gamma t$

Web thickness: $w = \frac{\alpha(1-B)}{\gamma} B$ (6.7)

Stiffener area: $A_{st} = \alpha\, b\, t$

Flange area: $A_f = \beta\, A_{st}$

Where b is the stiffener spacing.

Since plate slenderness $\frac{b}{t}$ has no effect in this anaylsis, the stiffener spacing is not given in this analysis. To complete the design of a stiffened plate panel, either the cross-sectional area of a stiffener or the stiffener spacing must be decided from a consideration other than this strength analysis. The stiffener cross-sectional area would be influenced by the availability of the structural sections which conform to the given β and γ. The consideration of the construction cost may affect the selection of the stiffener spacing. When the stiffener to be used is chosen first, the stiffener spacing is given by

$$b = \frac{A_{st}}{\alpha t} \tag{6.8}$$

Limitations on the Plate and Stiffener Dimensions

Longitudinally stiffened plate panels consist of three plate components; the plate, the stiffener flange and the stiffener web. When plate components are subjected to axial compression, plate buckling inevitably takes place either in the elastic or plastic range. To prevent premature local buckling, the plate slenderness of the plate components should be of such magnitude that the plate buckling load is at least equal to, or greater than the ultimate axial load of the stiffened plate panel.

A study of the strain distribution in the cross section at the ultimate condition shows that the strain in the plate does not greatly exceed the yield strain, but the strains in the stiffeners may become much greater than the yield strain. A precise plate slenderness requirement is not yet available for the strain conditions of the structure described above. For design, however, the requirements of

various specifications derived for more or less similar conditions will serve as a guide. According to the AISC Specification[73] the plate slenderness requirements are as follows:

$$\text{plate: } \frac{b}{t} \leq 44\sqrt{\frac{33}{\sigma_{yp}}}$$

$$\text{stiffener web: } \frac{d}{w} \leq 43\sqrt{\frac{33}{\sigma_{yp}}}$$

$$\text{stiffener flange: } \frac{b_f}{t_f} \leq 8.5\sqrt{\frac{33}{\sigma_{yp}}}$$

yield stress σ_{yp} is in ksi

Design Chart

In the design procedure described above, $\bar{p}$, $\bar{Q}$, $\bar{L}$ curves must be prepared for various sets of α, β, and γ. Since the lateral load parameter $\bar{Q}$ and the residual stress parameter G_{rc} vary for each set of α, β, and γ, the number of curves would become considerable. For design it is desirable to present all curves on the same sheet of paper. However, the crowding of curves greatly hampers the reading of $\bar{p}$. By a close study of $\bar{p}$, $\bar{Q}$, $\bar{L}$ curves for all sets of α, β, and γ, the following observations were made:

1. The modification factor, that is, the ratio between $\bar{p}$ for the Standard Section and $\bar{p}$ for the given section in which only one of the three geometric parameters differs from the Standard Section, is a function of $\bar{p}$ for the Standard Section, $\bar{Q}$, and the geometric parameter under the consideration.

2. The value of $\bar{p}\ (\alpha_1, \beta_1, \gamma_1)$ is obtained with reasonable accuracy (less than 4% error) by modifying $\bar{p}$ for the Standard Section with the three modification factors described in Item 1 for three different section.

3. The above discussion is also valid for a section with residual stresses, if the Standard Section is considered to have the same residual stress parameters as the given section.

Three modification charts were constructed with the above reasoning in mind. By using these charts, one can execute the modification graphically instead of multiplying modification factors numerically. Each modification chart consists of a set of curves for various values of $\bar{Q}$ and the geometric parameter under consideration. The coordinates of a curve give values of $\bar{p}$ before and after the modification. In Fig. 6.2 is shown a sketch of three modification charts and the $\bar{p}$- $\bar{Q}$ -$\bar{L}$ curves for the Standard Section. The required plate thickness t for a cross section with $\alpha = \alpha_1$, $\beta = \beta_1$, $\gamma = \gamma_1$, and $\bar{Q} = \bar{Q}_1$ is evaluated as follows:

1) Obtain $\bar{p}$ for the Standard Section and $\bar{Q} = \bar{Q}_1$ as described in the preceding section, point A.

2) Proceeding horizontally from point A, find the appropriate modification curve for $\gamma = \gamma_1$ and $\bar{Q} = \bar{Q}_1$, point B.

3) Proceeding vertically from point B, find the appropriate modification curve for $\beta = \beta_1$, point C.

4) Proceeding horizontally to the right from point C, find the appropriate modification curve for $\alpha = \alpha_1$, and $\bar{Q} = \bar{Q}_1$, point D.

5) Drawing the vertical line through point D, find the final value $\bar{p}_f$ on the $\bar{p}_f$- axis.

6) Using the final $\bar{p}_f$, determine the plate thickness t from Eq. 6.5.

Complete design charts for pinned end and fixed end stiffened plate panels are given in Figs. 6.3 and 6.4, respectively. On these charts, a scale for the value of "a" is given on an inclined axis. The design condition is easily placed on the chart by drawing a straight line connecting the origin of the $\bar{L}$ - $\bar{p}$ axis and the given point on the a-scale.

An illustrative example of the design procedure of a stiffened plate panel is given in Appendix 10.3.

7. SUMMARY

A longitudinally stiffened plate panel is composed of a plate and equally spaced tee stiffeners. It is subjected to the combined action of an axial load applied at the ends and a hydrostatic pressure acting on the plate surface.

This dissertation presents the result of an investigation into the ultimate strength of longitudinally stiffened plate panels having low b/t ratios. The study can be divided into two parts: 1) the investigation of the parameters which have an effect on the ultimate strength of longitudinally stiffened plate panels and 2) the development of the design procedure which provides the most advantageous structure without requiring excessive design time.

The investigation is summarized in the following numbered paragraphs.

7.1 METHOD OF ANALYSIS

When the plate slenderness of the plate components of the cross section is small the ultimate strength was determined using the following steps:

1. Moment-curvature relationship of the cross section was computed for a given axial load.
2. Using the established moment-curvature relationship the panel length-deflection relationship was evaluated by a stepwise integration.
3. The length of the stiffened panel, for which a given load is the ultimate load, was determined by means

of an instability criterion.

4. The above steps were repeated for various axial loads, and the ultimate strength curve (ultimate axial load vs. panel length curve) was constructed for a given cross section.

All the computations were carried out on a digital computer, G.E. 225. Numerical results showed good correlation with the experimental results obtained previously.[36,37]

7.2 MOMENT-CURVATURE-THRUST RELATIONSHIP

Due to the unsymmetry in geometry and residual stress distribution, moment vs. curvature ($m - \Phi$) curves of longitudinally stiffened plate panels differ considerably from those of symmetric sections, such as WF shapes. The main differences are:

1. Branches of an $m - \Phi$ curve in positive (plate in compression) and negative (plate in tension) bending are not identical. The cross section usually has a greater capacity for positive bending than for negative bending.

2. Axial thrust does not necessarily reduce the flexural rigidity of the cross section. In positive bending, axial thrust may have a reinforcing effect on the flesural rigidity of the cross section.

7.3 PARAMETERS

The ultimate strength of a longitudinally stiffened plate panel depends on the following parameters:

1. Residual stresses
2. Intensity of hydrostatic pressure
3. Stiffener area ratio (A_{st}/bt)
4. Stiffener flange area ratio (A_f/A_{st})
5. Stiffener depth to plate thickness ratio (d/t)

The analysis of the numerical results revealed the following trends in the effect of these parameters on the ultimate strength:

1. Residual stresses in the plate have considerable effect on the ultimate strength, while the effect of residual stresses in the stiffener flange is negligible.
2. Hydrostatic pressure on the plate surface influences the ultimate axial load considerably.
3. The optimum stiffener area ratio is a function of the slenderness of the stiffened plate panel. For a long stiffened plate panel, a high A_{st}/bt is advantageous, while a low A_{st}/bt is advantageous for a short stiffened plate panel.(Fig. 5.4)
4. The stiffener flange area ratio A_f/A_{st} has only a small effect on the ultimate strength.
5. A higher stiffener depth to plate thickness ratio d/t gives a greater ultimate strength. Nevertheless, since a change in d/t leads to a sensitive change in the plate slenderness of the plate components, b/t and d/w, the magnitude of the applicable d/t is limited by the plate slenderness requirement to

prevent local buckling.

In the analysis, parameters were varied one at a time, and the total cross-sectional area was kept constant.

7.4 DESIGN CHART

A wide variation of a stiffener-plate combination is possible in the longitudinally stiffened plate panels. No straight forward analytical approach is available for finding an optimum combination of the plate and stiffeners. A trial and error procedure would require too much time and labor to be practical.

A design chart was developed by reorganizing the numerical results, on which the optimum combination of geometric parameters, A_{st}/bt, A_f/A_{st} and d/t can be easily obtained for a given set of material properties, loading, panel length, and an assumed residual stress distribution. The actual dimensions of the cross section can be determined to conform to these optimum geometric parameters.

7.5 LIMITATION OF PRESENT STUDY AND RECOMMENDATION FOR FUTURE RESEARCH

The present ultimate strength analysis dealt only with a limited range of longitudinally stiffened plate panels. The most important limitation was imposed by the assumption that local buckling does not take place until the ultimate load is reached. This assumption imposes a requirement that the plate slenderness be less than approximately 44 for a steel with a yield stress of 33 ksi. In practice, however, there are many occasions where a larger plate slenderness would be used. An opinion has been expressed that a maximum

plate slenderness of about 60 provides a well balanced design[2]. To investigate the ultimate strength of longitudinally stiffened plate panels of such dimensions, the analysis should take into account the post-buckling behavior of the plate. Furthermore, it would be desirable to present the results of such an analysis in the form of a design chart, similar to those developed in this study.

In the present study, only the lateral load acting on the outer surface of the plate was considered. It is possible, however, to have a net hydrostatic pressure on the stiffener side of the plate also, especially in the bottom plating of tankers. Due to the unsymmetry of the cross section, the behavior of stiffened plate panels is expected to be somewhat different depending on the direction of the lateral load. The analysis of longitudinally stiffened plate panels under axial load and lateral loads acting on the stiffener side of the plate can be conducted using the computer program developed in this study.

Although the primary concern in the design of bottom plating of ships is the combined action of compression and lateral load, longitudinally stiffened plate panels may also experience tension and shear in varying proportions and directions. No ultimate strength analysis of longitudinally stiffened plate panels subjected to these external loads is available at present. To achieve the rational design of bottom plating of ships, more information on the loading and on the inelastic behavior of stiffened plate panels under various loading conditions would be necessary.

248.13
(8)

8. REFERENCES

1. Beedle, L. S.
PLASTIC DESIGN OF STEEL FRAMES
John Wiley & Sons, New York, 1958

2. Vasta, J.
APPLICATION OF PLASTICITY TO PROBLEMS IN NAVAL SHIP STRUCTURES
2nd Symposium Naval Structural Mechanics, April, 1960

3. Drucker, D. C.
PLASTIC DESIGN METHOD-ADVANTAGES AND LIMITATIONS
Trans. SNAME, Vol. 65, 1957

4. Bryan, G. H.
ON THE INSTABILITY OF A PLATE UNDER THRUSTS IN ITS OWN PLANE WITH APPLICATION ON THE "BUCKLING" OF THE SIDES OF A SHIP
Proc. London Math. Soc., 1891

5. Bleich, F.
BUCKLING STRENGTH OF METAL STRUCTURES,
McGraw-Hill, New York, 1952

6. Timoshenko, S. and Gere, J. M.
THEORY OF ELASTIC STABILITY
2nd Ed., McGraw-Hill, New York, 1961

7. Bijlaard, P. P.
SOME CONTRIBUTION TO THE THEORY OF ELASTIC AND PLASTIC STABILITY
Publ. Intern. Assoc. Bridge and Structural Eng., Vol. VIII, 1947

8. Ilyushin, A. A.
STABILITY OF PLATES AND SHELLS BEYOND THE PROPORTIONAL LIMIT
NACA T.M. 1116, October, 1947

9. Handelman, D. C. and Prager, W.
PLASTIC BUCKLING OF A RECTANGULAR PLATE UNDER EDGE THRUST
NACA T.N. 1530, 1948

10. Stowell, E. Z.
A UNIFIED THEORY OF PLASTIC BUCKLING OF COLUMNS AND PLATES
NACA Rep. 898, 1948

11. Stowell, E. Z. and Pride, R. A.
THE EFFECT OF COMPRESSIBILITY OF THE MATERIAL ON PLASTIC BUCKLING
J. Aero, Sci., Vol. 18, 1951

12. Pearson, G. E.
BIFURCATION CRITERION AND PLASTIC BUCKLING OF PLATES AND COLUMNS
J. Aero, Sci. Vol. 17, 1950

248.13
(8)

13. Haaijer, G.
PLATE BUCKLING IN THE STRAIN-HARDENING RANGE
Proc. ASCE, 83 (EM2), April, 1957

14. Haaijer, G. and Thürlimann, B.
ON INELASTIC BUCKLING IN STEEL
Proc. ASCE, 84 (EM2), April, 1958

15. Yoshiki, M. Fujita, Y. and Kawai, T.
INFLUENCE OF RESIDUAL STRESSES ON THE BUCKLING OF PLATES
Jour. Soc. of Naval Arch. of Japan, Vol. 107, 1960
(Japanese with English Abstract)

16. Ueda, Y.
ELASTIC, ELASTIC-PLASTIC AND PLASTIC BUCKLING OF PLATES WITH RESIDUAL STRESSES, Ph.D. Dissertation, Lehigh University, 1961

17. Nishino, F.
BUCKLING STRENGTH OF COLUMNS AND THEIR COMPONENTS PLATES
Fritz Laboratory Report 290.10, Lehigh University, 1964

18. Timoshenko, S.
UBER DIE STABILITÄT VERSTEIFTER PLATTEN
Der Eisenbau, Vol. 12, 1921

19. Chwalla, E.
DAS ALLGEMEINE STABILITÄTSPROBLEM DER GEDRÜCKTEN, DURCH RANDWINKEL VERSTÄRKTEN PLATTE,
Ingenieur Archiv., Vol. 5, 1934

20. Gerard, G.
HANDBOOK OF STRUCTURAL STABILITY. PART V - COMPRESSIVE STRENGTH OF FLAT STIFFENED PLATE
NACA T.N. 3785, 1957

21. Kusuda, T.
BUCKLING OF STIFFENED PANELS IN ELASTIC AND STRAIN-HARDENING RANGE
Rep. of Transportation Tech. Research Inst. No. 39, October, 1959

22. Levy, S., Goldenberg, D. and Zibritosky, G.
SIMPLY SUPPORTED LONG RECTANGULAR PLATE UNDER COMBINED AXIAL LOAD AND NORMAL PRESSURE
NACA T.N. 949, 1944

23. Corrick, J. N. and Levy, S.
CLAMPED LONG RECTANGULAR PLATE UNDER COMBINED AXIAL LOAD AND NORMAL PRESSURE
NACA T.N. 1047, 1946

24. McPherson, A. E., Levy, S. and Zibritosky, G.
EFFECT OF NORMAL PRESSURE ON STRENGTH OF AXIALLY LOADED SHEET-STRINGER PANELS
NACA T.N. 1041, 1946

25. Gerard, G.
HANDBOOK OF STRUCTURAL STABILITY PART IV- FAILURE OF PLATES AND COMPOSITE ELEMENTS
NACA T.N. 3784, 1957

26. Jombock, J. R. and Clark, J. W.
POSTBUCKLING BEHAVIOR OF FLAT PLATES
Trans. ASCE, Vol. 127, Part II, 1962

27. Schuman, L. and Beck, G.
STRENGTH OF RECTANGULAR FLAT PLATES UNDER EDGE COMPRESSION
NACA T.R. 356, 1930

28. von Karman, T., Sechler, E. E. and Donnell, L. H.
THE STRENGTH OF THIN PLATES IN COMPRESSION
Trans. ASME, Vol. 54, 1932

29. Frankland, J. M.
THE STRENGTH OF SHIP PLATING UNDER EDGE COMPRESSION
David Taylor Model Basin Report 469, 1940

30. Stowell, E. Z., Heimerl, G. J., Libove, C. and Lundquist, E. E.
BUCKLING STRESSES FOR FLAT PLATES AND SECTIONS
Trans. ASCE, Vol. 117, 1952

31. Vasta, J.
THE ULTIMATE AND CRITICAL COMPRESSIVE STRENGTH OF TEE STIFFENERS
United States Experimental Model Basin Report No. 445, February, 1938

32. Vasta, J.
COMPRESSION TESTS OF SHIP-STRUCTURE ASSEMBLIES
United States Experimental Model Basin Report No. 452, June, 1938

33. Bengston, H. W.
SHIP PLATING UNDER COMPRESSION AND HYDROSTATIC PRESSURE
Trans. SNAME, Vol. 47, 1939

34. Lee, T. T.
ELASTIC-PLASTIC ANALYSIS OF SIMPLY SUPPORTED LECTANGULAR PLATES UNDER COMBINED AXIAL AND LATERAL LOADING
Fritz Laboratory Report 248.7, Lehigh University, 1961

35. Vasta, J.
LESSONS LEARNED FROM FULL SCALE SHIP STRUCTURAL TESTS
Trans. SNAME, Vol. 66, 1958

36. Ostapenko, A. and Lee, T. T.
TESTS ON LONGITUDINALLY STIFFENED PLATE PANELS SUBJECTED TO LATERAL AND AXIAL LOADING
Fritz Laboratory Report 248.4, Lehigh University, 1960

37. Rampetsriter, R. H., Lee, T. T. and Ostapenko, A.
TESTS ON LONGITUDINALLY STIFFENED PLATE PANELS
Fritz Laboratory Report 248.5, Lehigh University, 1962

38. Kondo, J. and Ostapenko, A.
TESTS ON LONGITUDINALLY STIFFENED PLATE PANELS WITH FIXED ENDS
Fritz Laboratory Report 248.12, Lehigh University, 1964

39. Terazawa, K., Yagi, J. and Yasukawa, W.
ON THE ELASTIC BENDING OF PARALLEL INVERTED ANGLES WITH PLATING
Journal of the Soc. of Naval Arch. of Japan, Vol. 112, 1962
(Japanese with English Abstract)

40. Young, D. H.
RATIONAL DESIGN OF STEEL COLUMNS
Trans. ASCE, Vol. 101, 1936

41. von Kármán, T.
UNTERSUCHEN ÜBER KNICKFESTIGKEIT
Mitteilungen über Forschungsarbeiten auf dem Gebiete des Ingenieurwesens No. 81, 1910

42. Chwalla, E.
DER EINFLUSS DER QUERSCHNITTSFORM AUF DAS TRAGVERMÖGEN AUSSERMITTIG GEDRÜCKTER BAUSTAHLSTÄBE
Der Stahlbau, Vol. 8, 1935

43. Baker, J. F., Horne, M. R., and Roderick, J. W.
THE BEHAVIOR OF CONTINUOUS STANCHIONS
Proc. of the Royal Soc. of London, Series A, Vol. 198, 1949

44. Ježek, K.
DIE TRAGFÄHIGKEIT DES EXENTRISCH BEANSPRUCHTEN UND DES QUERBELASTETEN DRUCKSTABES AUS EINEM IDEAL PLASTISCHEN MATERIAL
Sitzungsberichte der Akademie der Wissenschaften in Wein, Abt. IIa, Vol. 143, 1934

45. Ježek, K.
DIE TRAGFÄHIGKEIT DES GLEICHMÄSSIG QUERBELASTETEN DRUCKSTABES AUS IDEAL-PLASTISCHEN STAHL
Der Bautechnik, Vol. 5, 1935

46. Ketter, R. L., Kaminsky, E. L. and Beedle, L. S.
PLASTIC DEFORMATION OF WIDE-FLANGE BEAM COLUMNS
Trans. ASCE, Vol. 120, 1955

47. Roš, M.
DIE BEMESSUNG ZENTRISCH UND EXZENTRISCH GEDRÜCKTER STÄBE AUF KNICKUNG
Rept. 2nd Internat. Cong. Bridge and Structural Eng., Vienna, 1928

48. Ježek, K.
NÄHERUNGSBERECHNUNG DER TRAGKRAFT EXEZENTRISCH GEDRÜCKTER STAHLSTÄBE
Der Stahlbau, Vol. 8, 1935

49. Ketter, R. L.
STABILITY OF BEAM COLUMNS ABOVE THE ELASTIC LIMIT
Proc. ASCE, Vol. 81, Separate No. 692, 1955

50. Westergaard, H. M., and Osgood, W. R.
STRENGTH OF COLUMNS
Trans. ASME, Vols. 49, 50, APM-50-9, 1928

51. Clark, J. W.
PLASTIC BUCKLING OF ECCENTRICALLY LOADED ALUMINUM ALLOY COLUMNS
Proc. ASCE, Vol. 79, Separate No. 299, 1953

52. Chwalla, E.
THEORIE DES AUSSERMITTIG GEDRÜCKTEN STABES AUS BAUSTAHL
Die Bautechnik, Vol. 7, 1934

53. Chwalla, E.
AUSSERMITTIG GEDRÜCKTE BAUSTAHLSTÄBE MIT EINGESPANNTEN ENDEN UND VERSCHIEDEN GROSSEN ANGRIFFSHEBELN
Die Bautechnik, 1937, Vol. 10

54. Ojalvo, M.
RESTRAINED COLUMNS
Proc., ASCE, 86 (EM5) October, 1960

55. Levi, V. and Driscoll, G. C. Jr.
RESPONSE OF COLUMNS TO IN-PLANE LOADING
Fritz Laboratory Report 237.10, Lehigh University, 1963

56. Ojalvo, M. and Fukumoto, Y.
NOMOGRAPHS FOR THE SOLUTION OF BEAM-COLUMN PROBLEMS
Weld. Res. Council Bull. 78, June 1962

57. Fukumoto, Y.
MOMENT-CURVATURE-THRUST PROGRAM FOR WIDE-FLANGE SHAPES
Fritz Laboratory Report 205A.37, Lehigh University, 1963

58. Birnstiel, C. and Michalos, J.
ULTIMATE LOAD OF H-COLUMNS UNDER BIAXIAL BENDING
Proc. ASCE 89 (ST2), April 1963

59. Johnston, B. G. and Opila, F.
COMPRESSION AND TENSION TESTS OF STRUCTURAL ALLOYS
Proc. ASTM Vol. 41, 1941

60. Collins, L. W. and Dolan, T. J.
PHYSICAL PROPERTIES OF FOUR LOW-ALLOY HIGH STRENGTH STEELS
Proc. ASTM, Vol. 38, Part II, 1938

61. Rampetsreiter, R. H.
COMPRESSIVE PROPERTIES OF THIN STEEL COUPONS
Fritz Laboratory Report 248.10, Lehigh University, 1962

62. Griffiths, G. H. R.
RESIDUAL STRESSES IN BUTT-WELDED STEEL PLATES
The Welding Journal, Vol. 20, September 1941

63. Cordovi, M. A.
BEHAVIOUR OF RESIDUAL STRESSES UNDER EXTERNAL LOAD AND THEIR EFFECT ON STRENGTH OF WELDED STRUCTURES
(by Acad. E. O. Patton, Prof. B. M. Gorbounov and Ing. D. O. Bershtein, Ukranian Academy of Sciences, Kiev 1937, translated and abstracted from Russian literature) The Welding Journal, Vol. 23, September 1944

64. Wilson, W. W. and Hao, G. C.
RESIDUAL STRESSES IN WELDED STRUCTURES
Bulletin No. 361, University of Illinois, February, 1946

65. Nagaraja Rao, N. R. and Tall, L.
RESIDUAL STRESSES IN WELDED PLATES
Fritz Laboratory Report 249.7, Lehigh University, 1960

66. FINAL REPORT OF A BOARD OF INVESTIGATION TO INQUIRE INTO THE DESIGN AND METHODS OF CONSTRUCTION OF WELDED STEEL MERCHANT VESSELS
Government Printing Office, Washington, 1947

67. Osgood, W. R.
RESIDUAL STRESSES IN METALS AND METAL CONSTRUCTION
Reinhold Publishing Corporation, New York, 1954

68. Beedle, L. S. and Tall, L.
BASIC COLUMN STRENGTH
Proc. ASCE 86 (ST7), July 1960

69. Feder, D. and Lee, G. C.
RESIDUAL STRESS AND THE STRENGTH OF MEMBERS OF HIGH STRENGTH STEEL
Fritz Laboratory Report 269.2, Lehigh University, 1959

70. Newmark, N. M.
NUMERICAL PROCEDURES FOR COMPUTING DEFLECTIONS, MOMENTS AND BUCKLING LOADS
Trans. ASCE Vol. 108, 1943

71. Hoffmann, G. H.
THE EFFECTIVE I OF H.M.S. WOLF
Trans. INA, Vol. 70, 1928

72. Kell, C. O.
INVESTIGATION OF STRUCTURAL CHARACTERISTICS OF DESTROYERS PRESTON AND BRUCE
Trans. SNAME, Vol. 39, 1931

73. SPECIFICATION FOR THE DESIGN, FABRICATION AND ERECTION OF STRUCTURAL STEEL FOR BUILDINGS
AISC, April 1963

74. McDonald, J. H. and MacNaught, D. F.
INVESTIGATION OF CARGO DISTRIBUTION IN TANK VESSELS
Trans. SNAME, Vol. 57, 1949

75. de Luce, H. and Budd, W. I. H.
THE DESIGN OF A CLASS OF 28,000-TON TANKERS;
Trans. SNAME, Vol. 58, 1950

76. General Electric Company
GE225 WIZ SYSTEM REFERENCE MANUAL
General Electric, Computer Department, Phoenix, Arizona

9. NOMENCLATURE

A	area of the cross section
A_{st}	area of the cross section of the stiffener
A_f	area of the cross section of the stiffener flange
A_b	cross-sectional area per unit width
A_e	area of elastic core of the cross section
A_{pc}	area of the part of the cross section yielded in compression
A_{pt}	area of the part of the cross section yielded in tension
$A_{bt} = \frac{A}{bt}$	
$a = \frac{\bar{p}}{\bar{L}}$	
B	breadth of a ship
$B_{rt} = \frac{b_{rt}}{b}$	
b	spacing of the stiffener
b_f	width of stiffener flange
b_{rt}	width of tensile residual stress zone in the plate
b_{rc}	width of compressive residual stress zone in the plate
D_h	depth of hull
$D_1 = \frac{d_1}{t}$	
$D_2 = \frac{d_2}{t}$	
d	depth of a stiffener
d_1	distance from elastic neutral axis to the extreme fibre in the plate

d_2 distance from elastic neutral axis to the extreme fibre in the stiffener flange

E modulus of elasticity

$G_1 = \frac{\epsilon_1}{\epsilon_{yp}}$

$G_{st} = \frac{\sigma_{st}}{\sigma_{yp}}$

$G_{rc} = \frac{\sigma_{rc}}{\sigma_{yp}}$

$G_{fc} = \frac{\sigma_{ft}}{\sigma_{yp}}$

$H = \frac{h}{\sigma_{yp} A}$

H_s depth of fluid cargo in the tank

H resultant force acting on the cross section in z-direction

I moment of inertia of the cross section

I_e moment of inertia of the elastic core of the cross section

J_q modification factor for lateral load

J_e modification factor for end restraint

K_r modification factor for residual stress

K_α modification factor for stiffener area ratio

K_β modification factor for stiffener flange area ratio

$L = \frac{\sigma_{yp}}{E} \frac{\ell}{r}$

$\bar{L} = \frac{\sigma_{yp}}{E} \frac{\ell}{t}$

$L.F.$ load factor

ℓ length of a longitudinally stiffened plate panel

M bending moment

M_{hog} hogging moment

M_{sag} sagging moment

M_{np} full plastic moment of the cross section in positive bending

M_{nn} full plastic moment of the cross section in negative bending

$$m = \frac{M}{\sigma_{yp} S}$$

$$m_{np} = \frac{M_{np}}{\sigma_{yp} S}$$

N axial thrust

N^o axial thrust acting at mid-span

$$n = \frac{N}{\sigma_{yp} A}$$

$$n^o = \frac{N^o}{\sigma_{yp} A}$$

P external axial load

P_c external compressive axial load

P_t external tensile axial load

P_{cr} elastic column buckling load

$\overline{P}_{cr}$ inelastic column buckling load

$$P_y = \sigma_{yp} A$$

$$p = \frac{P}{P_y}$$

$$\overline{p} = \frac{P_c}{\sigma_{yp} Bt}$$

$$Q = \frac{\mathfrak{E} b d_2}{\sigma_{yp}^2 A}$$

$\overline{Q} = \frac{qE}{\sigma_{yp}2}$

q hydrostatic pressure

r radius of gyration of the cross section

$R = \frac{r}{t}$

S section modulus for the stiffener flange

$S_{bt} = \frac{S}{bt^2}$

S_s gradient of a structure load-deflection curve

S_f gradient of a loading system load-deflection curve

ds_p length of the outer surface of the plate corresponding to part of the centrodial axis with length ds

Δs a segmental length of the centroidal axis in the stepwise integration

t thickness of the plate

t_f thickness of the stiffener flange

$v = \frac{Vd_2}{\sigma_{yp}Ar}\sqrt{\frac{E}{\sigma_{yp}}}$

V resultant force acting on the cross section in y-direction

w thickness of the stiffener web

$Y = \frac{y}{r}$

y lateral deflection

$Z = \frac{z}{r}\sqrt{\frac{\sigma_{yp}}{E}}$

z distance between loading ends

α stiffener area ratio

γ	ratio of the stiffener depth to the thickness of the plate
γ_w	unit weight of water
γ_c	unit weight of cargo
ϵ	strain
ϵ_1	strain at the outer surface of the plate
ϵ_2	strain in the stiffener flange
ϵ_c	strain at the centroid
ϵ_y	yield strain
ϵ_{yt}	tensile yield strain
ϵ_{yc}	compressive yield strain
$\bar{\epsilon}_{yt}$	effective tensile yield strain
$\bar{\epsilon}_{yc}$	effective compressive yield strain
$\epsilon_{yp} = \frac{\sigma_{yp}}{E}$	
$\epsilon_{st} = \frac{\sigma_{st}}{E}$	
ϵ_r	residual strain
$\epsilon_{rc} = \frac{\sigma_{rc}}{E}$	
$\epsilon_{fc} = \frac{\sigma_{fc}}{E}$	
$\epsilon_{ft} = \frac{\sigma_{ft}}{E}$	
ϵ_{pi1}	plastic strain at the lowest fiber of the i-th sub-area
ϵ_{pi2}	plastic strain at the upper most fiber of the i-th sub-area

η	distance from the elastic neutral axis
η_{1i1}	distance from the outer surface of the plate to the lowest fiber of the i-th sub-area
η_{1i2}	distance from the outer surface of the plate to the upper most fiber of the i-th sub-area
$\bar{\eta}_{np}$	distance from the elastic neutral axis to the neutral axis of fully plastified cross section in positive bending
$\bar{\eta}_{nn}$	distance from the elastic neutral axis to the neutral axis of fully plastified cross section in negative bending.
θ	slope
σ	stress
σ_{yp}	yield stress of the plate
σ_{st}	yield stress of the stiffener
σ_{rc}	compressive residual stress in the plate
σ_{fc}	residual stress at the stiffener flange tip
σ_{ft}	residual stress at the center of the stiffener flange
$\Phi = \frac{\phi}{\phi_y}$	
$\Phi^o = \frac{\phi^o}{\phi_y}$	
ϕ	curvature
ϕ^o	curvature at mid-span
$\phi_y = \frac{\sigma_{yp}}{Ed_2}$	

10. APPENDICES

10.1 MOMENT-CURVATURE-THRUST RELATIONSHIP

Geometric Constants

Geometric constants included in Eqs. 3.24 and 3.25 are

$$\frac{d_1}{d_2},\ \frac{d_2}{t},\ \frac{bd_2}{A},\ \frac{Ad_2}{S},\ \frac{btd_2}{S},\ \frac{b_{rt}}{b},\ \frac{b_{rc}}{b},\ \frac{w}{t},\ \frac{A_f}{bd_2},\ \frac{d+t}{t},\ \frac{d}{t}\ .$$

Among them, $\frac{b_{rt}}{b}$ and $\frac{b_{rc}}{b}$ are defined by the residual stress distribution.

$$\frac{b_{rt}}{b} = B_{rt}$$

$$\frac{b_{rc}}{b} = 1-B_{rt} \qquad (10.1)$$

The rest of the geometric constants are expressed by the algebraic combinations of non-dimensionlized geometric parameters, $\alpha = \frac{A_{st}}{bt}$, $\beta = \frac{A_f}{A_{st}}$ and $\gamma = \frac{d}{t}$. Using geometric parameters, α, β, and γ, one can express all sub-sectional sreas, and lengths parallel and perpendicular to the stiffener web are given as linear functions of bt, t and b, respectively.

$$A = (1+\alpha)bt$$

$$A_{st} = \alpha bt \qquad (10.2)$$

$$A_f = \alpha\beta\, bt$$

$$d = \gamma t$$

$$d_2 = \frac{\frac{1}{2} + \gamma - \frac{1}{2}\alpha(1-\beta)\gamma}{1 + \alpha} \tag{10.3}$$

$$d_1 = (1 + \gamma - \frac{\frac{1}{2}\alpha(1-\beta)\gamma}{1 + \alpha})t$$

$$w = \frac{\alpha(1 - \beta)}{\gamma} b \tag{10.4}$$

Using these same parameters, the section modulus for the stiffener flange S becomes a linear function of bt^2:

$$S = \frac{(\frac{1}{12} + (\frac{1}{2} - \gamma)^2 + \frac{\alpha(1-\beta)\gamma^2}{3} - (1 - \alpha)\gamma^2)\ (1 + \alpha)bt^2}{\frac{1}{2} + \gamma + \frac{1}{2}\alpha(1 - \beta)\gamma} \tag{10.5}$$

Then, the section modulus, the cross-sectional area and the basic linear dimensions are non-dimensionalized to:

$$S_{bt} = \frac{S}{bt^2} = \frac{(\frac{1}{12} + (\frac{1}{2} + \gamma)^2 + \frac{\alpha(1 - \beta)\gamma^2}{3} - (1 - \alpha)\gamma^2)\ (1 + \alpha)}{\frac{1}{2} + \gamma + \frac{1}{2}\alpha(1 - \beta)\gamma}$$

$$A_{bt} = \frac{A}{bt} = 1 + \alpha$$

$$D_1 = \frac{d_1}{t} = 1 + \gamma - \frac{\frac{1}{2} + \gamma - \frac{1}{2}\alpha(1 - \beta)\gamma}{1 + \alpha} \tag{10.6}$$

$$D_2 = \frac{d_2}{t} = \frac{\frac{1}{2} + \gamma - \frac{1}{2}\alpha(1 - \beta)\gamma}{1 + \alpha}$$

By Eqs. 10.1 through 10.6, all geometric constants are obtained in terms of α, β, γ, and B_{rt} only.

$$\frac{d_1}{d_2} = \frac{D_1}{D_2}$$

$$\frac{bd_2}{A} = \frac{D_2}{A_{bt}}$$

$$\frac{Ad_2}{S} = \frac{A_{bt} D_2}{S_{bt}}$$

$$\frac{btd_2}{S} = \frac{D_2}{S_{bt}}$$

$$\frac{w}{b} = \frac{\alpha(1 - \beta)}{\gamma} \tag{10.7}$$

$$\frac{A_f}{bd_2} = \frac{\alpha\beta}{D_2}$$

$$\frac{d - t}{t} = 1 + \gamma$$

$$\frac{d}{t} = \gamma$$

Using Eqs. 10.7, Eqs. 3.24 and 3.25 become:

$$n = (G_1 \frac{D_1}{D_2} \Phi) - \frac{D_2}{2\Phi A_{bt}} \sum_{j=1}^{8} (C_{j1}(G_1 - C_{j2})^2) \tag{10.8}$$

$$m = \Phi + (G_1 \frac{D_1}{D_2} \Phi - n) \frac{A_{bt} D_2}{S_{bt}}$$

$$- \frac{D_2}{2\Phi S_{bt}} \sum_{j=1}^{6} (C_{j1}(G_1 - C_{j2})^2 (C_{j3} - \frac{G_1 - C_{j2}}{\Phi} \frac{D_2}{3}) \tag{10.9}$$

Equation 10.8 can be further rearranged as a quadratic function of G_1:

$$AG_1^2 - 2BG_1 - C = 0 \qquad (10.10)$$

where

$$A = \sum_{j=1}^{8} C_{j1}$$

$$B = \frac{\Phi}{D_2} A_{bt} + \sum_{j=1}^{8} C_{j1}C_{j2}$$

$$C = -2 \frac{\Phi}{D_2} A_{bt}(n + \frac{\Phi}{D_2})D_1) + \sum_{j=1}^{8} C_{j1}C_{j2}^2$$

Selection of G_1

Coefficients C_j are dependent on the yield configuration. The yield configuration is defined by Φ and G_1. When the true yield configuration corresponding to a set of Φ_1 and n values is known, the yield configuration corresponding to a slightly increased curvature Φ_2 ($\Phi_2 = \Phi_1 + \delta\Phi$) would be (1) the same, or (2) slightly different.

(1) When the yield configuration is the same, the correct set of coefficents is obtained by assuming G_1 to be equal to that for Φ_1 ($G_a = G_1$). The true value of G_c is given by solving 10.10.

(2) When the yield configuration is different, the coefficients obtained under the above mentioned assumption are not correct. However, the solution of Eq. 10.10 with such incorrect coefficients gives G_c somewhat larger than G_a due to an increase in Φ. By using G_c, a new set of

coefficients are obtained and the same procedure is repeated until the correct yield configuration is achieved, that is when G_c equals G_a.

If the selected coefficients are not correct, it is possible that equation 10.10 does not have real roots. In such a case, the assumed G_a is increased by a small amount δG and the whole procedure is repeated.

The above procedure can be used if G_1 is derived for a decreased curvature by taking negative values for $\delta\Phi$ and δG.

In numerical computation, the first set of $\Phi - G_1 -$ m values is computed for the elastic limit, that it, for Φ at the first yield. The values of Φ are given by the following formulas:

Positive bending, $\Phi_{90} = n + G_{st} + G_{ft}$

or $\Phi_{90} = (1-G_{rc}-n)\frac{D_2}{D_1}$ (The smaller of the two)

(10.11)

Negative bending, $\Phi_{91} = n - G_{st} + G_{fc}$

or $\Phi_{91} = n\frac{D_2}{D_1}$ (The smaller of the two)

(10.12)

For these Φ's the true G_1 is given by the elastic relationship.

$$G_1 = n + \Phi \frac{D_1}{D_2} \qquad (10.13)$$

When a thrust higher than that given by equation 10.14 is present, the elastic range does not exist, even under a zero bending moment.

$$n = 1 - G_{rc} - \frac{1 - G_{rc} - G_{st} + G_{fc}}{1+\gamma} \frac{D_1}{D_2} \qquad (10.14)$$

For the axial thrust in this range, the first Φ values chosen for convenience are:

$$\Phi_{90} = 0.01$$
$$\Phi_{91} = -0.01 \qquad (10.15)$$

Equation 10.13 does not give the true G_1 for a Φ given by Eq. 10.15 but by the successive approximation method discussed, a satisfactory result can be obtained.

Increment of Curvature $\delta\Phi$

The m - Φ curve for a specified n consists of three kinds of curves. In the elastic range, the m - Φ curve is a straight line. For large $|\Phi|$ values, the m - Φ curve is a nearly straight curve asymptotically approaching the straight line $m = m_{np}$ or $m = m_{nn}$. The third kind is a curved portion connecting the straight line and nearly straight curve. The computation of the moment-curvature-thrust relationship is to be made with sufficient number of points to represent the complete m - Φ curve. An intermediate point between two computed points can be estimated by an appropriate interpolation. In the numerical integration described in Chapter 4, the linear interpolation was adopted for its simplicity. The increment which

gives the required accuracy varies in accordance with $\frac{d^2m}{d\Phi^2}$ at the location on the m - Φ curve. In a nearly straight part of the curve, larger increments can be used than in the curved part. Moreover, it is desirable to use the maximum permissible increment at each point to cover a significant portion of M - Φ curve with a limited number of points. In the elastic range, the maximum and minimum elastic limit values of m and Φ give the correct intermediate values by linear interpolation. In the inelastic range, three predetermined values of increment were used.

$$\delta\Phi = 0.02,\ 0.1 \text{ and } 0.5 \qquad (10.16)$$

After the evaluation of each moment m, the appropriateness of the increment used was checked against the possible error. The difference between the computed moment for Φ_n and the estimated moment by the extrapolation of m_{n-2} and m_{n-1} is given by:

$$E_r = m_{n-z} + (m_{n-1} - m_{n-2}) \frac{\delta\Phi n}{\delta\Phi_{n-1}} - m_n \qquad (10.17)$$

where $\delta\Phi_n = \Phi_n - \Phi_{n-1}$

$\delta\Phi_{n-1} = \Phi_{n-1} - \Phi_{n-2}$

The increment of Φ which satisfied the following condition was selected.

$$0.001 > \left|\frac{E_r}{m_n}\right| > 0.000015 \qquad (10.18)$$

If $\left|\frac{E_r}{m_n}\right|$ was larger than 0.001, the increment was changed to the next smaller value and Φ_n and m_n were recomputed. If $\left|\frac{E_r}{m_n}\right|$ was smaller than

0.000015, a larger increment might be used without losing accuracy. Φ_n was reassigned with a larger increment $\delta\Phi_n$. The recomputation and check was made for m_n until condition 10.18 was satisfied.

$\left|\frac{E_r}{m_n}\right|$ is not a relative error of linear interpolation over the span of $\delta\Phi$, but an error of linear extrapolation over the span of $(\delta\Phi_{n-1} + \delta\Phi_n)$. Since a linear interpolation was used over the span of $\delta\Phi$ in the numerical integration, the error included can be expected to be much less than 0.1%.

10.2 STEPWISE INTEGRATION AND DETERMINATION OF ULTIMATE STRENGTH

A numerical method for determination of ultimate strength described in Art. 4.2 was programmed in WIZ language[76] for a digital computer, G.E. 225. Its flow diagram is shown in Fig. 10.2. Before the start of the numerical integration, a moment-curvature-thrust relationship was computed for a given set of cross-sectional dimensions α, β, γ, material properties G_{st}, residual stresses G_{rc}, G_{fc}, G_{ft} and the axial thrust n. The moment-curvature-thrust relationship was then stored in the computer memory by means of labeled arrays in Φ, m and G in reverse order of the magnitude of curvature. In this article, subscript i designates the i-th location in the array.

In view of the limited storage space in the computer memory, the number of variables used in the determination of the ultimate strength was kept minimum by taking advantage of repetitive procedures.

Superscripts P and F are used to designate pinned and fixed-end conditions, respectively.

Initial Values

To commence the stepwise integration, the curvature at mid-span of the stiffened panel must be assumed. Since it was found that the plate panel fails after full plastification of either the plate or the stiffener flange, the first value of the curvature at mid-span Φ^o was assumed in the following manner:

$$\Phi^0 = \Phi_i - 0.4 \tag{10.19}$$

where Φ_i is the largest stored curvature which satisfies either one of the following two conditions

$$\begin{aligned} &G_i B_{rt} - (1 - G_{rc}) B_{rc} \geq 1 \\ &G_i - \Phi_i \frac{1 + \nu}{D_2} + G_{st} \leq 0 \end{aligned} \tag{10.20}$$

The initial values in the first segment are determined as follows.

$$\text{Curvature:} \quad \Phi_o = \Phi^o \tag{10.21}$$

$$\text{Moment:} \quad m_o = m_i - \frac{\Phi_i - \Phi_o}{\Phi_i - \Phi_{i+1}} (m_i - m_{i+1}) \tag{10.22}$$

Under the high axial thrust, the moment computed by the equation above could have a negative value. In such a case, Φ^o is increased by 0.1 and Φ_o and m_o are recomputed until m_o becomes positive.

The rest of the initial values are given as follows:

$$\Delta S_1 = \Delta S_t$$

$$L_o = X_o = Y_o = \theta_o = 0$$

$$v_o = 0 \qquad (10.23)$$

$$h_o = n^o$$

$$G_o = G_i - \frac{\Phi_i - \Phi_o}{\Phi_i - \Phi_{i+1}} (G_i - G_{i+1})$$

Computation in the First Segment

First, the final value of curvature in the segment is assumed to be equal to the initial value.

$$\Phi_{1a} = \Phi_o \qquad (10.24)$$

Using this final curvature, the first approximation of the final moment is computed by the following equations:

$$\Delta Z = \cos \theta_o \Delta S_o - (\frac{\Phi_o}{3} + \frac{\Phi_{1a}}{6}) \sin \theta_o (\Delta S_o)^2 \sqrt{\epsilon_{yp}} \frac{R}{D_2}$$

$$\Delta Y = \sin \theta_o \Delta S_o \frac{1}{\sqrt{\epsilon_{yp}}} + (\frac{\Phi_o}{3} + \frac{\Phi_{1a}}{6}) \cos \theta_o (\Delta S_o)^2 \frac{R}{D_2}$$

$$m_1 = m_o - h_o \Delta Y \frac{D_2}{R} - v_o \Delta Z$$
$$-Q \left[\tfrac{1}{2}(\Delta Y)^2 \epsilon_{yp} + \tfrac{1}{2}(\Delta Z)^2 - \cos \theta_o \Delta_y \frac{D_1}{R} \epsilon_{yp} + \sin \theta_o \right.$$
$$\left. \Delta Z \frac{D_1}{R} \sqrt{\epsilon_{yp}}\right] \qquad (10.25)$$

The final curvature and strain corresponding to m_1 are evaluated by one of the following equations depending on the magnitude

of moment m_1:

$$\text{If } m_i > m_1 > m_{i+1} \quad (i = 0,1,2\ldots,199),$$

$$\Phi_{1c} = \Phi_i - \frac{m_i - m_1}{m_i - m_{i+1}} (\Phi_i - \Phi_{i+1}) \tag{10.26}$$

$$G_1 = G_i - \frac{m_i - m_1}{m_1 - m_{i+1}} (G_i - G_{i+1}$$

$$\text{If } m_{200} > m_1 > m_{nn},$$

$$\Phi_{1c} = \left(1 + \frac{m_{200} - m_{nn}}{m_1 - m_{nn}}\right) \Phi_{200} - \sqrt{\frac{\Phi_{200}(\Phi_{200} - \Phi_{199})(M_{200} - M_{nn})}{M_{199} - M_{200}}} \tag{10.27}$$

$$G_1 = \left(1 + \frac{M_{200} - M_{nn}}{M_1 - M_{nn}}\right) G_{200} - \sqrt{\frac{G_{200}(G_{200} - G_{199})(M_{200} - M_{nn})}{M_{199} - M_{200}}}$$

$$\text{If } m_{nn} > m_1,$$

segmental length is reduced to,

$$\Delta S_1 = \tfrac{1}{2} \frac{m_o - m_{nn}}{m_o - m_1} \Delta S_1 \tag{10.28}$$

and m_1 is recomputed by Eq. 10.25

The appropriateness of the assumed curvature Φ_{1a} is checked against the following condition.

$$\left| \frac{\Phi_{1c} - \Phi_{1a}}{\Phi_{1c}} \right| < 0.00001 \tag{10.29}$$

If the relative difference between Φ_{1a} and Φ_{1c} is greater than 10^{-5}, a new Φ_{1a} is assumed to be equal to Φ_{1c},

$$\Phi_{1a} = \Phi_{1c} \tag{10.30}$$

and ΔZ, ΔY, m_1, Φ_{1c} and G_1 are recomputed. If the inequality 10.29 is satisfied, the curvature in the segment is established and the rest of the final values are evaluated as follows:

$$\begin{aligned}
\Phi_1 &= \Phi_{1c} \\
\theta_1 &= \theta_o + \tfrac{1}{2}(\Phi_o + \Phi_1)\frac{R}{D_2}\Delta S_o\sqrt{\epsilon_{yp}} \\
h_1 &= h_o + Q\left[\Delta Y\frac{R}{D_2} + (\cos\theta_1 - \cos\theta_o)\frac{D_1}{D_2}\right]\epsilon_{yp} \\
v_1 &= v_o + Q\left[\Delta Z - (\sin\theta_1 - \sin\theta_o)\frac{D_1}{R}\sqrt{\epsilon_{yp}}\right] \\
Y_1 &= Y_o + \Delta Y \\
Z_1 &= Z_o + \Delta Z \\
L_1 &= L_o + \frac{2\Delta S_o}{2 - \left[G_o + G_1 - (\Phi_o + \Phi_1)\frac{D_1}{D_2}\right]\epsilon_{yp}}
\end{aligned} \tag{10.31}$$

At the completion of the computations in each segment, the final values are tested against the end conditions described in the following section. If the end conditions are not yet satisfied, the integration over the next segment is carried out with the same procedure using the final values of the present segment as initial values.

End Conditions

Two end conditions are considered in the program.

$$\begin{aligned} &\text{Pinned End:} \quad m = 0 \\ &\text{Fixed End :} \quad \theta = 0 \end{aligned} \tag{10.32}$$

Final moment or slope in a segment (m_j or θ_j) does not generally become zero. Since moment and slope are taken to be positive in the middle portion of the stiffened plate panel, the first negative m_j (or θ_j) indicates the presence of the end of the panel in the segment.

$$\begin{aligned} &\text{Pinned End:} \quad m_j < 0 \\ &\text{Fixed End :} \quad \theta_j < 0 \end{aligned} \tag{10.33}$$

In this case the segment can be divided into two parts: the one inside of the end of the stiffened plate panel and the other outside. The length ds of the centroidal axis of that part of the segment within the panel is computed assuming the variation of moment (or slope) to be parabolic.

For Pinned End:

$$\begin{aligned} &((m_j - m_j)\Delta S_{j-1} + (m_{j-2} - m_{j-1})\Delta S_j)(dS)^2 \\ &+((m_{j-2} - m_{j-1})(\Delta S_j)^2 - (m_j - m_{j-1})(\Delta S_{j-1})^2)(dS) \\ &+ \Delta S_j \Delta S_{j-1}(\Delta S_j - \Delta S_{j-1}) = 0 \end{aligned} \tag{10.34}$$

The length dS is determined by solving the quadratic equation above by Newton's method. The corresponding variables representing the deflected configuration of the stiffened panel are computed again

assuming the parabolic variation.

$$L_k^p \frac{(L_j-L_{j-1})\Delta S_{j-1}+(L_{j-2}-L_{j-1})\Delta S_j}{\Delta S_j \Delta S_{j-1}(\Delta S_j+\Delta S_{j-1})}(dS)^2 + \frac{(L_j-L_{j-1})(\Delta S_{j-1})^2-(L_{j-2}-L_{j-1})(\Delta S_j)^2}{\Delta S_j \Delta S_{j-1}(\Delta S_j-\Delta S_{j-1}} (dS)+L_{j-1} \quad (10.35)$$

Rest of variables Z_k^p, Y_k^p, θ_k^p are evaluated with Eq. 10.35 by replacing (L_j, L_{j-1}, L_{j-2}) with (Z_j, Z_{j-1}, Z_{j-2}), (Y_j, Y_{j-1}, Y_{j-2}), and $(\theta_j, \theta_{j-1}, \theta_{j-2})$, respectively.

For Fixed End:

The length dS is determined by solving the following equation:

$$[(\theta_j-\theta_{j-1})\Delta S_{j-1}+(\theta_{j-1}-\theta_{j-1})\Delta S_j](dS)^2 + [(\theta_{j-2}-\theta_{j-1})(\Delta S_{j-1})^2 - (\theta_j-\theta_{j-1})(\Delta S_{j-1})^2](dS) \quad (10.36)$$
$$+ \Delta S_j \Delta S_{j-1}(\Delta S_j + \Delta S_{j-1}) = 0$$

Panel length L_K^F chord length Z_K^F, deflection Y_K^F and fixed end moment M_K^F are evaluated by equations similar to Eq. 10.35.

At the completion of the stepwise integration for each assumed curvature at mid-span Φ^o, computed panel lengths are checked with the ultimate condition. If the ultimate condition is not yet reached, the curvature at mid-span is increased by small increment Φ_{inc} and the stepwise integration is repeated.

Ultimate Condition

The ultimate condition is defined by the zero slope on the panel length-deflection curve.

$$\left(\frac{dL}{d\Phi^o}\right)_{n^o = \text{const}} = 0 \qquad (4.26)$$

In numerical computation, the realization of this condition is detected by the reduction of the computed panel length in the consecutive integrations.

$$\begin{aligned} &\text{Pinned End:} \quad L_K^P < L_{K-1}^P \\ &\text{Fixed End:} \quad L_K^F < L_{K-1}^F \end{aligned} \qquad (10.37)$$

The length of panel which fails at a given set of axial and lateral loads is computed by assuming the panel length-deflection curve to be a 2nd order parabola.

For Pinned End:

$$L^P = L_{K-1}^P - \tfrac{1}{2} \frac{(L_{K-2}^P - L_{K-1}^P)^2}{L_{K-2}^P - 2L_{K-1}^P + L_K^P} \qquad (10.38)$$

The corresponding curvature at mid-span is given by the following equation:

$$\Phi^P = \Phi_K^o - \Phi_{inc} + \tfrac{1}{2} \frac{L_{K-2}^P - L_{K-1}^P}{L_{K-2}^P - 2L_{K-1}^P + L_K^P} \Phi_{inc} \qquad (10.39)$$

The deflection at mid-span Y^P is computed assuming that the deflection at mid-span is a quadratic function of Φ^o

$$Y^P = \frac{Y_K^P - 2Y_{K-1}^P - Y_{K-2}^P}{2\,\Phi_{inc}^2}(d\Phi)^2 + \frac{Y_K^P - Y_{K-2}^P}{2\Phi_{inc}}(d\Phi) + Y_{K-1}^P \qquad (10.40)$$

where,

$$d\Phi = \tfrac{1}{2}\,\frac{L_{K-2}^P - L_{K-1}^P}{L_{K-2}^P - 2L_{K-1}^P + L_K^P}\,\Phi_{inc}$$

Equations for the computation of chord length Z^P, slope at the end θ^P are of identical form to Eq. 10.39 and can be obtained by replacing $(Y_K^P, Y_{K-1}^P, Y_{K-2}^P)$ by $(Z_K^P, Z_{K-1}^P, Z_{K-2}^P)$ and $(\theta_K^P, \theta_{K-1}^P, \theta_{K-2}^P)$, respectively.

For fixed end, the same procedure was carried out. Equations used are identical to Eqs. 10.38, 10.39, and 10.40 except that the superscript P be replaced by a superscript F.

10.3 DESIGN OF BOTTOM PLATE PANEL OF A 28,000 D.W.T. TANKER

As an example, the bottom plate panel of a 28,00 D.W.T. tanker is designed using the design chart given in Chapter 6. Principal dimensions of the tanker are taken from Reference 74.

Length between perpendiculars	595 ft. - 0 in.
Breadth molded	84 ft. - 0 in.
Depth molded	44 ft. - 0 in.
Draft molded	33 ft. - 0 5/8 in.
Displacement	36,346 L. tons
Deadweight	28,081 L. tons

The standard longitudinal bending moments are calculated as follows:[74]

Sag bending moment	635,800 ft-tons
Hog bending moment	253,500 ft-tons

These moments were calculated for a ship subjected to the following conditions: The ship is loaded to deep load draft with all cargo tanks filled with gasoline whose specific gravity is 0.7351. The ship also contains a normal supply of fuel, fresh water, and other items needed to operate a ship. Under this case of loading, the hogging and sagging conditions are assumed to correspond to a ship supported statically on a wave of standard proportions. The length of the wave is assumed equal to the length of the ship. The height of the wave from crest to trough is assumed to be 1/20 of the wave length. The wave crest is assumed amidships for the hogging condition, while for the sagging condition, the wave crests are assumed at the extremities of the ship.

When a cargo with a unit weight greater than 0.7351 is carried by the ship only part of the cargo space needs to be filled in order to

put the vessel down to the designed draft; therefore, it becomes necessary to operate with some empty or partially filled tanks. The longitudinal bending moment varies according to the cargo distribution. Moreover, the standard bending moment can be exceeded by a considerable amount. High hogging moment will result if heavy cargo is disposed in the end tanks with the amidship tanks empty. Similarly, high sagging moment will occur if heavy cargo is disposed in the amidship tanks with the end tanks empty. Since the cargo distribution has an effect on the hogging and sagging bending moments in opposite directions, at least one of the standard bending moments is exceeded under a loading with partially filled tanks. Investigating various cargo distributions, McDonald and MacNaught gave the maximum bending moments under the optimum cargo distributions for the ship under consideration as follows:(74)

Maximum sagging moment	635,800 ft-tons
Maximum hogging moment	445,000 ft-tons

Taking these moments as the basis of design, the axial loads acting on the bottom plate panel are obtained by Eq. 6.1.

$$\text{Axial Tension } P_t = \frac{M_{sag}\ L.F.}{K\ D_h} = \frac{635{,}800 \times 2.2\ L.F.}{44\ K}$$

$$\text{Axial Compression } P_c = \frac{M_{hog}\ L.F.}{K\ D_h} = \frac{445{,}000 \times 2.2 L.F}{44\ K}$$

(10.41)

where coefficient K depends on the type of the hull structure.

In a tanker, the flanges of the hull girder are composed of the

single deck and bottom platings. Since we can neglect the contribution of the side walls and longitudinal bulkheads to the longitudinal bending resistance with reasonable accuracy on the safe side, K = 1 can be used.

The basis for the selection of the load factor (L.F.) is not yet well established in the ultimate strength design of ships. According to the conventional design method, the scantlings of this tanker are determined for the working stress of $8.30^{L.}$ ton/in^2 = 18.59 ksi.(75) Since the hull structure would fail in jack-knifing when either the deck or the bottom plating is plastified, this conventional design is equivalent to the ultimate design with load factor L.F.= $\frac{\sigma_{yp}}{18.59}$. For the material with yield stress of 33 ksi, the load factor becomes,

$$\text{L.F.} = \frac{33}{18.59} = 1.78$$

Using the load factor, L.F. = 1.8, the ultimate axial loads acting on the bottom plate panel are:

$$P_t = \frac{635{,}800 \times 2.2 \times 1.8}{44 \times 1} = 58{,}200_{\text{kips}} \text{(tension)}$$

$$P_c = \frac{445{,}000 \times 2.2 \times 1.8}{44 \times 1} = 40{,}700_{\text{kips}} \text{(compression)}$$

The maximum lateral load acting on the bottom plate panel of an empty tank in still water is

$$q = \gamma_w d_s \text{ L.F.} = \frac{64}{144} \times 33.05 \text{ L.F.} \text{ (upward)}$$

The maximum lateral load is hardly affected by the distribution of the cargo, but it may be influenced by the dynamic effect of waves to a greater extent than the axial load. Since there is no

better basis for the selection of the load factor, L.F. = 1.5 is tentatively used in this example.

$$q = \frac{64}{144} \times 33.05 \times 1.5 = 22.0_{psi} \text{(upward)}$$

The design condition of the bottom plate panel is summarized as follows:

Axial load (tension): P_t = 58,200 kips

Axial load (compression) P_c = 40,700 kips

Lateral load q = 22.0 psi = 0.022 ksi

Breadth of the ship B = 1008 in.

Length of the panel ℓ = 120 in*

Material Properties,

Yield Stress of plate σ_{yp} = 33 ksi*

Yield Stress of stiffeners σ_{st} = 33 ksi(G_{st} = 1)*

Compressive Residual Stress in Plate

$\sigma_{rc} = 1/8\ \sigma_{yp}$ (G_{rc} = 0.125)*

End Restraint Fixed*

Assumed Values*

In order to use the design chart, the design conditions are expressed in terms of $\bar{q}$ and a.

$$\bar{q} = \frac{29{,}600\ q}{\sigma_{yp}^2} = \frac{29{,}600 \times 0.022}{33^2} = 0.6 \qquad (10.42)$$

$$a = \frac{172\ P_c}{B\ell\sqrt{\sigma_{yp}}^3} = \frac{172 \times 40{,}700}{1008 \times 120 \times \sqrt{33}^3} = 0.306$$

The design procedure is as follows:

A straight line is drawn in the fourth quadrant of the design chart, Figure 6.4, passing through the origin and point a = 0.306 on the a-scale. The intersection of this straight line and the $\bar{p}$ $\bar{Q}$ $\bar{L}$ curve for $\bar{Q} = 0.6$ and $\sigma_{rc} = 0.125\ \sigma_{yp}$ gives the solution ($\bar{P}_f = \bar{p} = 1.170$) for the standard section ($\alpha = 0.3$, $\beta = 0.45$, $\gamma = 10$). Using the modification charts (Figure 6.4) one can obtain values of $\bar{P}_f$ for various cross sections as described in Article 6.2. Values of $\bar{p}$ at each step of the modification procedure are shown in Table 10.1 together with the final values $\bar{P}_f$. The required plate thickness is computed by Equation 6.7 and shown in Col. 8, Table 10.1.

$$t = \frac{P_c}{\sigma_{yp}\ B\ P_f} = \frac{40{,}700}{33 \times 1008\ \bar{P}_f} = \frac{1.222}{\bar{P}_f} \qquad (10.43)$$

The combined cross sectional area of the plate and stiffeners can be obtained by Equation 6.8.

$$A = (1 + \alpha)\ B\ t \qquad (6.8)$$

The total area per unit width A_b is shown in Col. 9, Table 10.1.

$$A_b = \frac{A}{B} = (1 + \alpha)\ t\ \text{in}^2/\text{in} \qquad (10.44)$$

Values of A_b are plotted against stiffener area ratios α for several promising combinations of β and γ in Figure 10.1. These curves show the minimum allowable area of the plate-stiffener combination for each combination of β and γ. Among the sections checked, the group with $\gamma = 15$, the total area is smaller for smaller stiffener area ratios α. However, the smallest allowable α is restricted by the occurrence of local buckling.

For material assumed, σ_{yp} = 33 ksi, the plate slenderness requirements of the plate components are:

$$\text{plate: } \frac{b}{t} \leq 44$$

$$\text{stiffener web: } \frac{d}{w} \leq 43$$

According to the definition of the stiffener area ratios, α can be expressed in terms of $\frac{b}{t}$ and $\frac{d}{w}$,

$$\alpha = \frac{A_{st}}{bt} = \frac{\gamma^2}{(1-\beta)\frac{b}{t}\frac{d}{w}} \tag{10.45}$$

Consequently, the limitation to α is

$$\alpha \geq 0.000529 \frac{\gamma^2}{1-\beta} \tag{10.46}$$

Thus the limit of α for the local buckling is given for each combination β and γ, and is shown in Fig. 10.1 as a local buckling curve.

Since the local buckling curve has a lowest point A, the minimum weight section is determined from the coordinate at A and the parameters, β and γ, pertinent to the total area curve passing through point A. These values are read off as:

$$\alpha = 0.170$$

$$\beta = 0.3$$

$$\gamma = 15$$

$$A_b = (1 + \alpha)t = 1.31$$

Then, the cross sectional dimensions of the minimum weight section become:

$$t = \frac{A_b}{1+\alpha} = \frac{1.31}{1+0.17} = 1.119 \text{ in.}$$

$$b = 44\,t = 44 \times 1.119 = 49.2 \text{ in.}$$

$$A_{st} = \alpha\, b\, t = 0.170 \times 49.2 \times 1.119 = 9.35 \text{ in.}^2$$

$$A_f = \beta\, A_{st} = 0.3 \times 9.35 = 2.80 \text{ in}^2$$

$$A_w = (1-\beta)\, A_{st} = 0.7 \times 9.35 = 6.55 \text{ in}^2$$

$$d = \gamma t = 15 \times 1.119 = 16.79 \text{ in.}$$

$$w = \frac{A_w}{d} = \frac{6.55}{16.79} = 0.390 \text{ in.}$$

In practice, the exact cross-sectional dimensions computed as above cannot be realized. The available cross section, which closely conforms to the minimum weight section, will be the best design.

Five trial cross sections are selected (Table 10.2). The plate thicknesses of these sections are 1 in. and 1-1/8 in. The relationship between α and A_b for sections with t = 1 in. and t = 1.125 in. are shown in Figure 10.1 by two straight lines. The stiffener depths are such that γ is approximately 15, except for trial section 5 where γ is approximately 10. In all trial sections, the plate slenderness of the stiffener web $\frac{d}{w}$ satisfies the plate slenderness requirement (Table 10.2, Line 5). Values of γ and β are computed for each trial section (Table 10.2,Line 3 and 4). The total sectional area curve for each combination of γ and β can be estimated by the interpolation in Figure 10.1. The minimum required α is obtained from the abscissa at the intersection of the estimated total cross sectional curve and the constant thickness line (Table 10.2, Line 6).

The stiffener spacing is computed with A_{st}, α, and t(Table 10.2, Line 7).

$$b \leq \frac{A_{st}}{\alpha\, t}$$

The computed stiffener spacing may not satisfy the plate slenderness requirement,

$$b \leq 44\, t$$

Therefore the stiffener spacing is determined as the rounded value which satisfies both the requirements (Table 10.2, Line 8).

Since the designed stiffener spacing differs from the computed b, α exceeds the minimum α. The total area per unit width A_b should be computed by the following equation (Table 10.2, Line 9):

$$A_b = \frac{bt + A_{st}}{b} \qquad (10.47)$$

Among the trial sections, trial section 2 requires the minimum cross-sectional area.

Trial Section 2:

Plate thickness t = 1 in.

Stiffener Spacing = b = 44 in.

Stiffener = 18 I 70.0 cut to d = 15 in.

Total area A_b = 1.341 in^2/in

Among the sections with readily available tee stiffeners, trial section 5 gives the best result.

Trial Section 5:

Plate thickness t = 1-1/8 in.

Stiffener spacing b = 48 in.

Stiffeners ST 12 I 39.95

Total Area A_b = 1.368 in^2/in

As shown in Line 9, Table 10.2, the required cross-sectional areas of 5 trial sections have only small differences (less than 4%), in spite of fairly large variations of α and β. Such results were obtained partly because an optimum stiffener spacing was selected for each stiffener. Some of stiffener spacings selected depart from the stiffener spacing used in practice to some extent. If such stiffener spacings were accepted, the designer can have fairly wide freedom in achieving practically the best cross section.

Since the available plate and stiffeners do not necessarily conform closely to the best theoretical combination of geometric parameters, the best theoretical geometric parameters do not dictate the best cross section. For example, trial section 5 (γ = 10) has a smaller required cross-sectional area than trial section 4(γ = 15). Therefore, in design, the second best combination of geometric parameters obtained by analysis should be kept for consideration.

From the economic point of view, the readily available tee stiffeners are far more desirable than the stiffeners cut out from I-beams. To perform the design procedure described in this example, a tabulation of available tee stiffeners in terms of β and γ(a function of the plate thickness) would be of great convenience.

10.4 AN APPROXIMATE SOLUTION USING A SIMPLIFIED MOMENT-CURVATURE-THRUST RELATIONSHIP

An approximate solution of the ultimate axial load-lateral load-panel length relationship can be obtained analytically, if the moment-curvature-thrust relationship is assumed to consist of three

straight line segments, an elastic portion, and two flat plastic portions as shown in Fig. 10.4. The levels of the plastic portions are equal to the full positive and negative plastic moments of the cross section, m_{np} and m_{nn}, which are functions of axial thrust p.

If the deflection of the stiffened plate panel is small, the differential equation (2.17) is valid in the stiffened plate panel.

$$EI \frac{d^4y}{dz^4} + H\frac{d^2y}{dz^2} = qb \qquad (2.17)$$

The equilibrium configuration of the panel can be obtained as a solution of this equation.

First, the stiffened plate panel with pinned ends is considered. Solving Eq. 2.17 for boundary conditions,

$$(y)_{z=0} = 0$$

$$\left(\frac{d^2y}{dz^2}\right)_{z=\frac{\ell}{2}} = 0$$

The equilibrium configuration is obtained as

$$y = \frac{qb}{Pk^2\cos u}(\cos k z - 1) + \frac{qb}{2P} z^2 \qquad (10.48)$$

where $$k = \sqrt{\frac{P}{EI}}; u = \frac{k\ell}{2}$$

When maximum moment at the mid-span reaches M_{np}, a plastic hinge forms at mid-span and the stiffened plate panel becomes unstable. Thus the ultimate condition is defined by

$$\left(\frac{d^2y}{dz^2}\right)_{z=0} = -\frac{M_{np}}{EI} \qquad (10.49)$$

From Eqs. 10.48 and 10.49, the length of the stiffend plate panel which fails at the given axial load is given by

$$\ell = \frac{2}{k} \sec^{-1} \left(1 + \frac{M_{np} P}{qbEI} \right) \qquad (10.50)$$

When both ends are fixed, the fixed end moments reach M_{nn} before the plastification at the mid-span, and the fixed ends become plastic hinges. The equilibrium configuration immediately prior to the ultimate collapse should be solved for the following boundary conditions:

$$(y)_{z=0} = 0$$

$$\left(\frac{d^2y}{dz^2}\right)_{z=\frac{\ell}{2}} = -\frac{M_{nn}}{EI}$$

Then the equilibrium configuration becomes

$$y = \frac{\frac{qb}{P} \frac{M_{nn}}{EI}}{k^2 \cos u} (\cos kz - 1) + \frac{qb}{2p} z^2 \qquad (10.51)$$

The length of a panel having an ultimate axial load equal to a given P is obtained by Eq. 10.52.

$$\ell = \frac{2}{k} \sec^{-1} \left(\frac{1 + \frac{M_{np} P}{qbEI}}{1 + \frac{M_{nn} P}{qbEI}} \right) \qquad (10.52)$$

Using the non-dimensionalized moment, axial thrust, lateral load and length introduced in Chapter 4,

$$m_{np} = \frac{M_{np}}{\sigma_{yp} S}$$

$$m_{nn} = \frac{M_{nn}}{\sigma_{yp} S}$$

$$p = \frac{P}{P_y}$$

$$Q = \frac{qEbd_2}{\sigma_{yp}{}^2 A}$$

$$L = \frac{\ell}{r} \sqrt{\frac{E}{\sigma_{yp}}}$$

Eqs. 10.50 and 10.52 then become

$$\text{For pinned ends:} \quad L = \frac{2}{\sqrt{p}} \sec^{-1} \left(1 + \frac{m_{np} p}{Q}\right) \qquad (10.53)$$

$$\text{For fixed ends:} \quad L = \frac{2}{\sqrt{p}} \sec^{-1} \left(\frac{1 + \frac{m_{np} p}{Q}}{1 + \frac{m_{nn} p}{Q}}\right) \qquad (10.54)$$

The approximate solutions of ultimate axial load--lateral load--panel length relationship for a section with $\alpha = 0.3$, $\beta = 0.45$, $\gamma = 10$, and $G_{st} = 1$ are shown in Figs. 10.6 and 10.7 for pinned and fixed ends, respectively. The approximate solution gives the ultimate axial load 2 to 10 percent higher than the exact solution.

Modification Factor for Lateral Load, J_q

The modification factor J_q given in Eq. 5.10 is derived from Eq. 10.53. Two values Q_1 and Q_2 are considered. The corresponding L values are given for the stiffened plate panels with pinned ends by

$$L_1 = \frac{2}{\sqrt{p}} \sec^{-1}\left(L + \frac{m_{np}P}{Q_1}\right)$$

$$L_2 = \frac{2}{\sqrt{p}} \sec^{-1}\left(1 + \frac{m_{np}P}{Q_2}\right)$$

These L's are a function of $p = \frac{P}{P_y}$, Q, and m_{np}; thus, they are functions of cross-sectional dimensions. However, taking the ratio of L_2 and L_1, m_{np} can be eliminated.

$$J = \frac{L_2}{L_1} = \frac{1}{u_1} \sec^{-1}\left[1 + \frac{\sec u_1 - 1}{\frac{Q_2}{Q_1}}\right] \quad (10.55)$$

Where $u_1 = \frac{1}{2}\sqrt{p}\, L_1$

The ratio of L_2 and L_1 is thus obtained as a function of u_1 and Q_2/Q_1. The relationship of J_q vs. Q_2/Q_1 is plotted in Fig. 5.11 as a family of curves for several values of u_1.

Modification Factor for End Restraint, J_e

The modification factor for end restraint is obtained in a similar manner to that used in computing J_q.

Let L of the stiffened plate panels with pinned ends and with fixed ends be L^p and L^f, respectively.

Then,

$$K = \frac{L^f}{L^p} = \frac{1}{u_{pin}} \sec^{-1}\left[\frac{\sec u^p}{1 + \frac{m_{nn}P}{Q}}\right] \quad (10.56)$$

where

$$u_{pin} = \tfrac{1}{2}\sqrt{p}\,L^{p}$$

J_e vs. $(-\frac{m_{nn}P}{Q})$ Relationship is shown in Fig. 5.12.

Since m_{np} is not smaller than $|m_{nn}|$ in the longitudinally stiffened plate panels, limiting value of J_e occurs when $m_{np} = |m_{nn}|$.

$$(J_e)_{limit} = \frac{\sec^{-1}\left[\dfrac{1-\frac{m_{nn}P}{Q}}{1+\frac{m_{nn}P}{Q}}\right]}{\sec^{-1}\left[1-\frac{m_{nn}P}{Q}\right]}$$

J_e limit increases gradually from $\sqrt{2}$ at $(-\frac{m_{nn}P}{Q}) = 0$ to 2 at $(\frac{m_{nn}P}{Q}) = \infty$ as shown in Fig. 5.12. For the practical range of the sectional dimensions and lateral load, $(-\frac{m_{nn}P}{Q})$ varies between 0 and 1, and the variation of J_e is limited to the range of 1.0 to 1.5.

11. T A B L E S

TABLE 3.1 EFFECTIVE YIELD STRAINS

Sub-area	i	Effective Yield Strain	
		Compression, $\bar{\epsilon}_{yci}$	Tension, $\bar{\epsilon}_{yti}$
1	1	$\bar{\epsilon}_{yc1} = 2\,\epsilon_{yp}$	$\bar{\epsilon}_{yt1} = 0$
2	2	$\bar{\epsilon}_{yc2} = \epsilon_{yp} - \epsilon_{rc}$	$\bar{\epsilon}_{yt2} = -\epsilon_{yp} - \epsilon_{rc}$
3	3	$\bar{\epsilon}_{yc3} = \epsilon_{st}$	$\bar{\epsilon}_{yt3} = -\epsilon_{st}$
4 at flange tip	4	$\bar{\epsilon}_{yc4} = \epsilon_{st} - \epsilon_{fc}$	$\bar{\epsilon}_{yt4} = -\epsilon_{st} - \epsilon_{fc}$
at center line	5	$\bar{\epsilon}_{yc5} = \epsilon_{st} - \epsilon_{ft}$	$\bar{\epsilon}_{yt5} = -\epsilon_{st} - \epsilon_{ft}$

Note: ϵ_{yp}; yield strain of the plate

ϵ_{st}; yield strain of the stiffener

ϵ_{rc}; compressive residual strain in the plate

ϵ_{fc}; residual strain at the flange tips

ϵ_{ft}; residual strain at the center line of the stiffener flange

Table 3.2 COEFFICIENTS IN EQS. 3.17 AND 3.18
(i = 1, 2, 3)

	$\epsilon_1 > -g_{ci1}$	$-g_{ci1} > \epsilon_1 > -g_{ti1}$	$-g_{ti1} > \epsilon_1$
c_{i11}	$-b_i$	0	$-b_i$
c_{i12}	g_{ci1}	----	g_{ti1}
	$\epsilon_1 > -g_{ci2}$	$-g_{ci2} > \epsilon_1 > -g_{ti2}$	$-g_{ti2} > \epsilon_1$
c_{i21}	b_i	0	b_i
c_{i22}	g_{ci2}	----	g_{ti2}

where, $g_{ci1} = -\bar{\epsilon}_{yci} - \emptyset\eta_{li1}$

$g_{ti1} = -\bar{\epsilon}_{yti} - \emptyset\eta_{li1}$

$g_{ci2} = -\bar{\epsilon}_{yci} - \emptyset\eta_{li2}$

$g_{ti2} = -\bar{\epsilon}_{yti} - \emptyset\eta_{li2}$

TABLE 3.3 COEFFICIENTS IN EQ. 3.19

	$\varepsilon_1 > -g_{c41}$	$-g_{c41} > \varepsilon_1 > -g_{t41}$	$-g_{t41} > \varepsilon_1$
c_{411}	$-\dfrac{\phi A_f}{\varepsilon_{fc} - \varepsilon_{ft}}$	0	$-\dfrac{\phi A_f}{\varepsilon_{fc} - \varepsilon_{ft}}$
c_{412}	g_{c41}	---	g_{t41}
	$\varepsilon_1 > -g_{c42}$	$-g_{c42} > \varepsilon_1 > -g_{t42}$	$-g_{t42} > \varepsilon_1$
c_{421}	$\dfrac{\phi A_f}{\varepsilon_{fc} - \varepsilon_{ft}}$	0	$\dfrac{\phi A_f}{\varepsilon_{fc} - \varepsilon_{ft}}$
c_{422}	g_{c42}	---	g_{t42}

where, $g_{c41} = -\bar{\varepsilon}_{yc4} - \phi \eta_{141}$

$g_{t41} = -\bar{\varepsilon}_{yt5} - \phi \eta_{141}$

$g_{c42} = -\bar{\varepsilon}_{yc5} - \phi \eta_{141}$

$g_{t42} = -\bar{\varepsilon}_{yt4} - \phi \eta_{141}$

TABLE 3.4 COEFFICIENTS IN EQS. 3.24 and 3.25

(a) C_{j1} and C_{j2} (j=1, 2, ---, 8)

	$G_1 > -X_{j+8}$	$-X_{j+8} > G_1 > -X_{j+16}$	$X_{j+16} > G_1$
C_{j1}	X_j	0	X_j
C_{j2}	X_{j+8}	---	X_{j+16}

$$X_1 = -X_2 = -B_{rt}$$

$$X_3 = -X_4 = B_{rt} - 1$$

$$X_5 = -X_6 = \frac{\alpha(\beta-1)}{\gamma}$$

$$X_7 = -X_8 = \frac{\alpha\beta\Phi}{(G_{ft}-G_{fc})D_2}$$

$$X_9 = -2$$

$$X_{10} = -2 - \frac{\Phi}{D_2}$$

$$X_{11} = -\ 1 + G_{rc}$$

$$X_{12} = -\ 1 + G_{cr} - \frac{\Phi}{D_2}$$

$$X_{13} = -\ G_{st} - \frac{\Phi}{D_2}$$

$$X_{14} = -G_{st} - \Phi\ (1+\frac{D_1}{D_2})$$

$$X_{15} = -G_{st} + G_{fc} - \Phi\ (1+\frac{D_1}{D_2})$$

$$X_{16} = -\ G_{st} + G_{ft} - \Phi\ (1+\frac{D_1}{D_2})$$

$$X_{17} = 0$$

TABLE 3.4 COEFFICIENTS IN EQS. 3.24 and 3.25 (Cont'd)

$$X_{18} = -\frac{\Phi}{D_2}$$

$$X_{19} = 1 + G_{rc}$$

$$X_{20} = 1 + G_{rc} - \frac{\Phi}{D_2}$$

$$X_{21} = G_{st} - \frac{\Phi}{D_2}$$

$$X_{22} = G_{st} - \Phi\left(1+\frac{D_1}{D_2}\right)$$

$$X_{23} = G_{st} + G_{ft} - \Phi\left(1+\frac{D_1}{D_2}\right)$$

where $G_{rc} = \frac{\sigma_{rc}}{\sigma_{yp}}$

$G_{st} = \frac{\sigma_{st}}{\sigma_{yp}}$

$G_{fc} = \frac{\sigma_{fc}}{\sigma_{yp}}$

$G_{fy} = \frac{\sigma_{ft}}{\sigma_{yp}}$

(b) C_{j3} $(j = 1, 2, ---,6)$

$C_{13} = 1 + \gamma$

$C_{23} = \gamma$

$C_{33} = 1 + \gamma$

$C_{43} = \gamma$

$C_{53} = \gamma$

$C_{63} = 0$

TABLE 4.1 BASIC SPECIMEN DATA

Specimen	T-5	T-6
Actual Dimensions (in.)		
Length, ℓ	60.875	61.0
Plate Width, B	51.0	51.0
Plate thickness, t	0.2610	0.2553
Stiffener Flange Width, b_f	3.96	1.88
Stiffener Flange Thickness, t_f	0.201	0.161
Stiffener Web Thickness, w	0.168	0.120
Stiffener Depth, d	2.92	3.32
Thickness of Stiffener Strips	0.1258	----
Width of Stiffening Strips	3.02	----
Material Properties (ksi)		
Yield Stress in Plate, σ_{yp}	39.7	39.5
Yield Stress in Stiffener Flange	37.5	35.9
Yield Stress in Stiffener Web	46.4	39.7
Test Results		
Ultimate Axial Load, P (kips)	648	463
Lateral Load, q (psi)	6.5	6.5

TABLE 4.2 PARAMETERS OF SIMPLIFIED CROSS SECTIONS

(T-5 and T-6)

Specimen	T-5	T-6
$\alpha = \frac{A_{st}}{bt}$	0.5185	0.2714
$\beta = \frac{A_f}{A_{st}}$	0.3921	0.4379
$\gamma = \frac{d}{t}$	10.805	12.706
$G_{st} = \frac{\sigma_{st}}{\sigma_{yp}}$	1.0	0.91
$G_{rc} = \frac{\sigma_{rc}}{\sigma_{yp}}$	0.234	0.185
$G_{fc} = \frac{\sigma_{fc}}{\sigma_{yp}}$	0.3	0.3
$G_{ft} = \frac{\sigma_{ft}}{\sigma_{yp}}$	0.3	0.3
$Q = \frac{qEbd_2}{\sigma_{yp}{}^2 A}$	0.689	1.080
$L = \frac{\ell}{r}\frac{\sqrt{\sigma_{yp}}}{E}$	1.96	2.01

TABLE 5.1 ANALYZED CROSS SECTIONS

Section No.	α	β	γ	G_{rc}
1 - A*	0.3	0.45	10	0
1 - B*	0.3	0.45	10	0.125
1 - C	0.3	0.45	10	0.125
2	0.3	0.45	5	0.125
3	0.3	0.45	15	0.125
4*	0.3	0.30	10	0.125
5	0.3	0.15	10	0.125
6 - A	0.5	0.45	10	0
6 - B*	0.5	0.45	10	0.125
6 - C	0.5	0.45	10	0.25
7	0.5	0.45	5	0.125
8	0.5	0.45	15	0
9 - A	0.5	0.30	15	0
9 - B	0.5	0.30	15	0.125
9 - C	0.5	0.30	15	0.25
10	0.5	0.30	10	0.125
11	0.5	0.15	10	0.125
12 - A	0.1	0.45	10	0
12 - B	0.1	0.45	10	0.125
12 - C	0.1	0.45	10	0.25
13	0.1	0.45	15	0.125
14	0.1	0.30	10	0.125

* Sections listed in Table 5.2.

TABLE 5.2 NUMERICAL RESULTS

Section 1 - A, $\alpha = 0.3$, $\beta = 0.45$, $\gamma = 10$, $G_{rc} = 0$

Pinned Ends

Q	p	L^P	Δ^P ($X10^{-3}$)	Y^P	Φ_o^P	θ^P ($X10^{-3}$ rad.)
0.5	0.6	3.169	7.92	0.7154	1.776	2.602
	0.7	2.958	3.21	0.5654	1.690	2.201
	0.8	2.608	3.02	0.2983	1.132	1.310
	0.9	2.124	2.66	0.1057	0.647	0.564
2.0	0.6	2.173	2.49	0.3769	2.184	1.967
	0.7	2.040	2.19	0.2928	1.930	1.633
	0.8	1.736	2.05	0.1472	1.407	0.958
	0.9	1.313	1.71	0.0484	0.920	0.404
3.5	0.6	1.769	1.66	0.2723	2.575	1.719
	0.7	1.667	1.87	0.2101	2.242	1.417
	0.8	1.400	1.75	0.1077	1.755	0.848
	0.9	1.037	1.41	0.0348	1.128	0.358
5.0	0.6	1.533	1.43	0.2150	2.847	1.552
	0.7	1.445	1.63	0.1636	2.405	1.261
	0.8	1.209	1.60	0.0888	2.092	0.994
	0.9	0.884	1.26	0.0299	1.240	0.332

Note: Q : lateral load

p : axial load

L : panel length

$\Delta = L - Z$: longitudinal deflection

TABLE 5.2 NUMERICAL RESULTS (Cont'd)

Y : lateral deflection

Φ_o: curvature at mid-span

θ^P: slope at pinned ends

m^F: fixed end moment

Section 1-A, Fixed Ends

Q	p	L^F	Δ^F ($X10^{-3}$)	Y^F	Φ_o^F	m^F
0.5	0.6	3.791	11.34	0.8831	1.644	-0.564
	0.7	3.446	6.37	0.6766	1.495	-0.430
	0.8	3.015	4.15	0.3540	1.026	-0.271
	0.9	2.450	3.33	0.1328	0.679	-0.147
2.0	0.6	2.562	8.79	0.4340	2.026	-0.557
	0.7	2.342	5.01	0.3488	1.835	-0.433
	0.8	1.986	2.74	0.1743	1.339	-0.292
	0.9	1.494	2.13	0.0566	0.874	-0.147
3.5	0.6	2.056	2.60	0.3233	2.373	-0.569
	0.7	1.898	2.78	0.2490	2.174	-0.432
	0.8	1.592	2.20	0.1050	1.769	-0.290
	0.9	1.176	1.76	0.0401	1.072	-0.148
5.0	0.6	1.776	2.23	0.2551	2.659	-0.569
	0.7	1.642	2.39	0.1951	2.368	-0.434
	0.8	1.370	1.94	0.0768	1.967	-0.289
	0.9	1.001	1.56	0.0320	1.217	-0.147

TABLE 5.2 NUMERICAL RESULTS(Cont'd)

Section 1-B, α = o.3, β = 0.45, γ = 10, G_{rc} = 0.125

Pinned Ends

Q	p	L^p	Δ^p ($X10^{-3}$)	Y^p	Φ_o^p	θ^p ($X10^{-2}$ rad.)
1.198	0.6	2.474	2.59	0.4772	2.090	2.163
	0.7	2.240	3.45	0.4816	2.553	2.347
	0.8	1.888	3.21	0.2872	2.087	1.680
	0.9	1.400	2.79	0.1256	1.590	1.068
2.397	0.6	1.778	2.03	0.3373	2.498	1.888
	0.7	1.841	2.77	0.3385	2.701	2.017
	0.8	1.541	2.67	0.1939	2.130	1.397
	0.9	1.141	2.26	0.0834	1.607	0.873
3.595	0.6	1.703	1.74	0.2731	2.912	1.751
	0.7	1.604	2.56	0.2556	2.755	1.660
	0.8	1.338	2.31	0.1486	2.230	1.221
	0.9	0.990	2.20	0.0618	1.614	0.430
4.793	0.6	1.520	1.53	0.2295	3.217	1.634
	0.7	1.435	2.16	0.2110	2.822	1.611
	0.8	1.198	2.08	0.1213	2.278	1.122
	0.9	0.884	1.75	0.0498	1.618	0.676

TABLE 5.2 NUMERICAL RESULTS (Cont'd)

Section 1 - B, $\alpha = 0.3$, $\beta = 0.45$, $\gamma = 10$, $G_{rc} = 0.125$

		Fixed Ends				
Q	p	L^F	$\Delta^F(\times 10^{-3})$	Y^F	Φ_o^F	m^F
1.198	0.6	2.941	3.89	0.5712	1.903	-0.557
	0.7	2.595	4.61	0.5259	2.230	-0.430
	0.8	2.173	4.30	0.3437	2.019	-0.289
	0.9	1.596	3.48	0.1529	1.570	-0.148
2.397	0.6	2.318	3.08	0.4117	2.434	-0.550
	0.7	2.104	3.92	0.4018	2.674	-0.420
	0.8	1.758	3.49	0.2330	2.122	-0.278
	0.9	1.291	2.84	0.1010	1.600	-0.149
3.595	0.6	1.991	2.73	0.3241	2.685	-0.568
	0.7	1.838	3.32	0.2993	2.706	-0.430
	0.8	1.515	3.07	0.1740	2.219	-0.275
	0.9	1.140	2.40	0.0704	1.609	-0.149
4.793	0.6	1.771	2.40	0.2717	3.067	-0.568
	0.7	1.634	3.02	0.2530	2.776	-0.433
	0.8	1.360	2.80	0.1439	2.231	-0.293
	0.9	0.994	2.20	0.0580	1.615	-0.143

TABLE 5.2 NUMERICAL RESULTS(Cont'd)

Section 4, $\alpha = 0.3$, $\beta = 0.30$, $\gamma = 10$, $G_{rc} = 0.125$

Pinned Ends

Q	p	L^p	Δ^p ($\times 10^{-3}$)	Y^p	ϕ_o^p	θ^p ($\times 10^{-2}$ rad.)
1.320	0.6	2.455	2.34	0.4325	2.116	1.990
	0.7	2.241	3.16	0.4392	2.582	2.146
	0.8	1.924	3.32	0.3075	2.368	1.769
	0.9	1.413	2.96	0.1386	1.945	1.141
2.641	0.6	1.951	1.38	0.3119	2.622	1.771
	0.7	1.832	2.57	0.3263	2.995	1.940
	0.8	1.583	2.72	0.2107	2.428	1.485
	0.9	1.155	2.43	0.0943	2.007	0.950
3.961	0.6	1.677	1.62	0.2592	3.148	1.682
	0.7	1.592	2.20	0.2469	3.145	1.692
	0.8	1.371	2.40	0.1621	2.579	1.306
	0.9	1.004	2.10	0.0705	2.031	0.817

TABLE 5.2 NUMERICAL RESULTS (Cont'd)

Section 4, $\alpha = 0.3$, $\beta = 0.30$, $\gamma = 10$, $G_{rc} = 0.125$

Fixed Ends

Q	p	L^F	Δ^F ($\times 10^{-3}$)	Y^F	Φ_o^F	m^F
1.320	0.6	2.945	3.56	0.5302	1.943	-0.618
	0.7	2.606	3.45	0.4929	2.312	-0.462
	0.8	2.203	4.56	0.3627	2.278	-0.320
	0.9	1.607	3.55	0.1562	1.930	-0.161
2.641	0.6	2.306	2.94	0.3673	2.337	-0.620
	0.7	2.103	3.69	0.3815	2.888	-0.466
	0.8	1.794	3.67	0.2505	2.404	-0.322
	0.9	1.302	3.05	0.119	1.982	-0.163
3.961	0.6	1.967	2.59	0.3116	3.033	-0.613
	0.7	1.820	3.24	0.2965	2.995	-0.474
	0.8	1.556	3.16	0.1891	2.433	-0.322
	0.9	1.128	2.58	0.0830	2.005	-0.163

TABLE 5.2 NUMERICAL RESULTS (Cont'd)

Section 6 - B, $\alpha = 0.5$, $\beta = 0.45$, $\gamma = 10$, $G_{rc} = 0.125$

Pinned Ends

Q	p	L^p	Δ^p ($\times 10^{-3}$)	Y^p	Φ_o^p	θ^p ($\times 10^{-2}$ rad.)
0.9603	0.6	2.380	3.23	0.5732	2.185	2.621
	0.7	2.077	3.02	0.3798	1.889	1.981
	0.8	1.725	2.81	0.2258	1.610	1.429
	0.9	1.254	2.40	0.1011	1.306	0.953
1.921	0.6	1.939	2.60	0.3948	2.325	2.219
	0.7	1.692	2.48	0.2593	1.993	1.663
	0.8	1.409	2.28	0.1526	1.657	1.191
	0.9	1.021	1.95	0.0673	1.329	0.780
2.881	0.6	1.680	2.21	0.3050	2.460	1.974
	0.7	1.466	2.14	0.2002	2.071	1.479
	0.8	1.222	1.98	0.1155	1.673	1.046
	0.9	0.883	1.69	0.0508	1.340	0.679

TABLE 5.2 NUMERICAL RESULTS (Cont'd)

Section 6 - B, $\alpha = 0.5$, $\beta = 0.45$, $\gamma = 10$, $G_{rc} = 0.125$

Fixed Ends

Q	p	L^F	Δ^F ($\times 10^{-3}$)	Y^F	Φ_o^F	m^F
0.9603	0.6	2.932	4.01	0.5698	1.606	-0.538
	0.7	2.547	3.82	0.3870	.1449	-0.407
	0.8	2.087	3.72	0.2895	1.393	-0.265
	0.9	1.509	3.18	0.1321	1.268	-0.141
1.921	0.6	2.343	4.07	0.5030	2.234	-0.546
	0.7	2.043	3.51	0.3229	1.849	-0.412
	0.8	1.689	3.23	0.1950	1.632	-0.276
	0.9	1.216	2.57	0.0878	1.317	-0.141
2.881	0.6	2.017	3.55	0.3854	2.345	-0.547
	0.7	1.759	3.34	0.2509	2.002	-0.412
	0.8	1.457	2.83	0.1468	1.647	-0.279
	0.9	1.049	2.27	0.0656	1.332	-0.142

TABLE 5.3 NON-DIMENSIONALIZED PANEL LENGTH L,
(p - Q - L RELATIONSHIP)

a. Pinned Ends

		p			
Section No.	Q	0.6	0.7	0.8	0.9
	0.5	2.885	2.574	2.147	1.650
	2.0	2.047	1.920	1.611	1.209
1 - C	3.5	1.687	1.601	1.346	1.002
	5.0	1.469	1.403	1.180	0.873
	1.2	2.479	2.247	1.895	1.404
2	2.4	1.981	1.844	1.548	1.144
	3.6	1.705	1.607	1.341	0.993
	4.8	1.522	1.441	1.200	0.887
	1.2	2.478	2.246	1.894	1.404
3	2.4	1.980	1.843	1.547	1.144
	3.6	1.704	1.606	1.341	0.993
	4.8	1.521	1.441	1.220	0.887
	1.48	2.429	2.229	1.935	1.469
5	2.96	1.928	1.811	1.601	1.203
	4.44	1.657	1.567	1.394	1.046
	1.0	2.490	2.207	1.818	1.280
6 - A	2.0	2.003	1.762	1.470	1.079
	3.0	1.700	1.491	1.230	0.890
	1.0	2.268	1.980	1.671	1.195
6 - C	2.0	1.869	1.627	1.368	1.000
	3.0	1.645	1.420	1.182	0.847

TABLE 5.3 NON-DIMENSIONALIZED PANEL LENGTH L,
(p - Q - L RELATIONSHIP)

a. Pinned Ends

Section No.	Q	p = 0.6	0.7	0.8	0.9
7	0.96	2.378	2.076	1.724	1.254
	1.92	1.938	1.691	1.409	1.021
	2.88	1.679	1.466	1.222	0.883
8	0.96	2.340	2.079	1.726	1.255
	1.92	1.940	1.693	1.410	1.021
	2.88	1.681	1.467	1.223	0.883
9 - A	1.0	2.558	2.325	1.969	1.368
	2.0	2.077	1.869	1.567	1.280
	3.0	1.768	1.590	1.332	0.920
9 - B	1.0	2.451	2.200	1.847	1.310
	2.0	1.998	1.784	1.518	1.221
	3.0	1.736	1.543	1.308	0.908
9 - C	1.0	2.340	2.103	1.780	1.276
	2.0	1.951	1.722	1.461	1.185
	3.0	1.713	1.512	1.273	0.880
10	1.0	2.449	2.198	1.846	1.309
	2.0	1.996	1.783	1.517	1.220
	3.0	1.735	1.542	1.307	0.908
11	1.0	2.501	2.308	1.960	1.383
	2.0	2.059	1.867	1.600	1.164
	3.0	1.792	1.619	1.388	0.986
12 - A	2.0	2.181	2.176	2.081	1.753
	3.0	1.879	1.864	1.782	1.578
	5.0	1.540	1.570	1.481	1.312

TABLE 5.3 NON-DIMENSIONALIZED PANEL LENGTH , L (Cont'd)

a. Pinned Ends

Section No.	Q	p 0.6	0.7	0.8	0.9
12 - B	2.0	2.173	2.156	2.046	1.753
	4.0	1.683	1.688	1.631	1.432
	6.0	1.426	1.437	1.398	1.231
12- C	2.0	2.171	2.152	2.002	1.608
	3.0	1.872	1.855	1.753	1.541
	5.0	1.547	1.548	1.471	1.308
13	2.0	2.172	2.155	2.045	1.751
	4.0	1.681	1.686	1.629	1.430
	6.0	1.424	1.435	1.397	1.230
14	2.0	2.182	2.173	2.100	1.738
	3.0	1.880	1.869	1.801	1.612
	5.0	1.533	1.551	1.507	1.352

b. Fixed Ends

Section No.	Q	p 0.6	0.7	0.8	0.9
1 - C	0.5	3.540	3.032	2.506	1.933
	2.0	2.420	2.230	1.810	1.364
	3.5	1.977	1.827	1.496	1.107
	5.0	1.716	1.596	1.334	0.980
2	0.5	3.536	3.028	2.503	1.931
	2.0	2.417	2.200	1.808	1.362
	3.5	1.975	1.825	1.494	1.105
	5.0	1.714	1.594	1.332	0.979

TABLE 5.3 NON-DIMENSIONALIZED PANEL LENGTH, L

a. Fixed Ends

Section No.	Q	p = 0.6	0.7	0.8	0.9
3	1.2	2.925	2.578	2.158	1.584
	2.4	2.309	2.109	1.758	1.284
	3.6	1.976	1.817	1.525	1.131
	4.8	1.758	1.627	1.353	0.962
5	1.48	2.926	2.615	2.231	1.654
	2.96	2.290	2.091	1.821	1.348
	4.44	1.953	1.803	1.571	1.166
6 - A	1.0	3.032	2.668	2.220	1.532
	2.0	2.401	2.110	1.760	1.258
	3.0	2.053	1.786	.1480	1.089
6 - C	1.0	2.840	2.443	2.012	1.456
	2.0	2.260	1.952	1.631	1.204
	3.0	1.941	1.680	1.402	1.027
7	0.96	2.929	2.544	2.084	1.507
	1.92	2.340	2.040	1.687	1.214
	2.88	2.014	1.757	1.455	1.047
8	0.96	2.934	2,549	2.089	1.510
	1.92	2.345	2.044	1.690	1.217
	2.88	2.019	1.761	1.458	1.050
9 - A	1.0	3.154	2.770	2.341	1.618
	2.0	2.486	2.200	1.868	1.320
	3.0	2.120	1.882	1.572	1.152

TABLE 5.3 NON-DIMENSIONLIZED PANEL LENGTH, L (Cont'd)

b. Fixed Ends

Section No.	Q	p = 0.6	0.7	0.8	0.9
9 - B	1.0	3.050	2.635	2.199	1.578
	2.0	2.401	2.112	1.780	1.291
	3.0	2.058	1.820	1.523	1.115
9 - C	1.0	2.980	2.557	2.116	1.530
	2.0	2.347	2.041	1.721	1.270
	3.0	2.013	1.775	1.484	1.091
10	1.0	3.047	2.633	2.197	1.576
	2.0	2.398	2.110	1.778	1.290
	3.0	2.056	1.818	1.521	1.114
11	1.0	3.223	2.760	2.312	1.701
	2.0	2.492	2.199	1.880	1.386
	3.0	2.113	1.898	1.611	1.193
12 - A	2.0	2.660	2.542	2.328	1.893
	3.0	2.281	2.199	2.040	1.716
	5.0	1.837	1.782	1.651	1.389
12 - B	2.0	2.620	2.488	2.270	1.874
	4.0	2.001	1.937	1.800	1.502
	6.0	1.680	1.643	1.534	1.313
12 - C	2.0	2.592	2.451	2.231	1.852
	3.0	2.230	2.148	1.979	1.670
	5.0	1.807	1.762	1.637	1.380
13	2.0	2.623	2.491	2.272	1.876
	4.0	2.003	1.939	1.802	1.503
	6.0	1.683	1.646	1.537	1.315

TABLE 5.3 NON-DIMENSIONALIZED PANEL LENGTH, L(Cont'd)

b. Fixed Ends

Section No.	Q	p 0.6	0.7	0.8	0.9
	2.0	2.637	2.540	2.329	1.921
14	3.0	2.275	2.203	2.051	1.730
	5.0	1.832	1.791	1.675	1.420

Table 10.1 DESIGN TABLE

1	2	3	4	5	6	7	8	9
Geometric Parameters								
γ	β	α	$\bar{p}$	$\bar{p}_\gamma$	$\bar{p}_\beta$	$\bar{p}_f$	t(in)	$(1+\alpha)t$
	0.15	0.3			1.014	1.014	1.209	1.570
	0.30	0.3			1.041	1.041	1.176	1.529
5		0.1		1.051		0.829	1.480	1.628
	0.45	0.3			1.051	1.051	1.164	1.512
		0.5				1.190	1.030	1.546
	0.15	0.3			1.152	1.152	1.061	1.380
		0.1				0.989	1.240	1.361
	0.30	0.3			1.168	1.168	1.050	1.365
10		0.5		1.170		1.329	0.923	1.383
		0.1	1.170			0.990	1.239	1.360
	0.45	0.3			1.170	1.170	1.048	1.361
		0.5				1.333	0.919	1.378
		0.1				1.024	1.198	1.317
	0.15	0.3			1.200	1.200	1.021	1.330
		0.5				1.370	0.895	1.341
		0.1				1.034	0.185	1.302
15	0.30	0.3		1.210	1.208	1.208	1.016	1.320
		0.5				1.381	0.886	1.330
		0.1				1.036	1.182	1.300
	0.45	0.3			1.210	1.210	1.012	1.318
		0.5				1.383	0.855	1.329

Table 10.2 TRIAL SECTIONS

			Trial Section	Trial Section	Trial Section	Trial Section	Trial Section	Remarks
			1	2	3	4	5	
Plate thickness t (in)		1	1	1	1	1.125	1.125	
Stiffeners		2	18I54.7 cut to d= 15	18I70.0 cut to d= 15	ST15WF58	20I65.4 cut to d= 17	ST12I39.95	
Stiffener Dimensions (Relative)	γ	3	15	15	15	15.1	10.68	Computed for the cross sectional dimensions of selected stiffeners
	β	4	0.376	0.288	0.505	0.366	0.486	
	$\frac{d}{w}$	5	32.6	21.1	26.6	34	24	
Minimum	α	6	0.319	0.322	0.318	0.165	0.207	Read from Fig. 10.1
Maximum	b	7	34.5	46.5	53.6	77.5	50.1	$b = \frac{A_{st}}{\alpha t}$
Designed Spacing	stiffener b	8	32	44	44	48	48	b should not exceed 44 for t = 1, and 49.5 for t = 1.125
Total Area per unit width A_b		9	1.345	1.341	1.388	1.374	1.368	$A_b = \frac{b\,t + A_{st}}{b}$

12. FIGURES

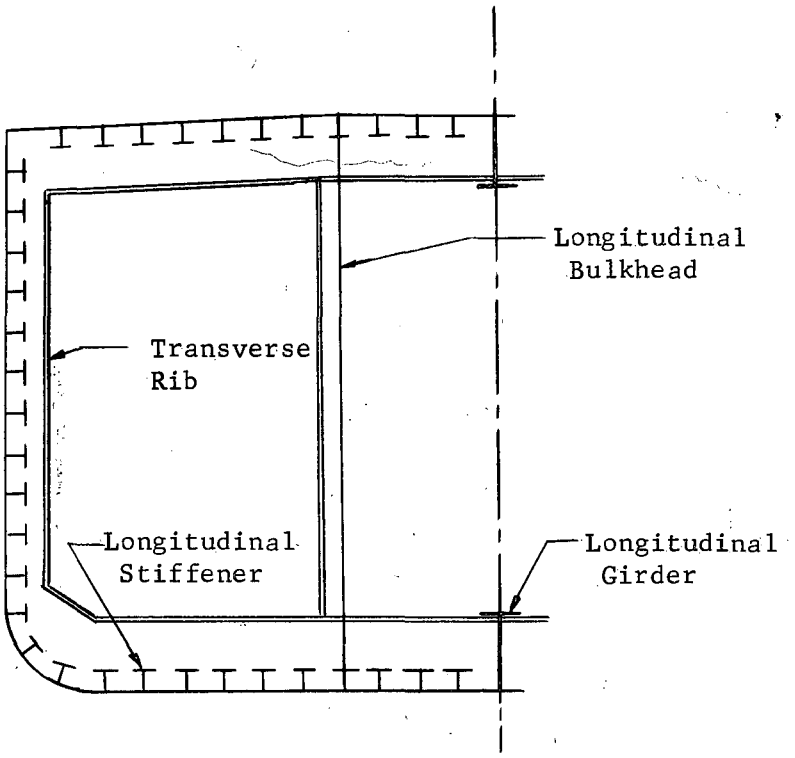

(a) TYPICAL MID-SHIP CROSS SECTION

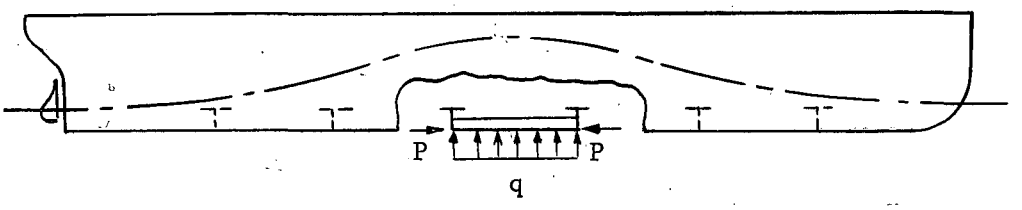

(b) LOADING ON THE SHIP BOTTOM PANEL DUE TO WAVE ACTION-HOGGING

Fig. 1.1 LONGITUDINALLY STIFFENED PLATE PANELS IN THE SHIP BOTTOM STRUCTURE.

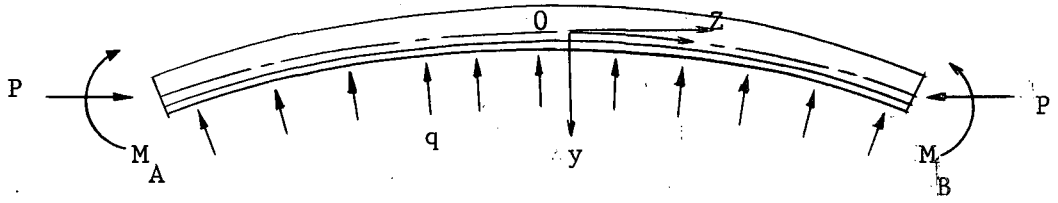

(a) LONGITUDINALLY STIFFENED PLATE PANEL UNDER COMBINED LOADING

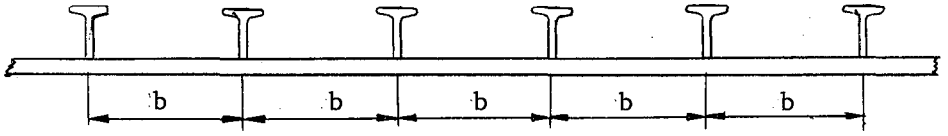

(b) CROSS SECTION

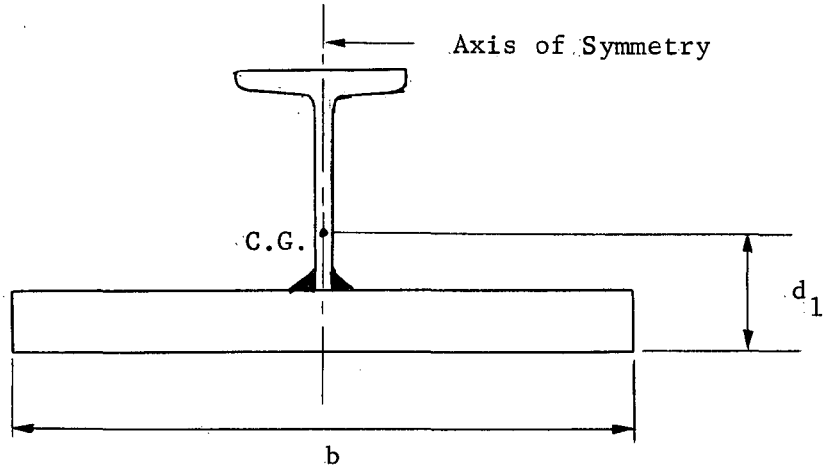

(c) SYMPLIFIED CROSS SECTION

Fig. 2.1 CONDITION OF LOADING AND CROSS SECTION

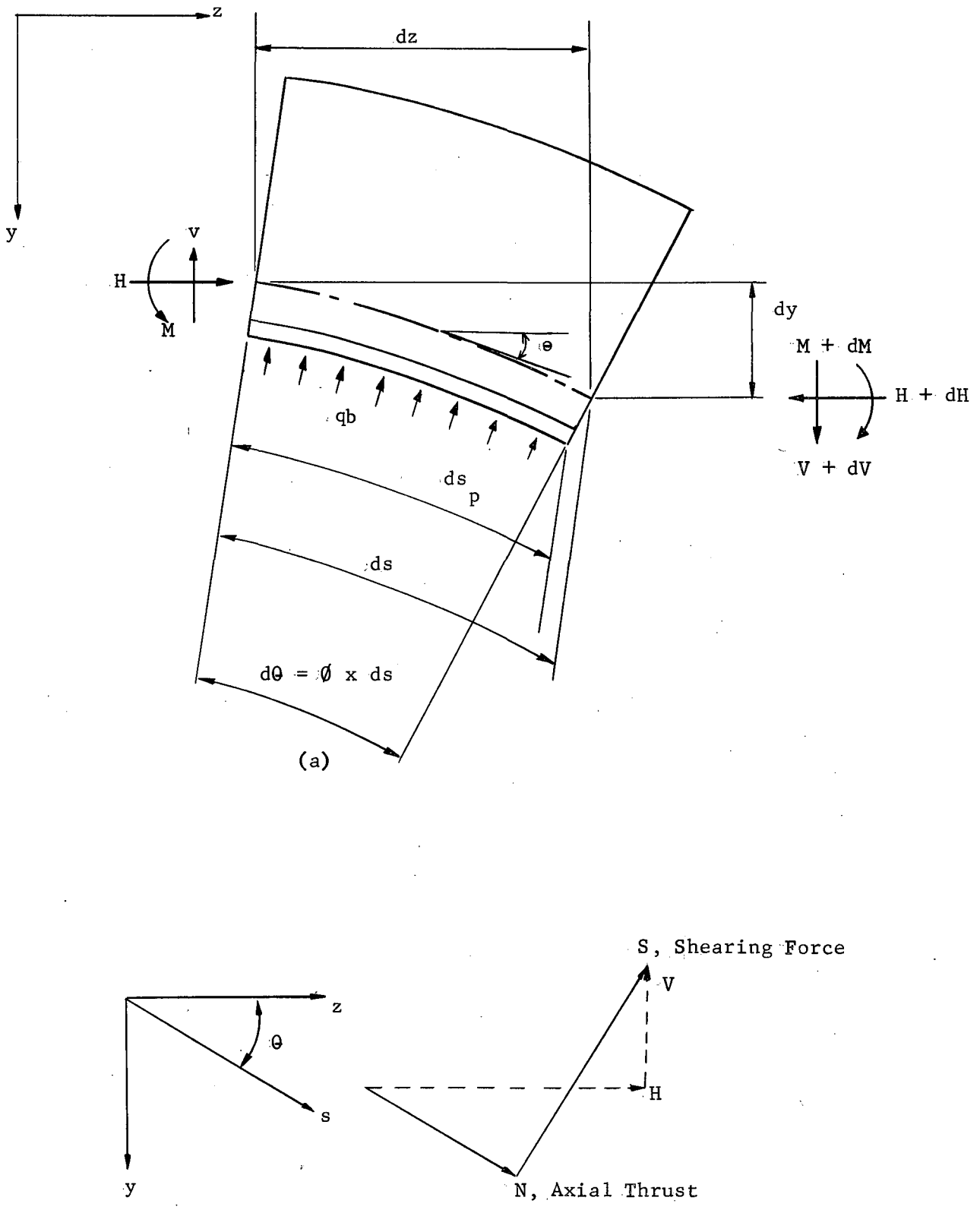

Fig. 2.2 EQUILIBRIUM OF AN ELEMENT OF LENGTH ds.

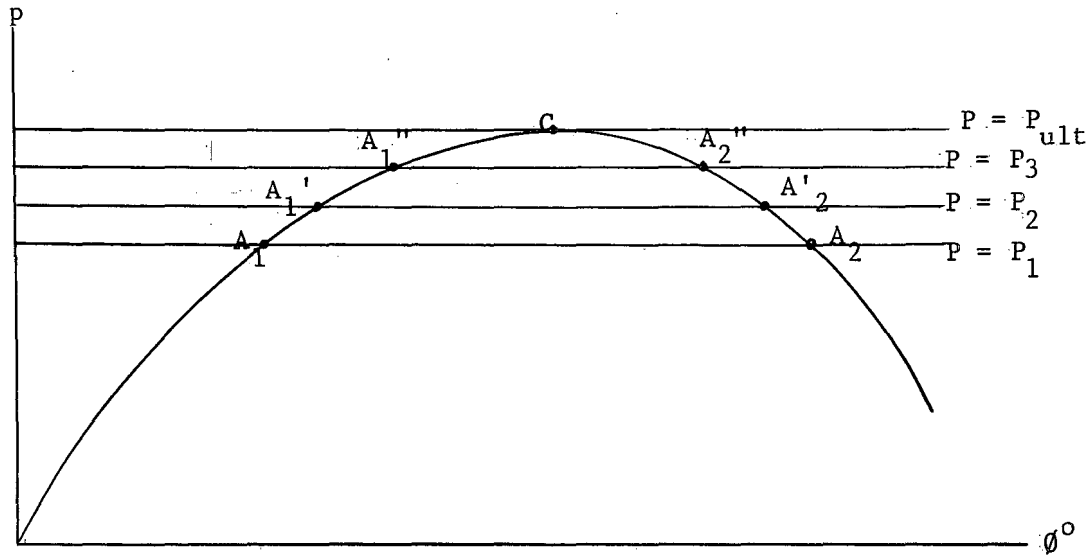

Fig. 2.3 LOAD DEFLECTION CURVE

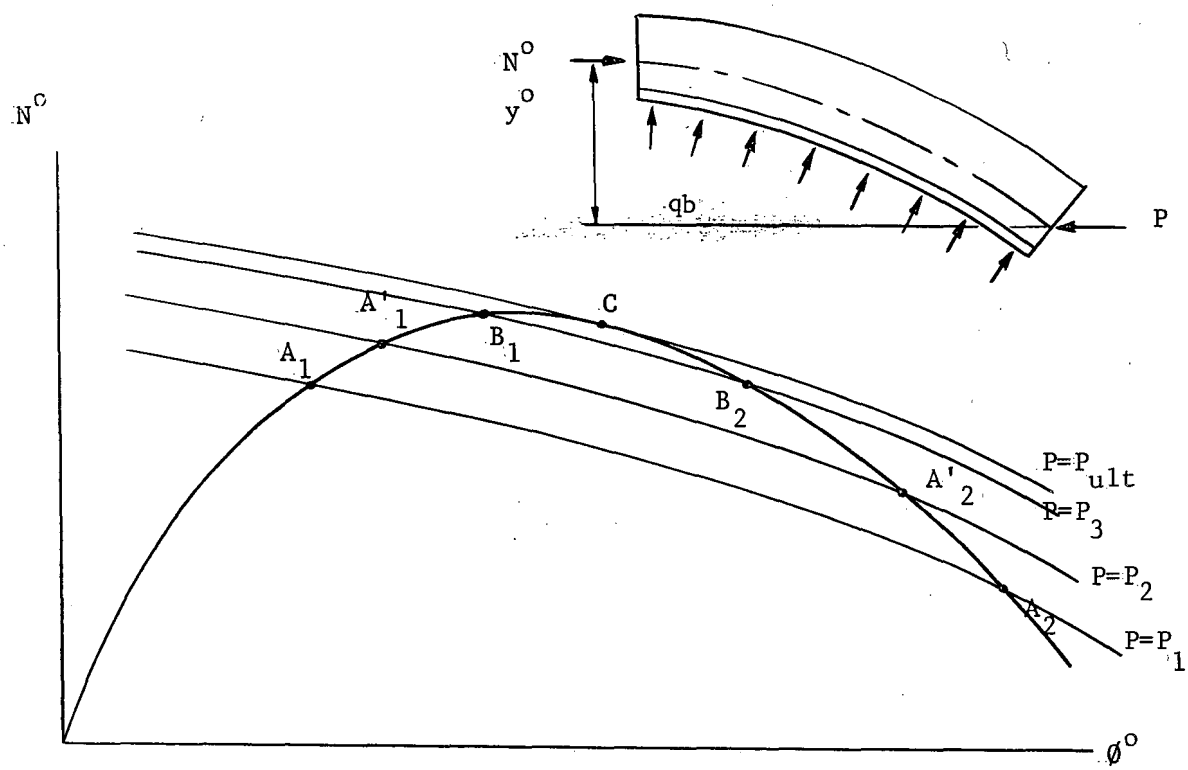

Fig. 2.4 LOAD DEFLECTION CURVE TERMS OF N^o AND ϕ^o

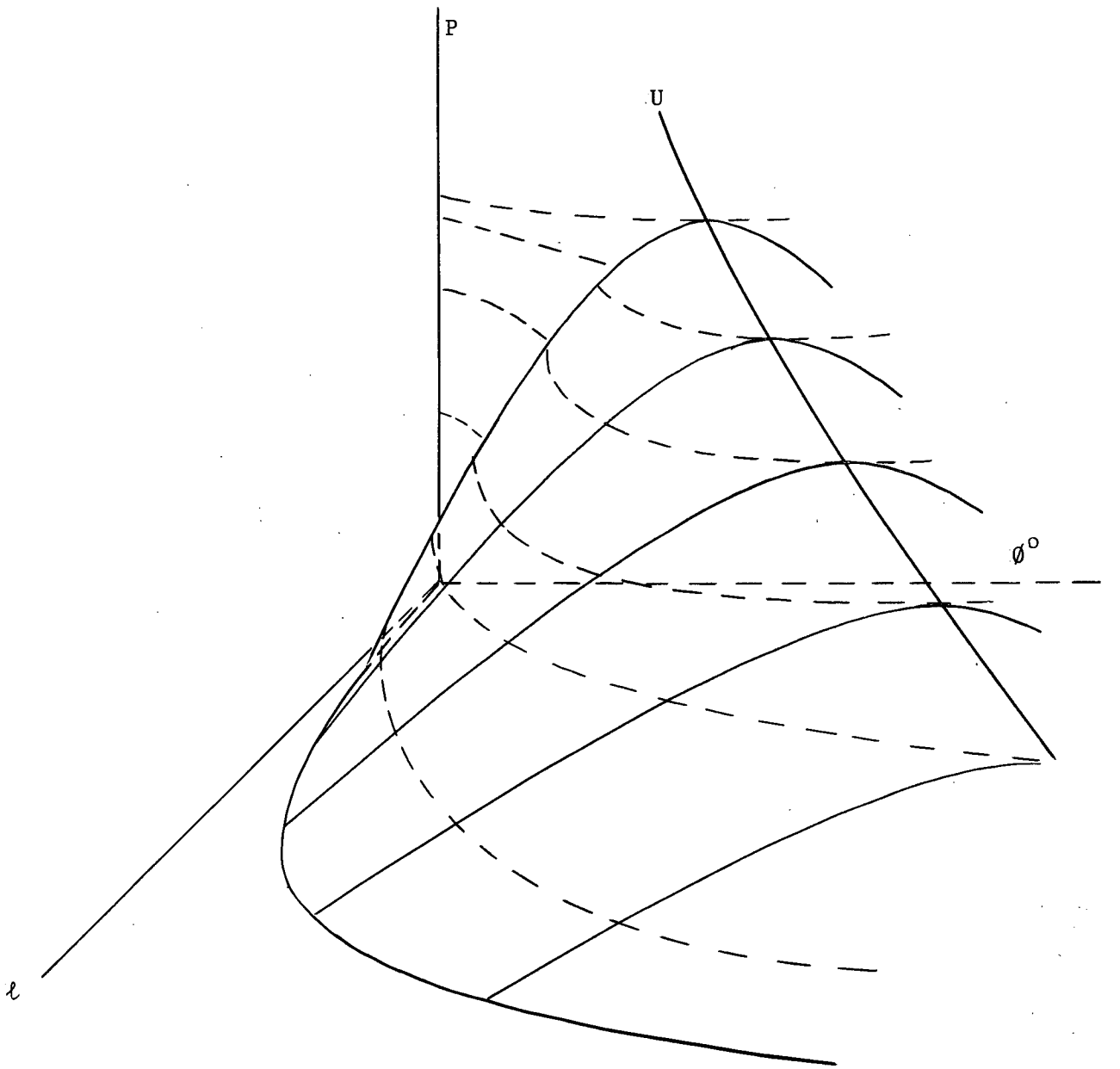

Fig. 2.5 AXIAL LOAD--DEFLECTION--PANEL LENGTH RELATIONSHIP

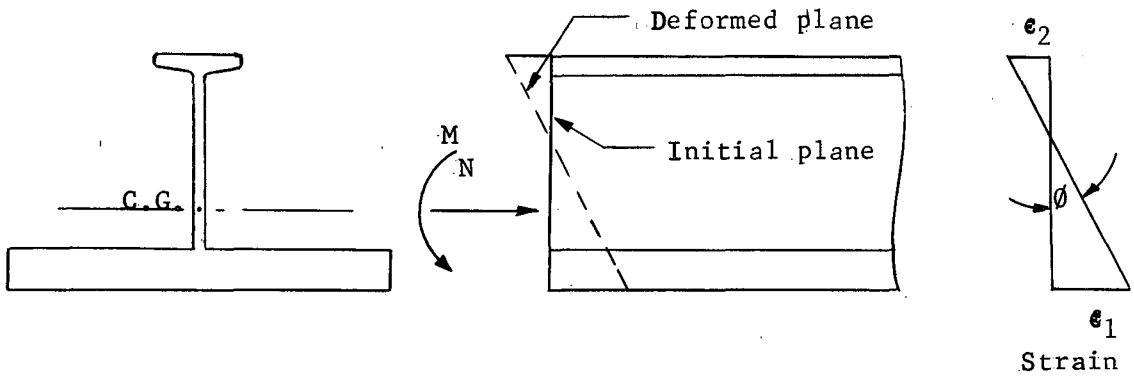

Fig. 3.1 STRAIN DUE TO LOADING

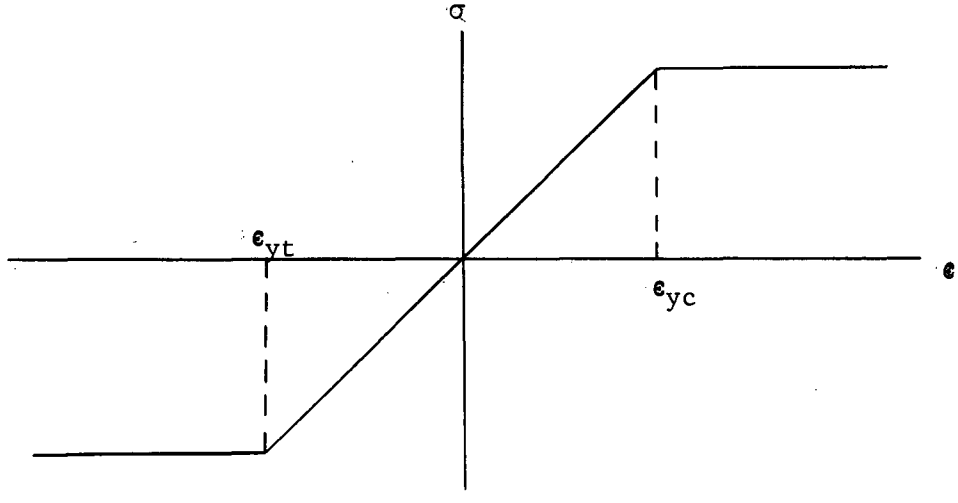

Fig. 3.2 IDEALIZED STRESS-STRAIN DIAGRAM

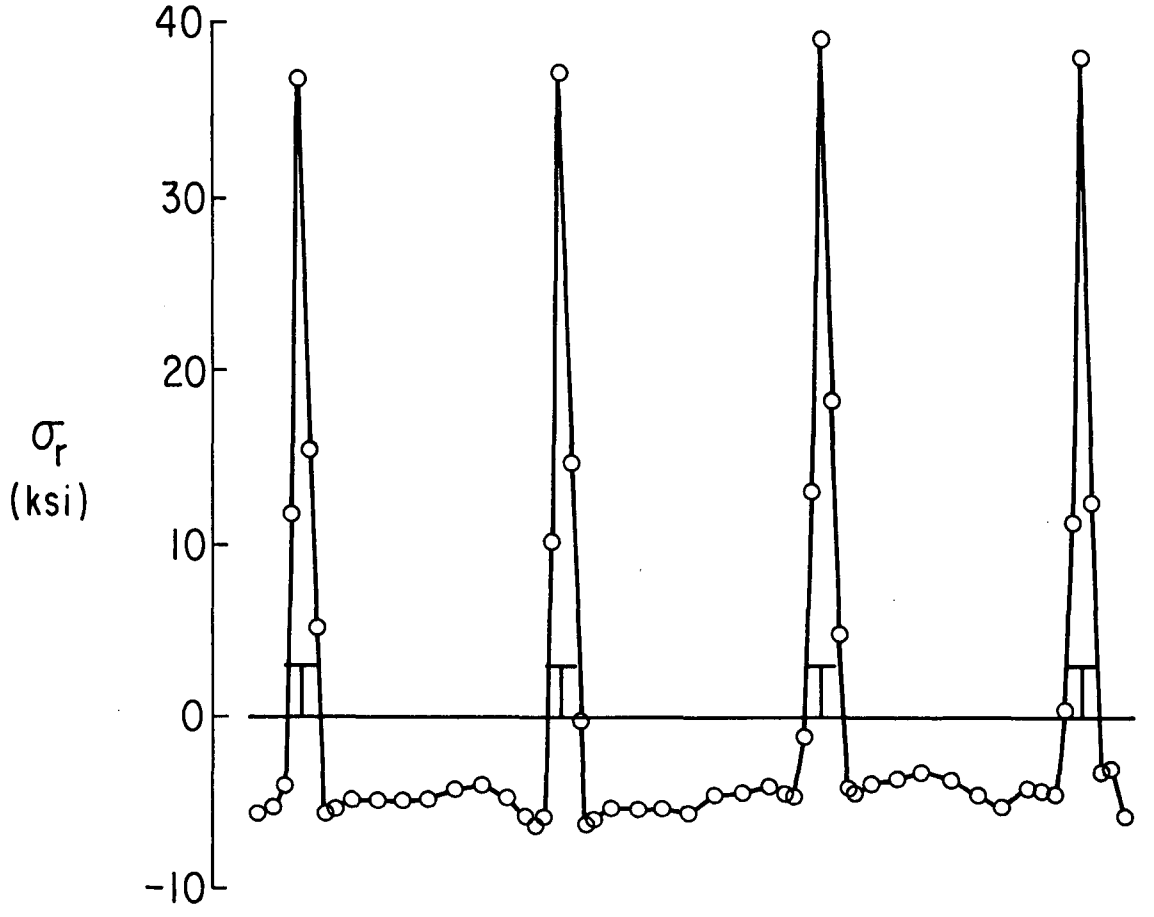

FIG. 3.3 RESIDUAL STRESSES IN PLATE

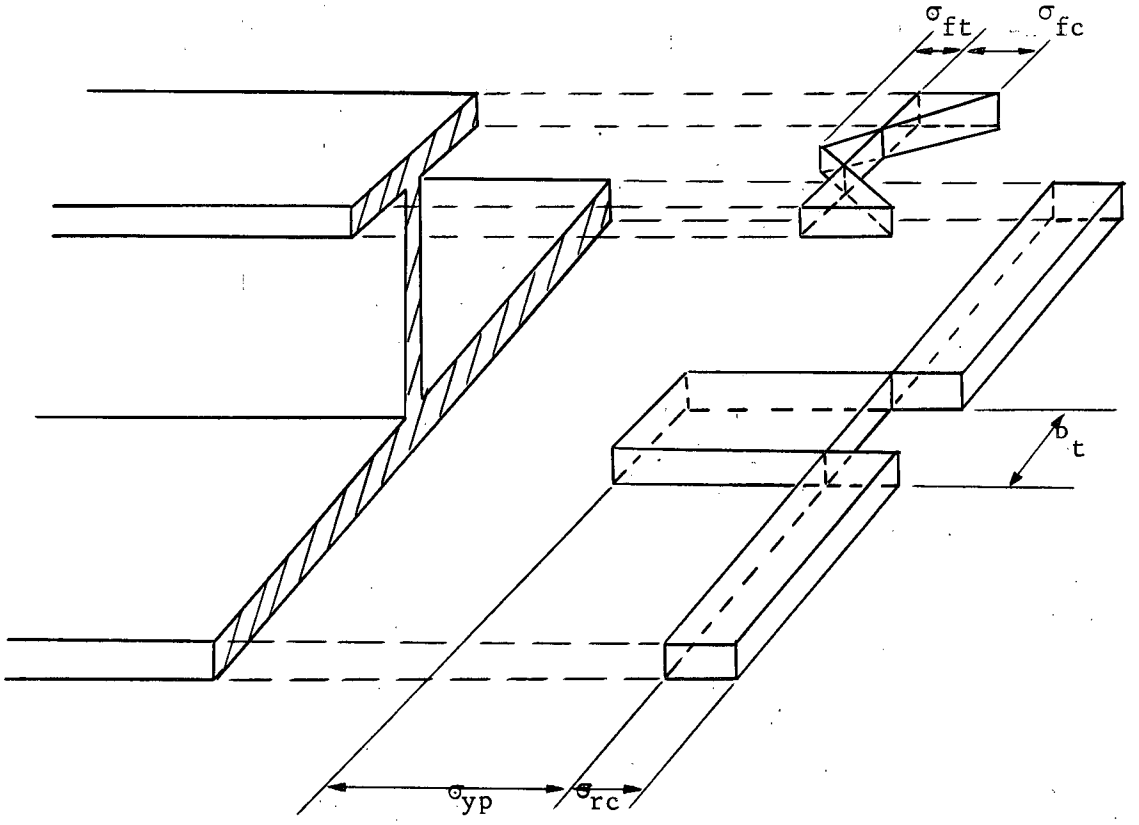

Fig. 3.4 SIMPLIFIED RESIDUAL STRESS DISTRIBUTION

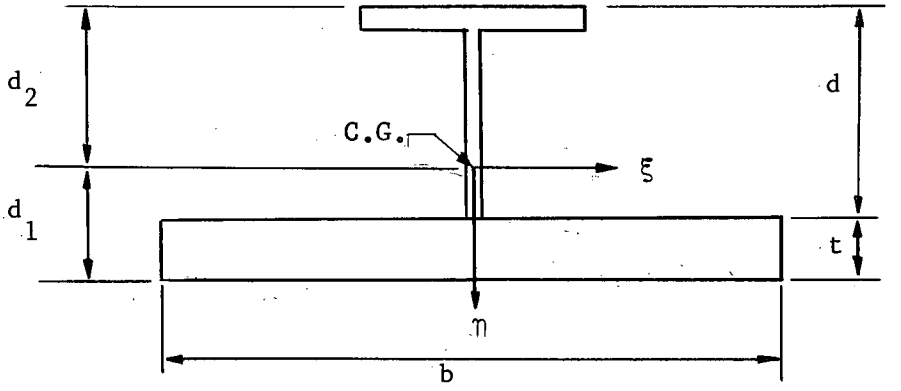

Fig. 3.5 IDEALIZED CROSS SECTION

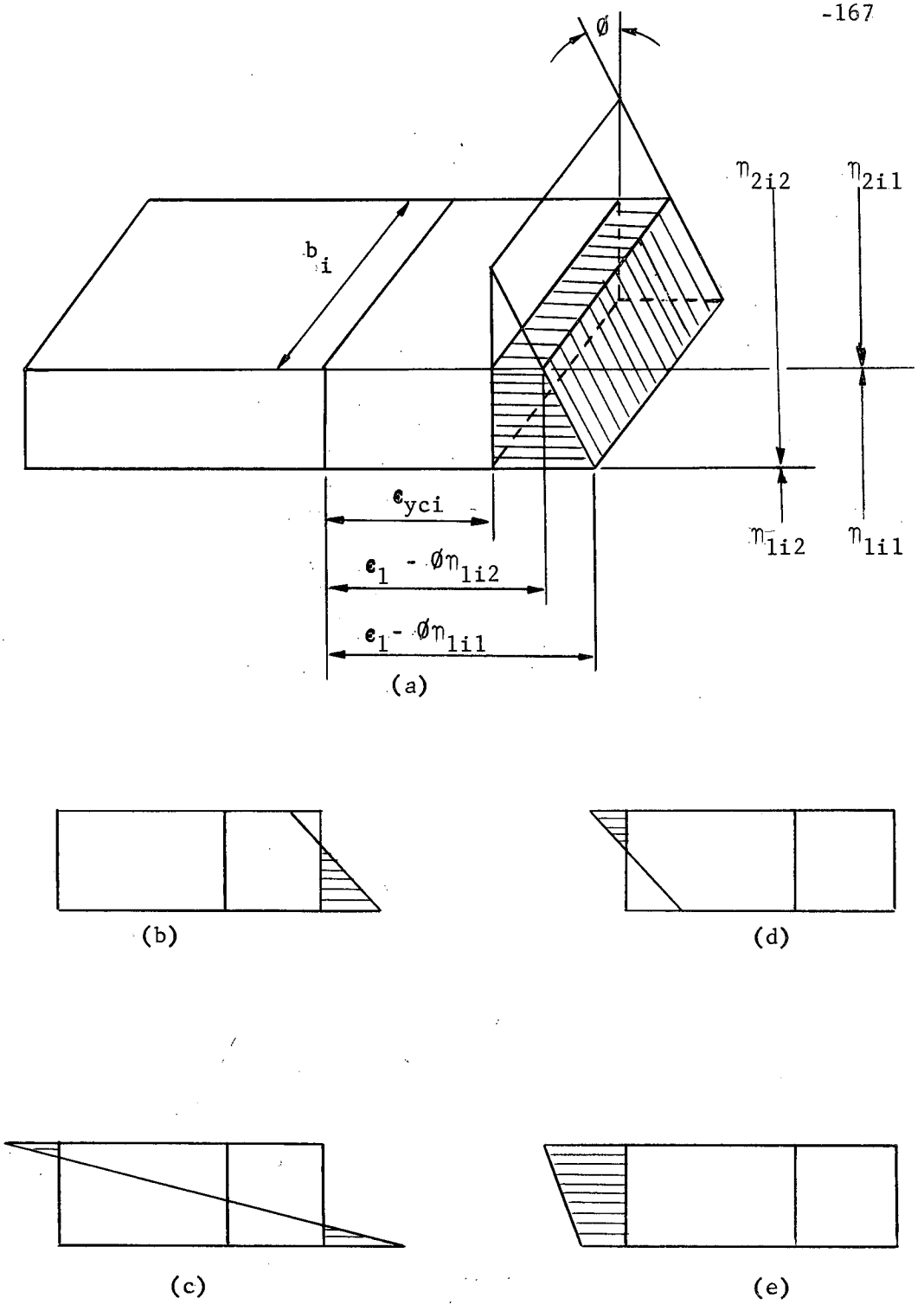

Fig. 3.6 PLASTIC STRAINS, CONSTANT EFFECTIVE YIELD STRAIN

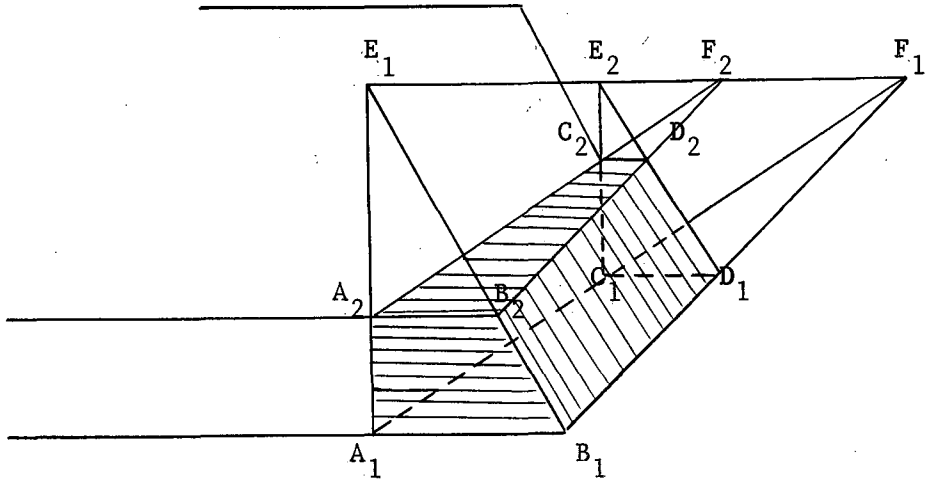

$$(\text{SHADED VOLUME}) = (A_1 E_1 B_1 F_1 - A_2 E_1 B_2 F_2) - (C_1 E_2 D_1 F_1 - C_2 E_2 D_2 F_2)$$

(a)

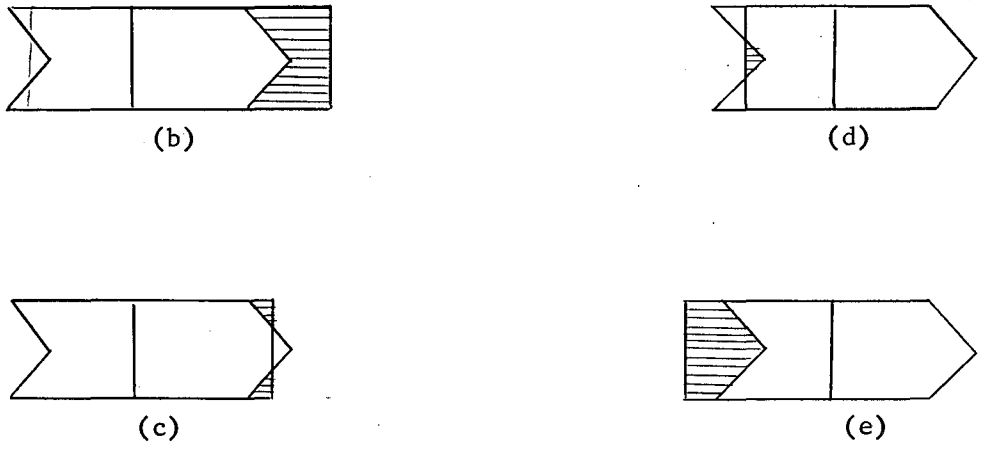

Fig. 3.7 PLASTIC STRAINS, LINERARLY VARYING EFFECTIVE YIELD STRAIN

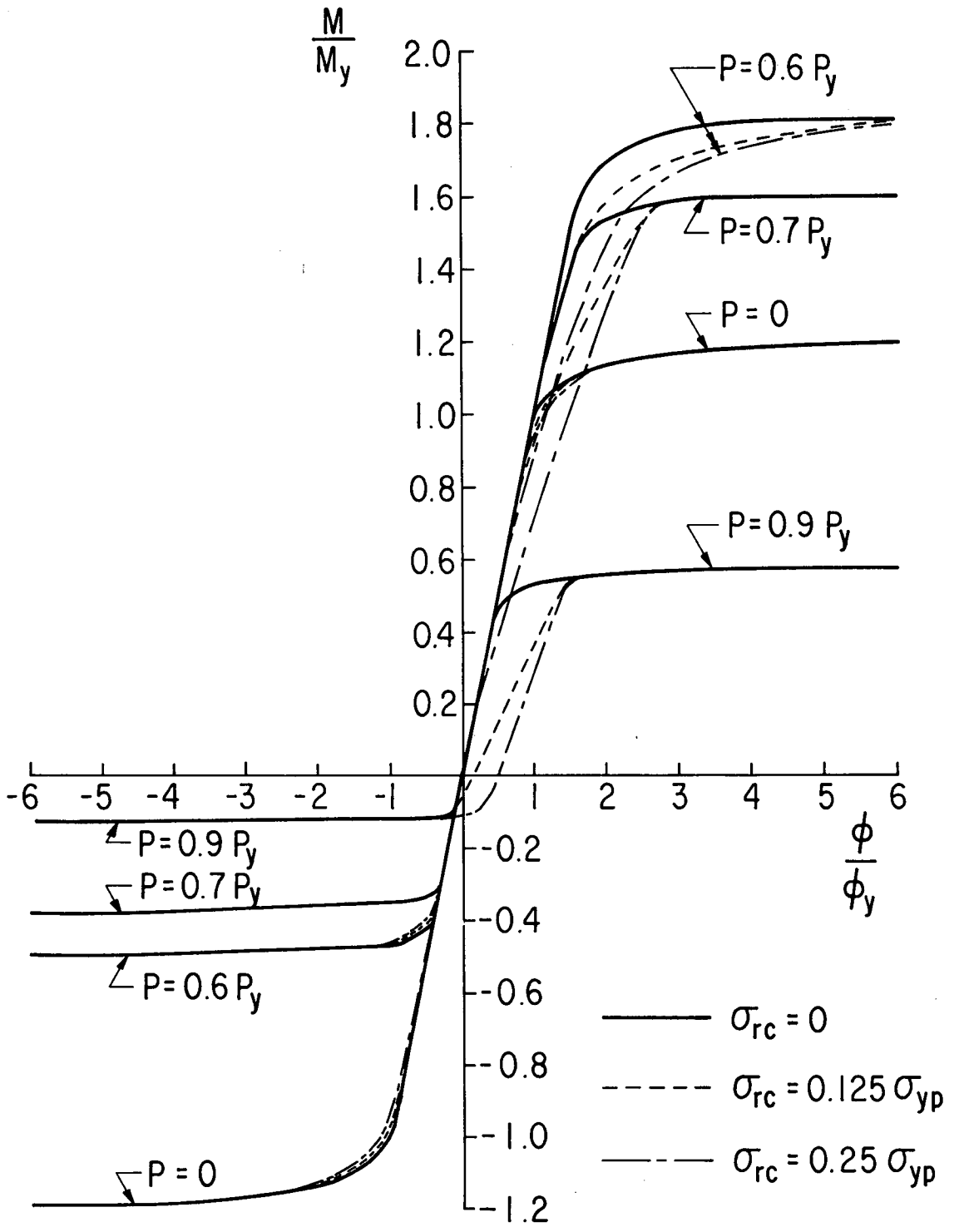

FIG. 3.8 TYPICAL MOMENT-CURVATURE CURVES

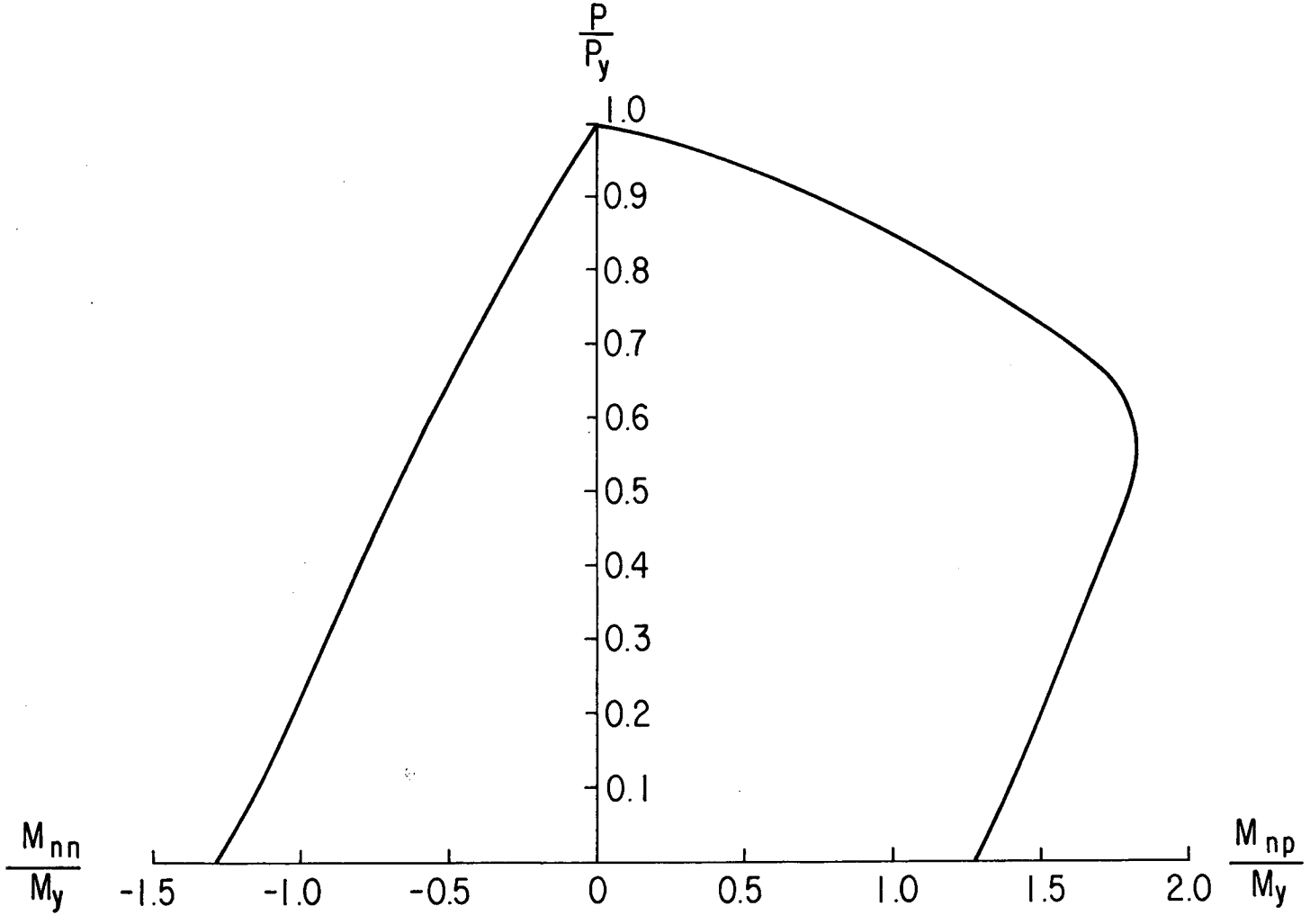

FIG. 3.9 FULL PLASTIC BENDING MOMENT OF A CROSS SECTION

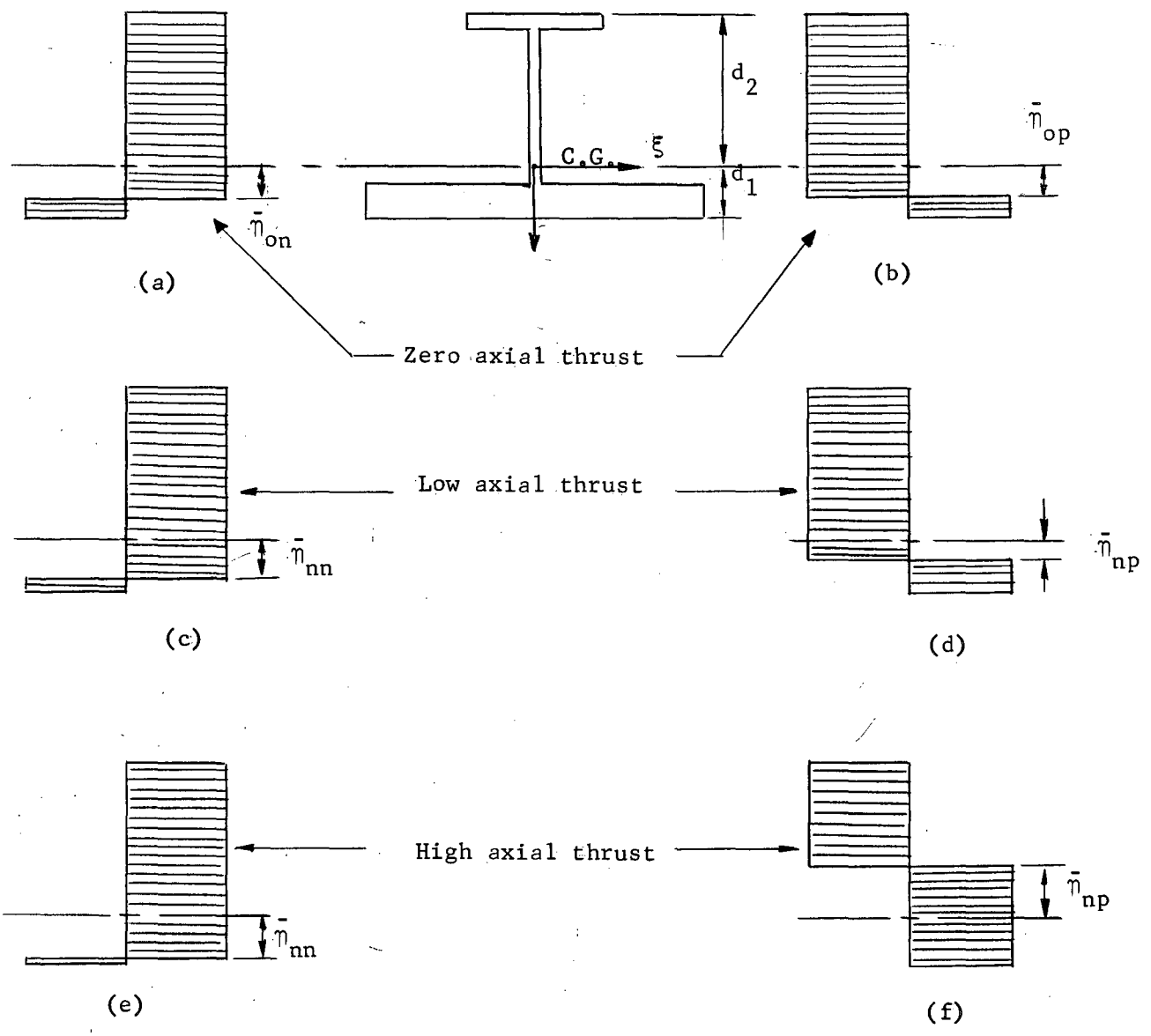

Fig. 3.10 STRESS DISTRIBUTION AT FULL PLASTIFICATION OF THE CROSS SECTION

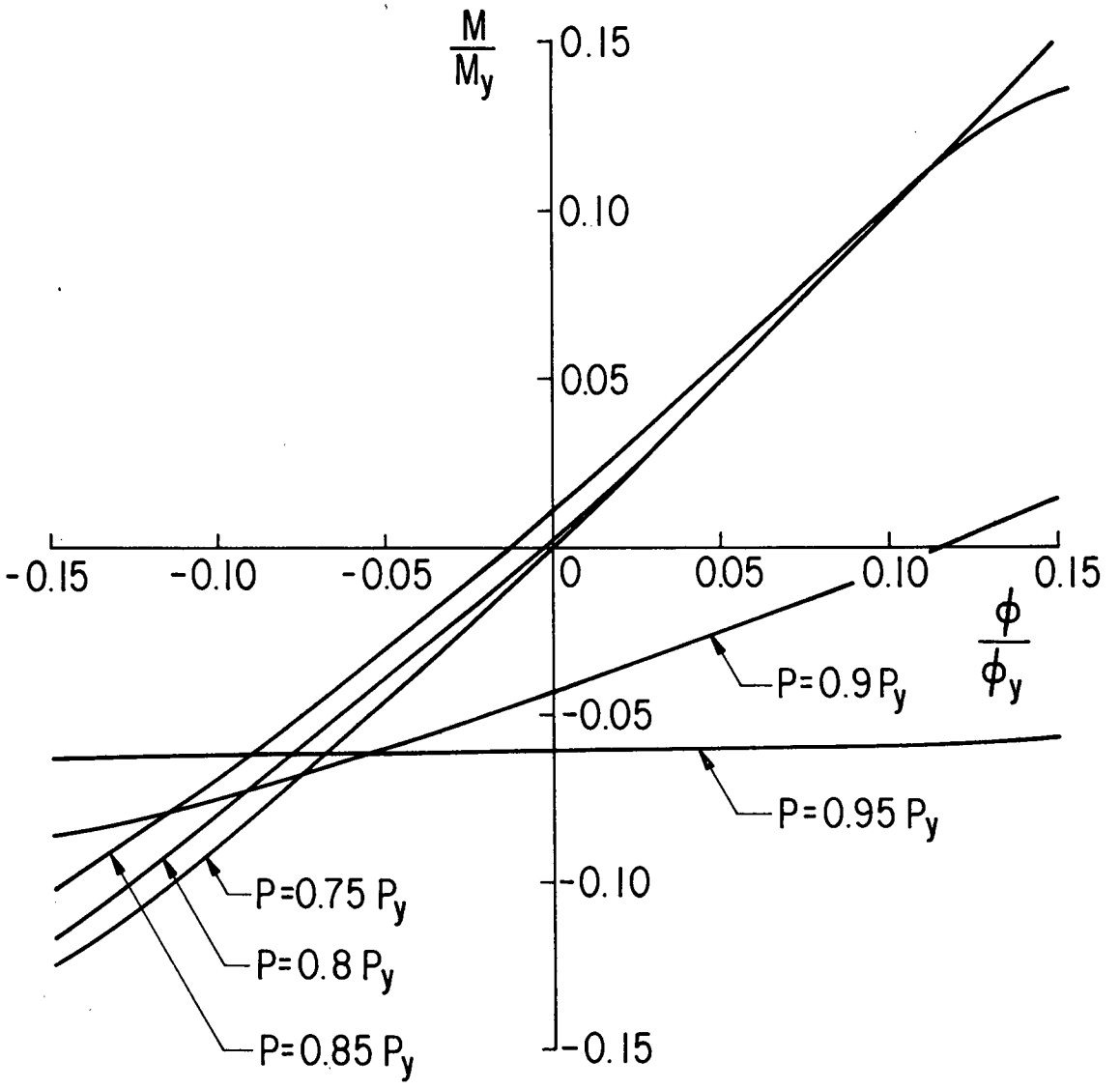

FIG. 3.11 SHIFT OF MOMENT-CURVATURE CURVES FROM ORIGIN, $\sigma_{rc} = 0.125\ \sigma_{yp}$

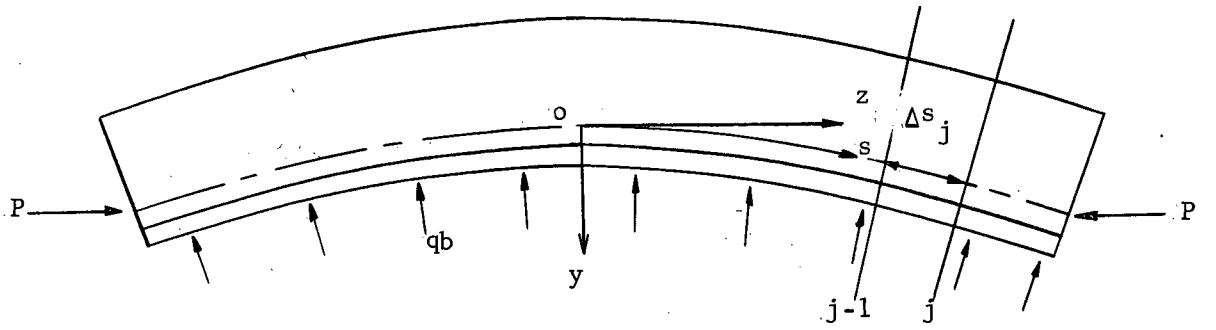

(a)

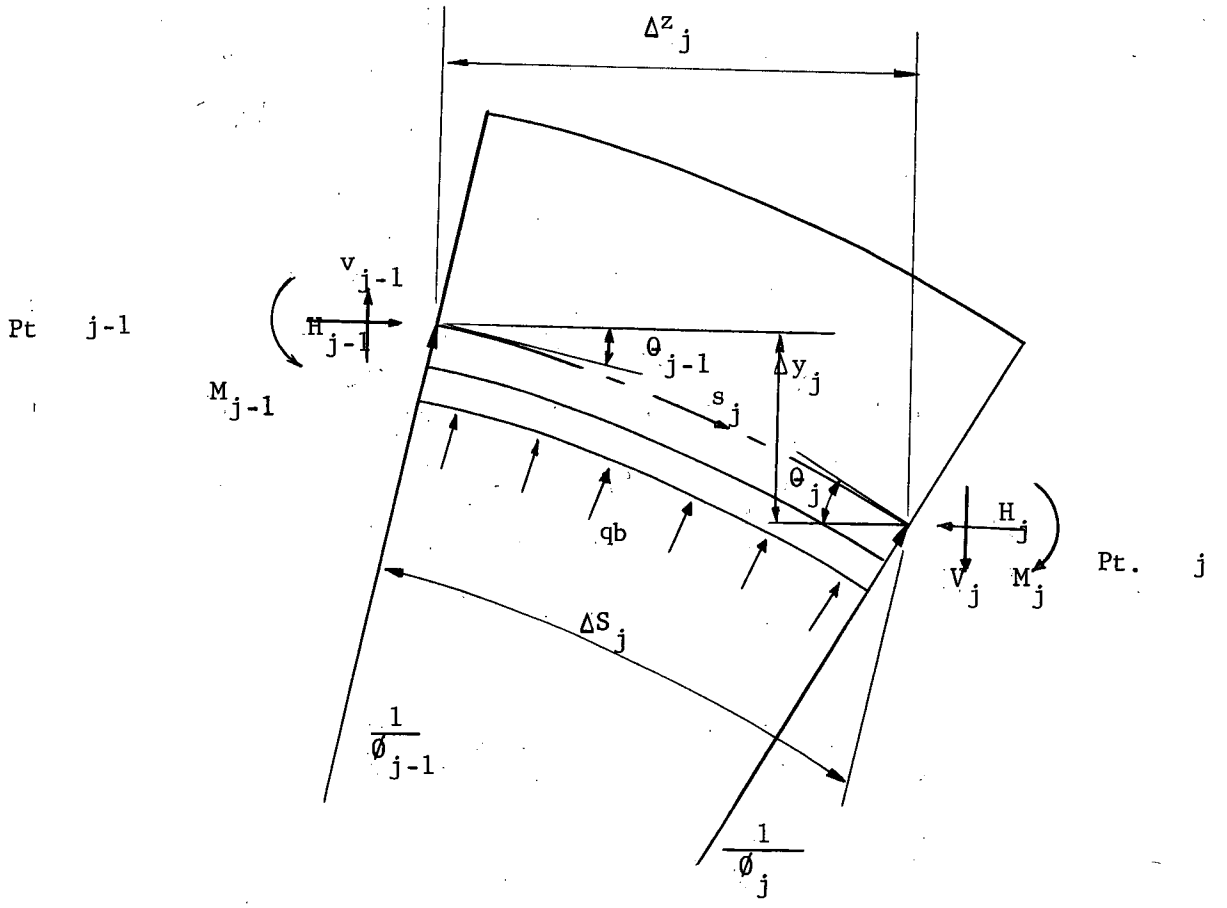

(b)

Fig. 4.1 THE j-TH SEGMENT OF STEPWISE INTEGRATION

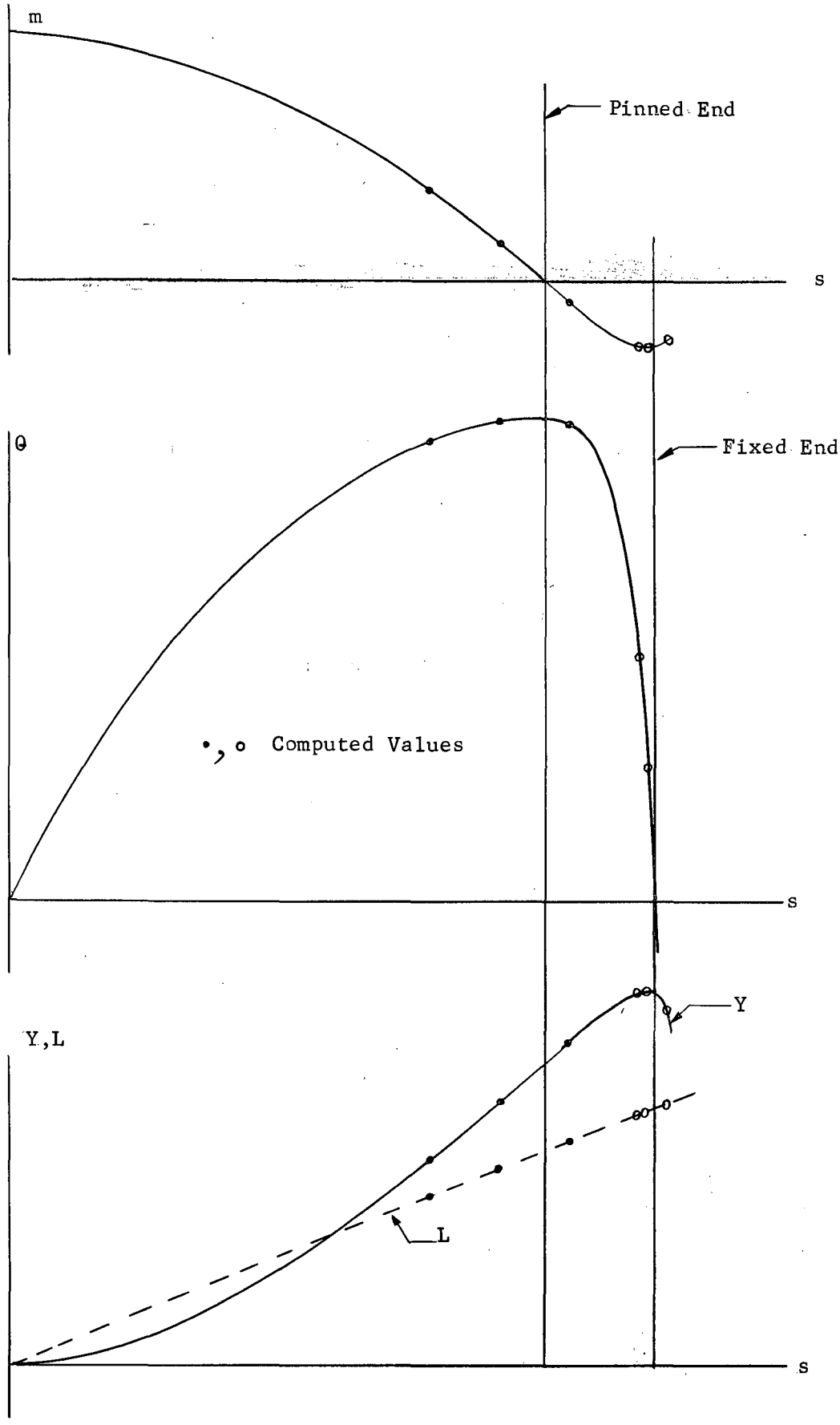

Fig. 4.2 VARIATION OF VARIABLES, m θ, Y, and L, ALONG THE CENTROIDAL AXIS

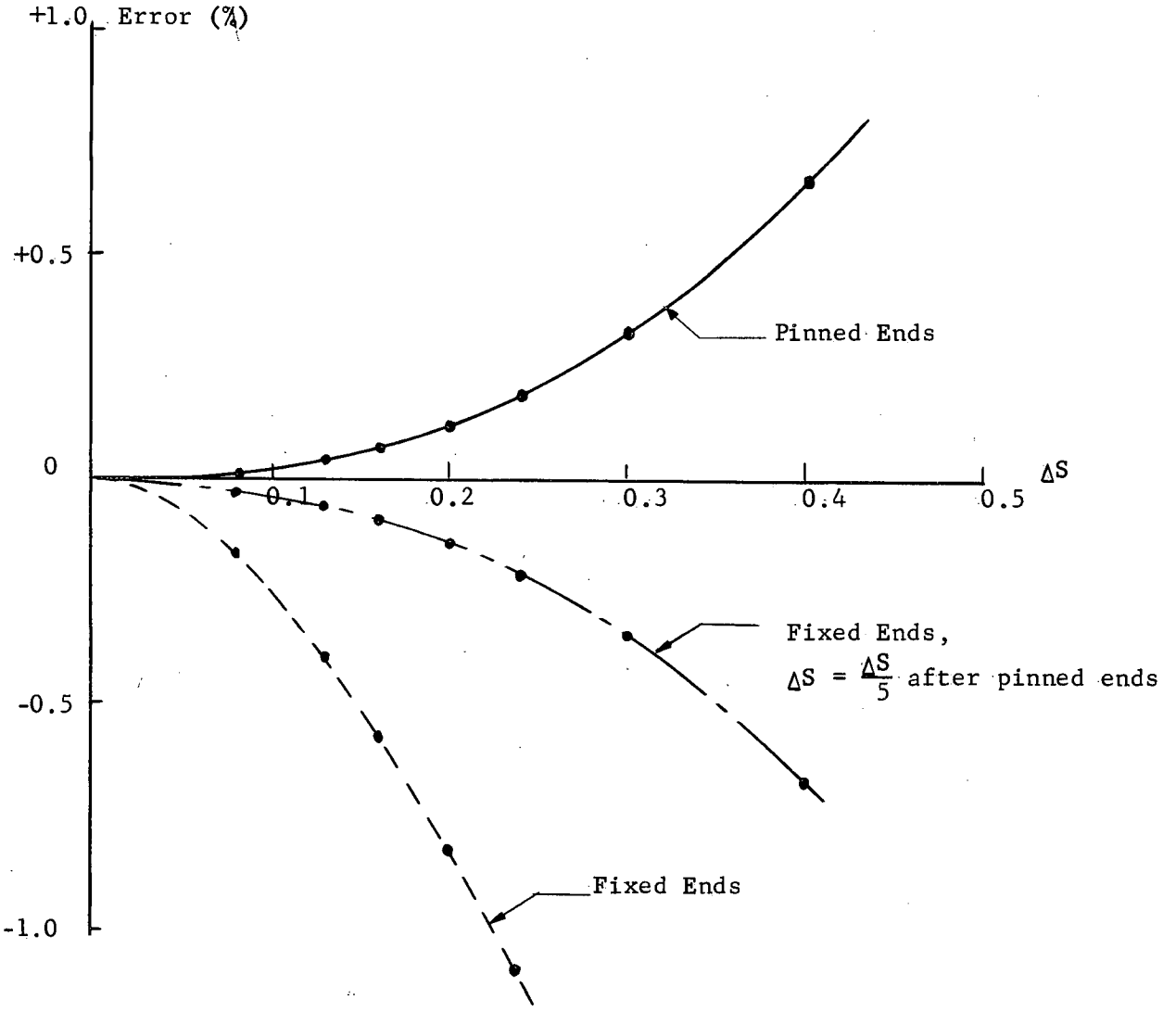

Fig. 4.3 ERROR IN STEPWISE INTEGRATION, ERROR vs. SEGMENTAL LENGTH

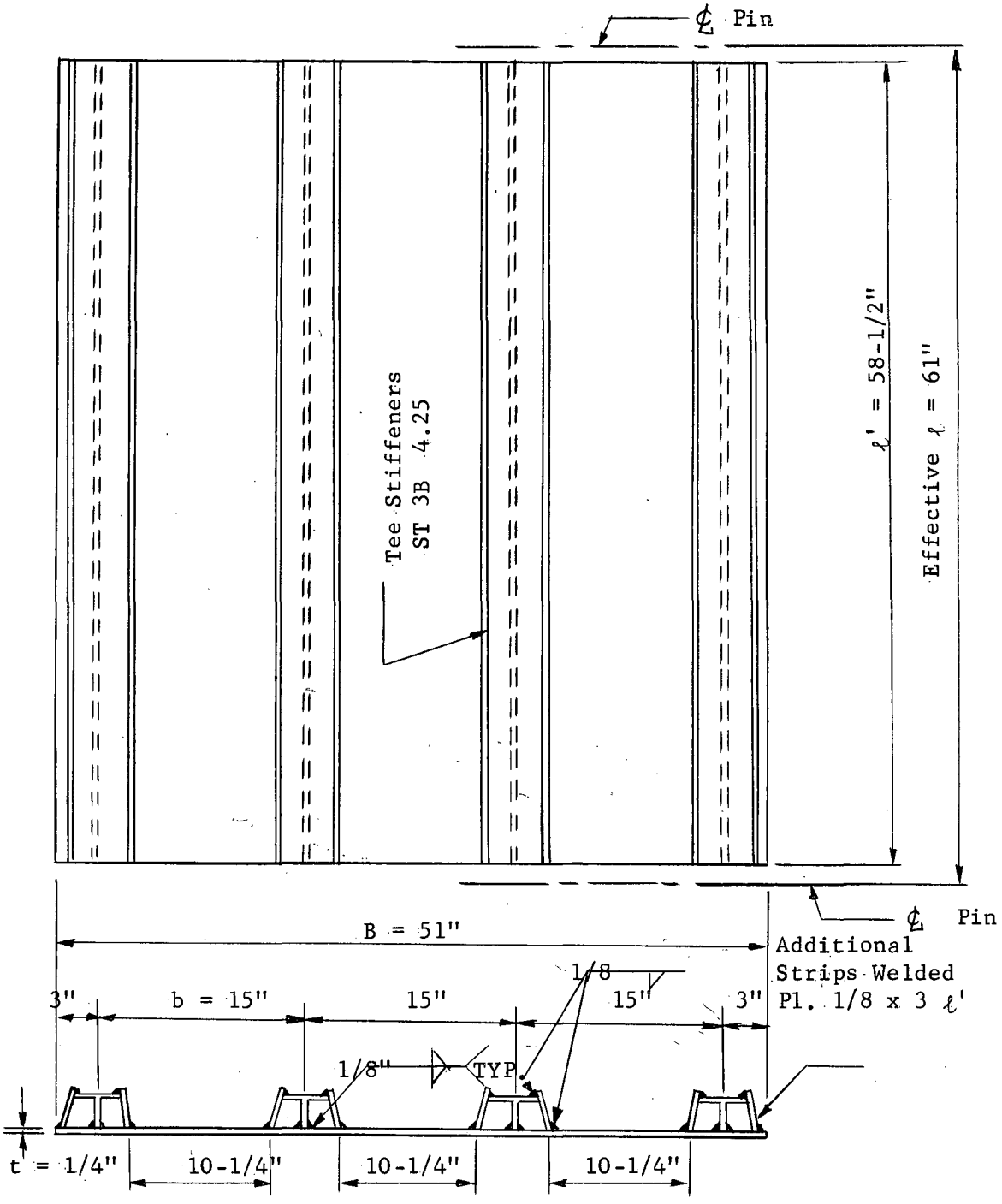

Fig. 4.4 TEST SPECIMEN DIMENSIONS (T-5)
Scale: 1" = 1'-0"

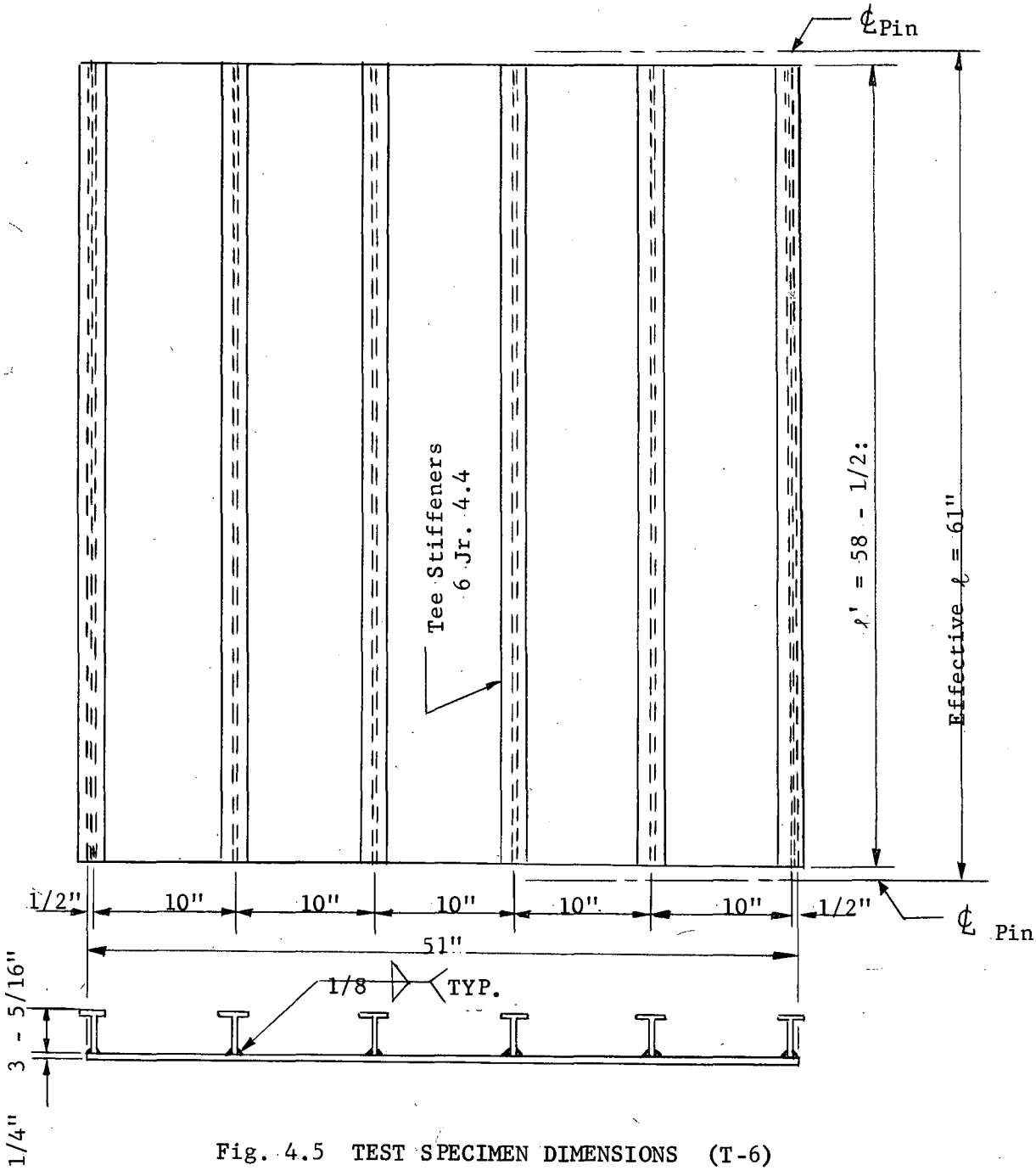

Fig. 4.5 TEST SPECIMEN DIMENSIONS (T-6)

Scale: 1" = 1'-0"

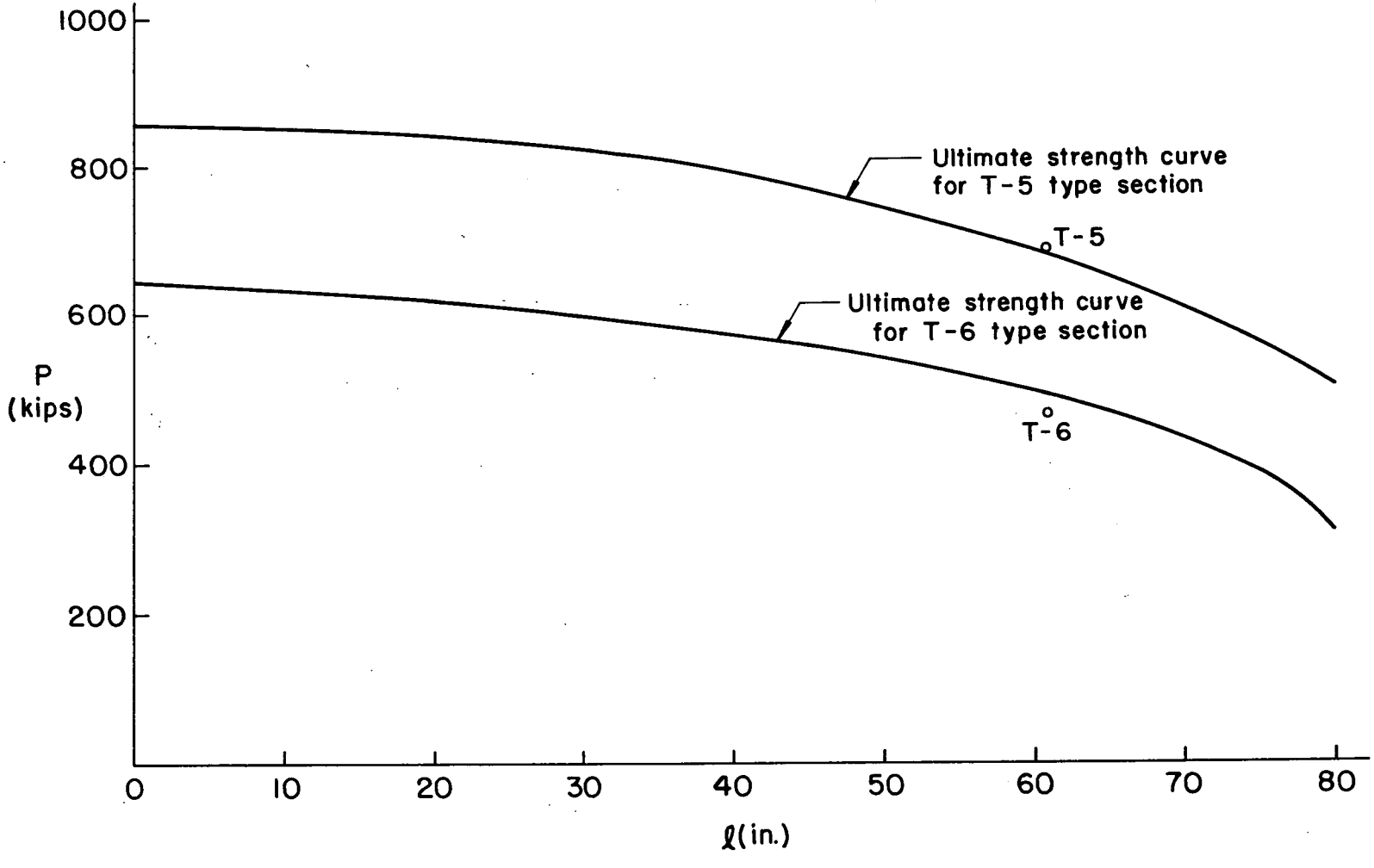

FIG. 4.6 ULTIMATE STRENGTH CURVES AND TEST RESULTS

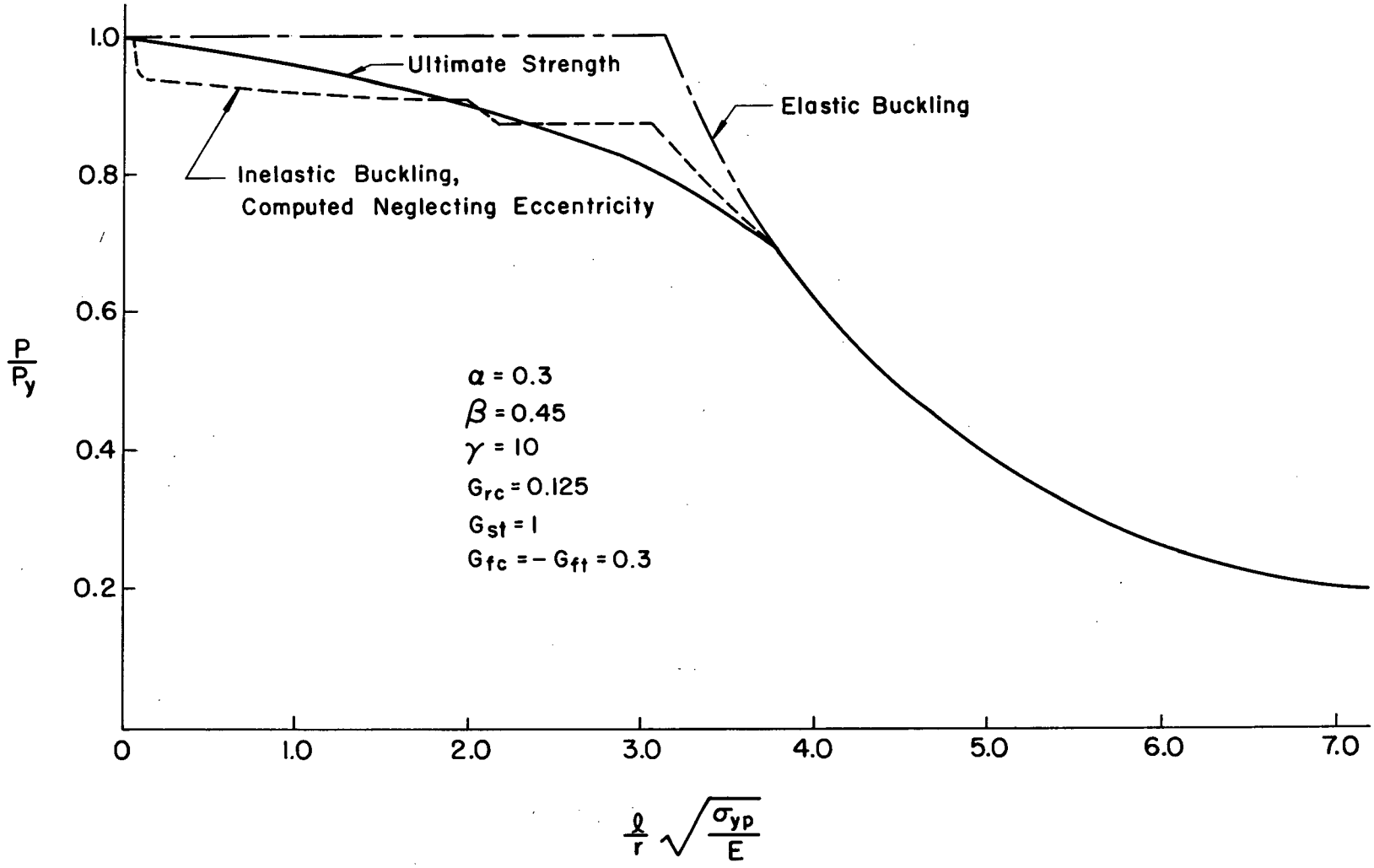

FIG. 4.7 ULTIMATE STRENGTH OF CENTRALLY LOADED STIFFENED PLATE PANELS, PINNED ENDS

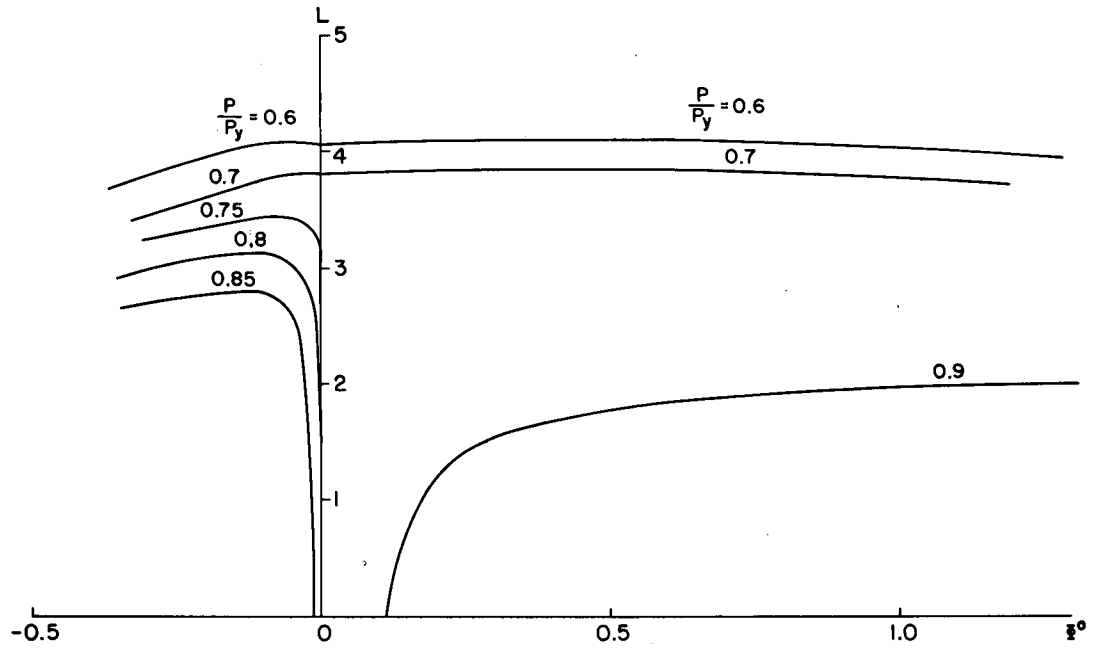

FIG. 4.8 PANEL LENGTH vs. DEFLECTION RELATIONSHIP OF CENTRALLY LOADED STIFFENED PLATE PANEL, PINNED ENDS

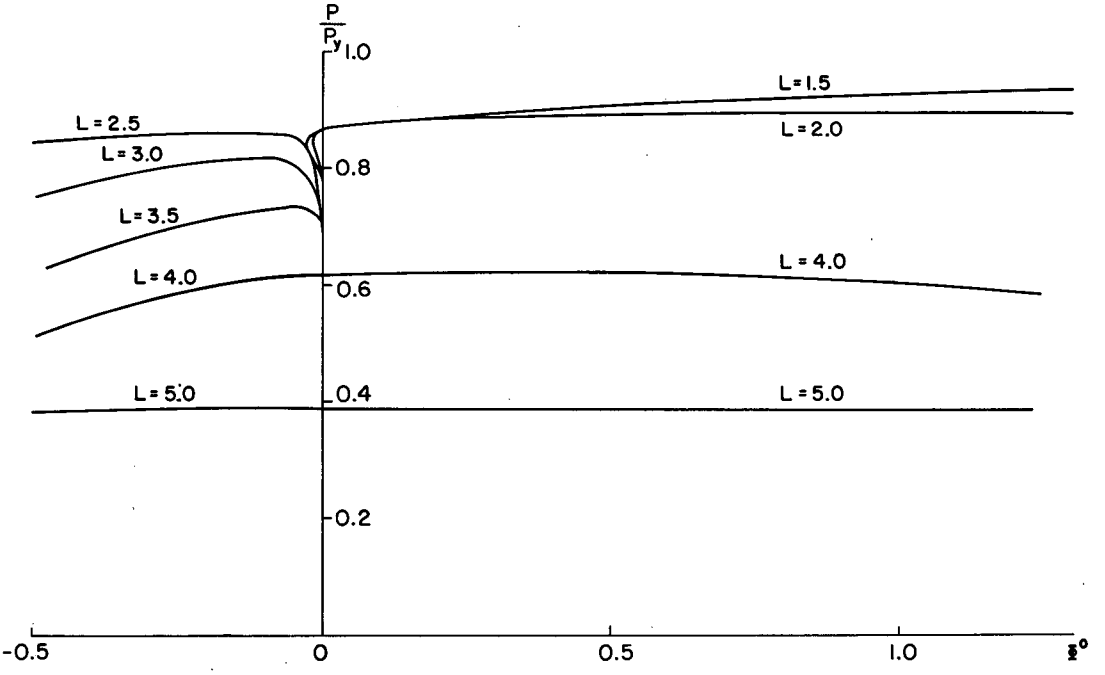

FIG. 4.9 LOAD DEFLECTION CURVES FOR CENTRALLY LOADED STIFFENED PLATE PANELS, PINNED ENDS

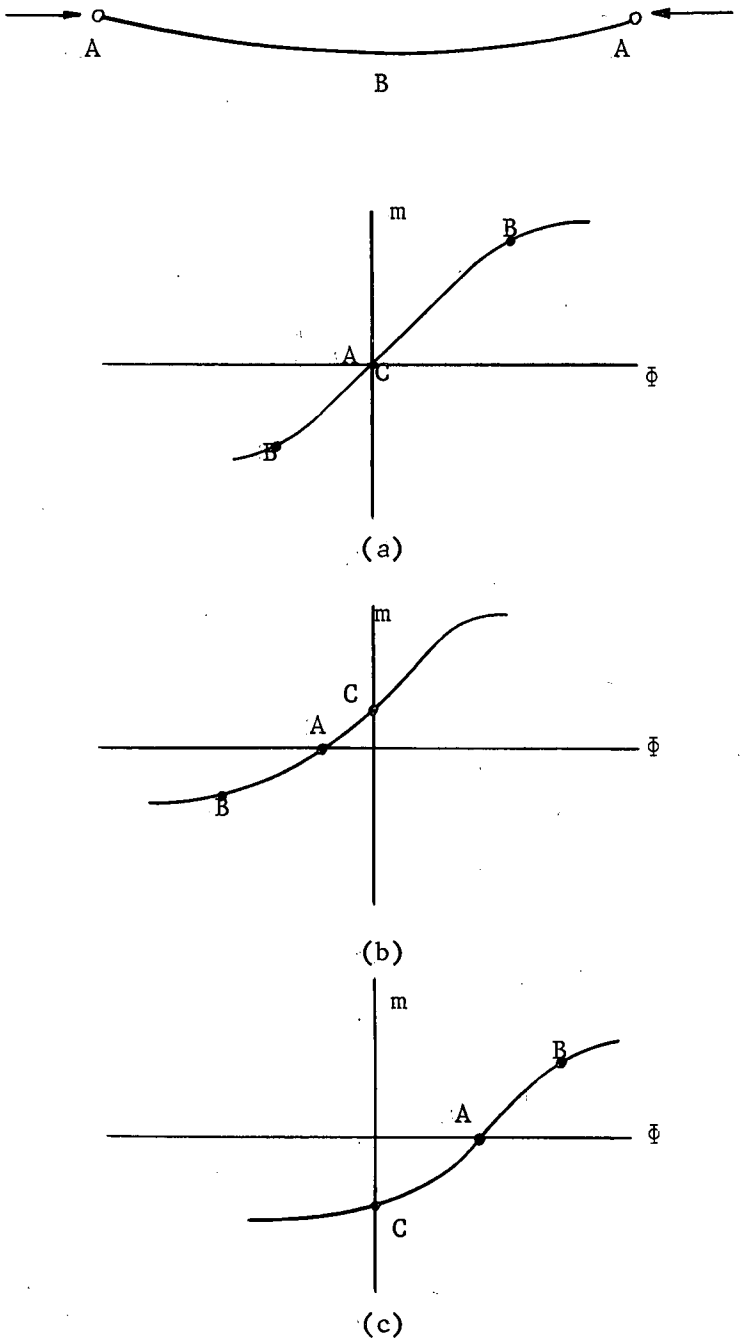

Fig. 4.10 MOMENT-CURVATURE RELATIONSHIP IN CENTRALLY LOADED STIFFENED PLATE PANELS, PINNED ENDS

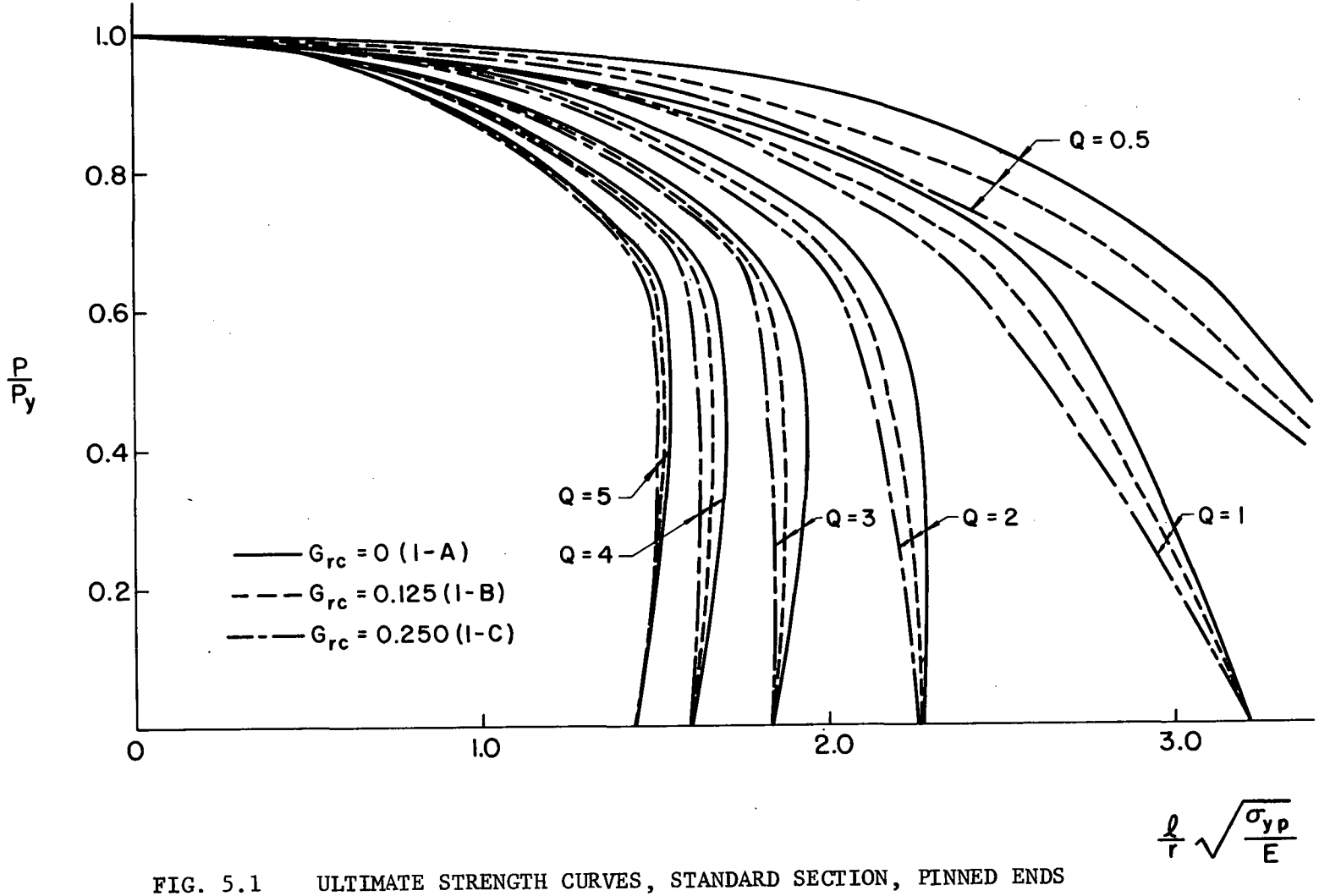

FIG. 5.1 ULTIMATE STRENGTH CURVES, STANDARD SECTION, PINNED ENDS

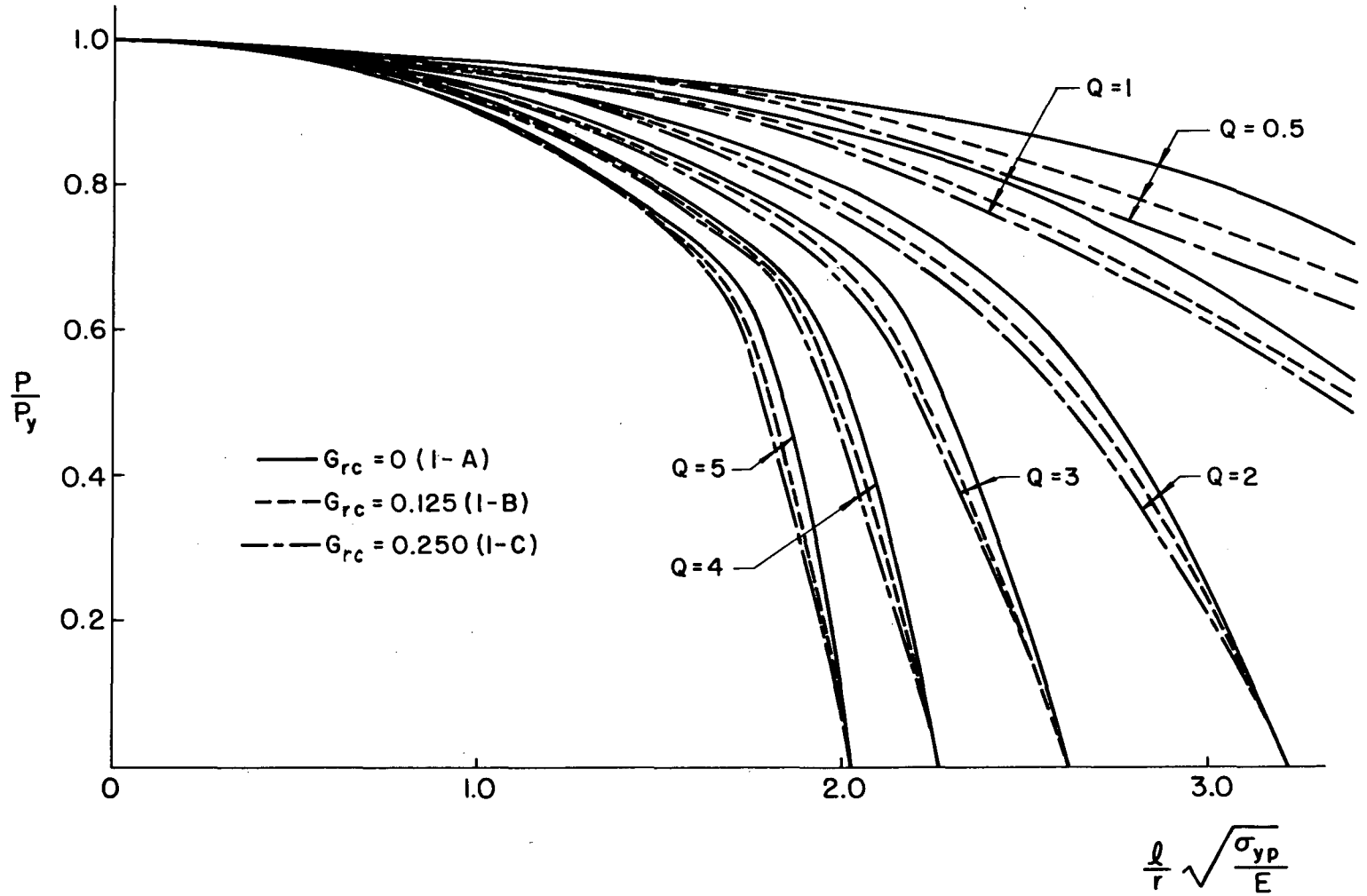

FIG. 5.2 ULTIMATE STRENGTH CURVES, STANDARD SECTION, FIXED ENDS

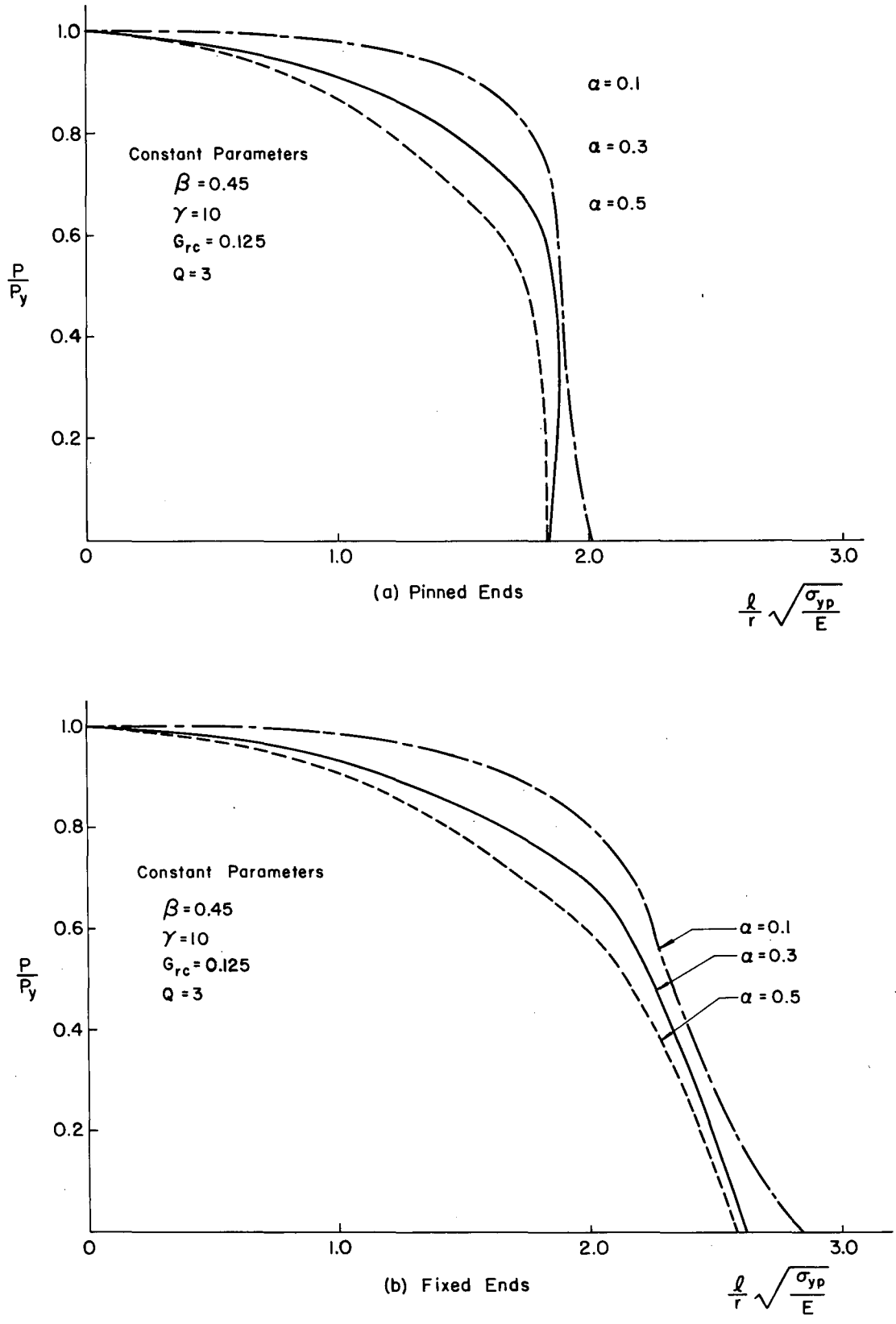

FIG. 5.3 ULTIMATE STRENGTH CURVES, EFFECT OF STIFFENER AREA RATIO

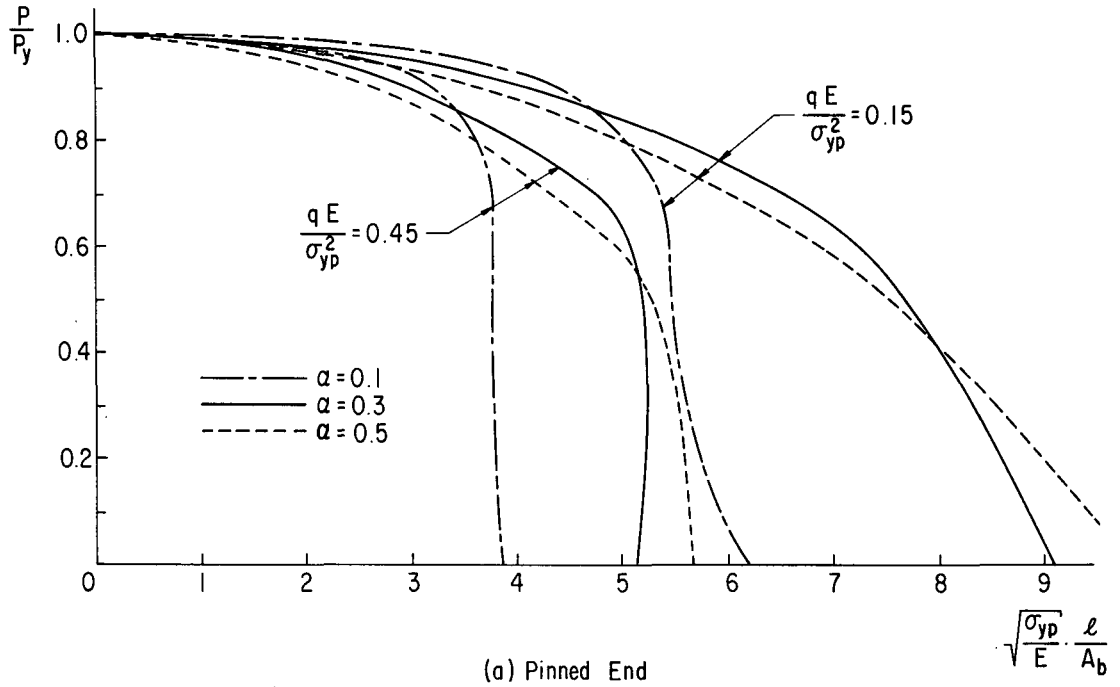

(a) Pinned End

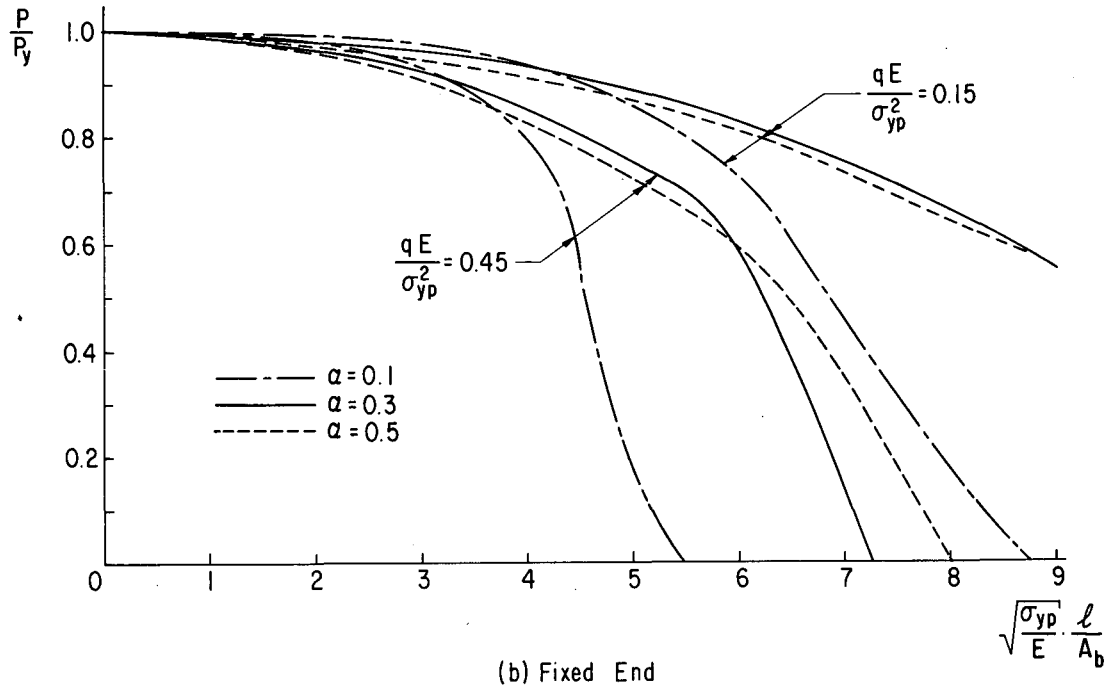

(b) Fixed End

FIG. 5.4 EFFECT OF STIFFENER AREA RATIO

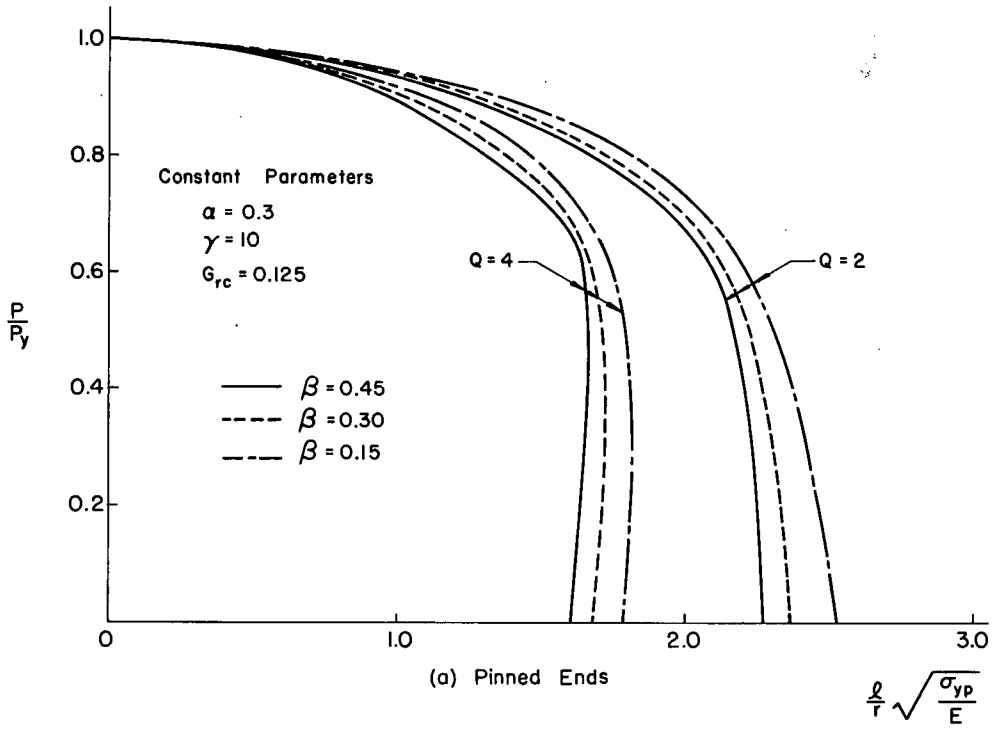

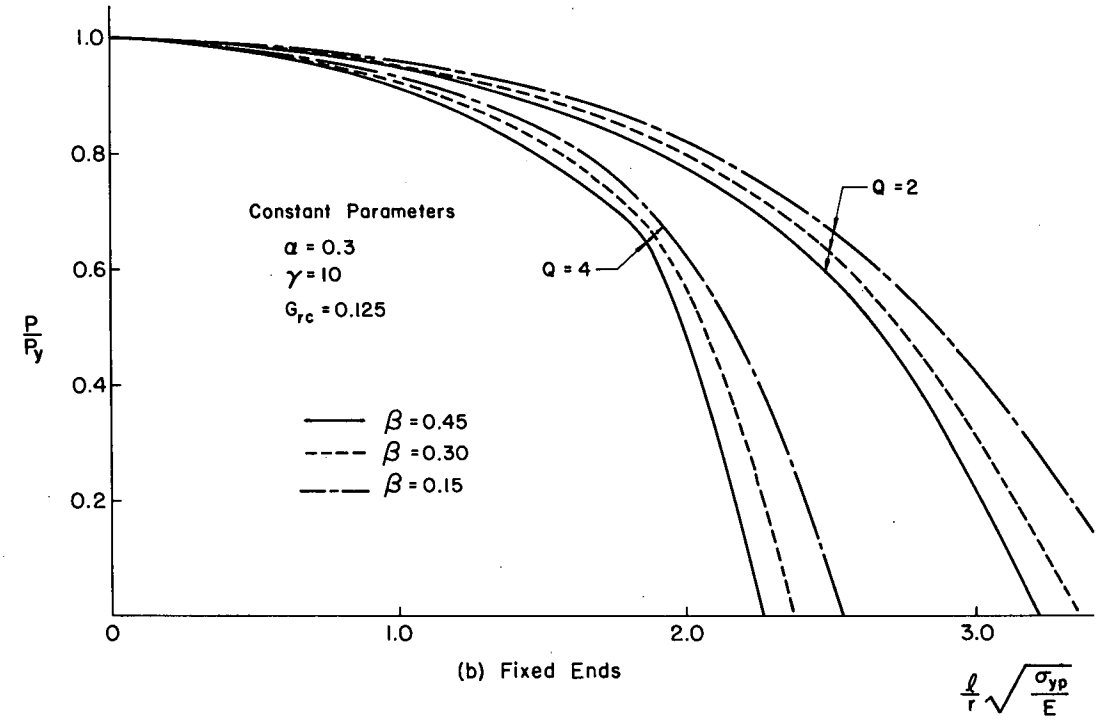

FIG. 5.5 ULTIMATE STRENGTH CURVES, EFFECT OF STIFFENER FLANGE AREA RATIO

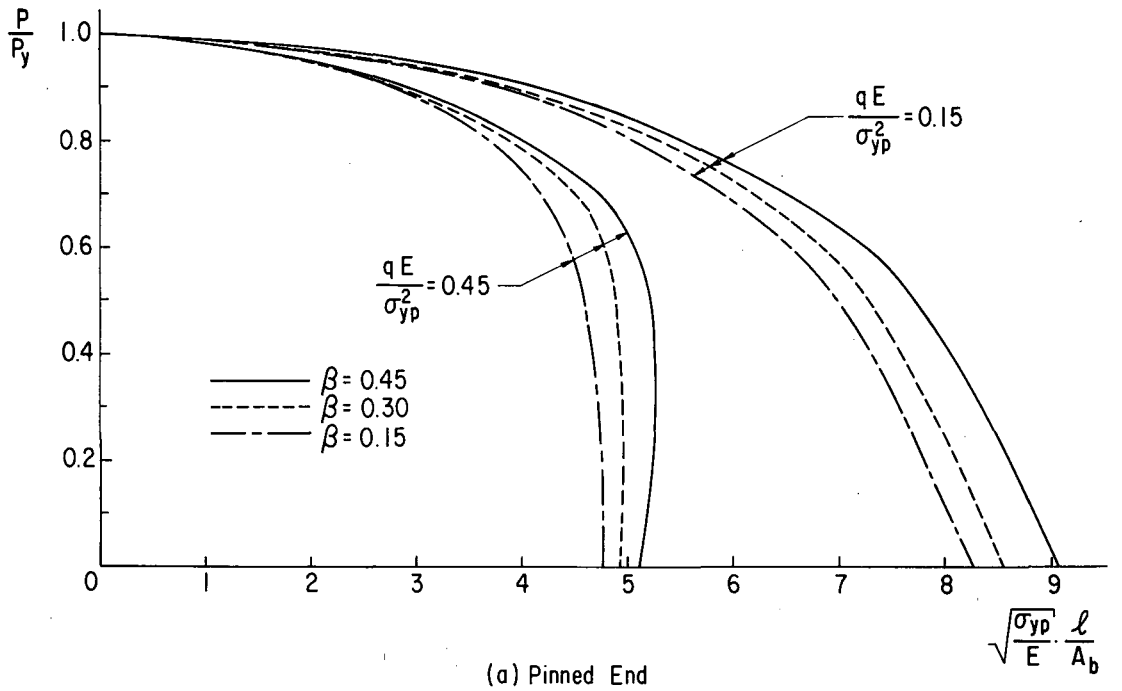

(a) Pinned End

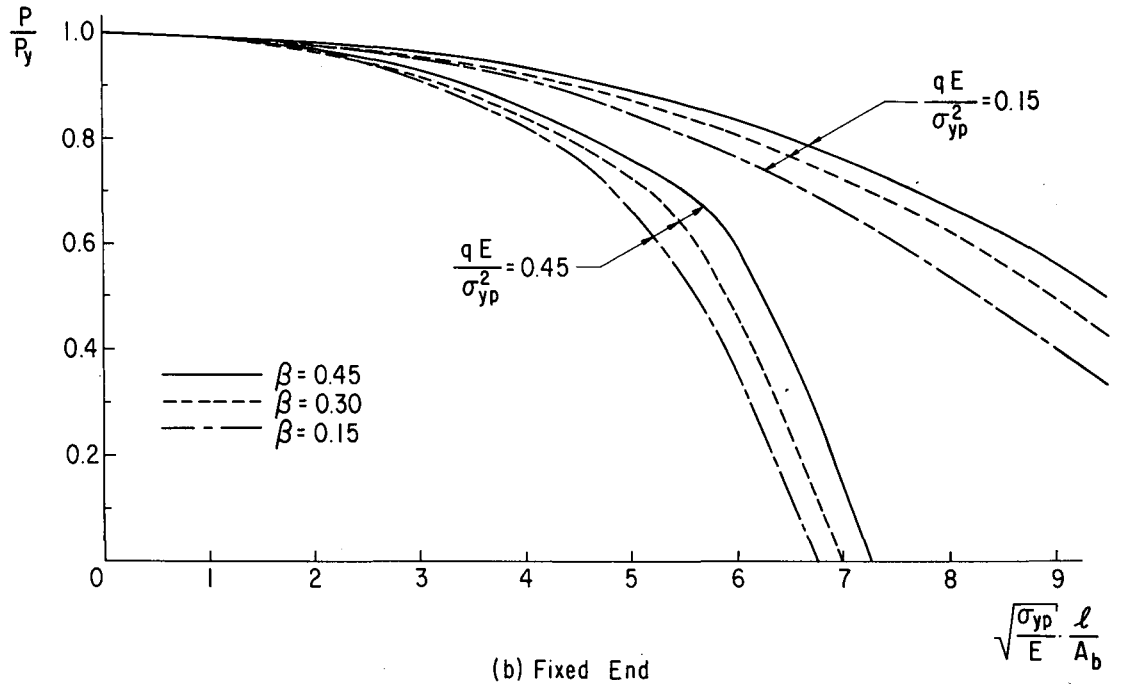

(b) Fixed End

FIG. 5.6 EFFECT OF STIFFENER FLANGE AREA RATIO

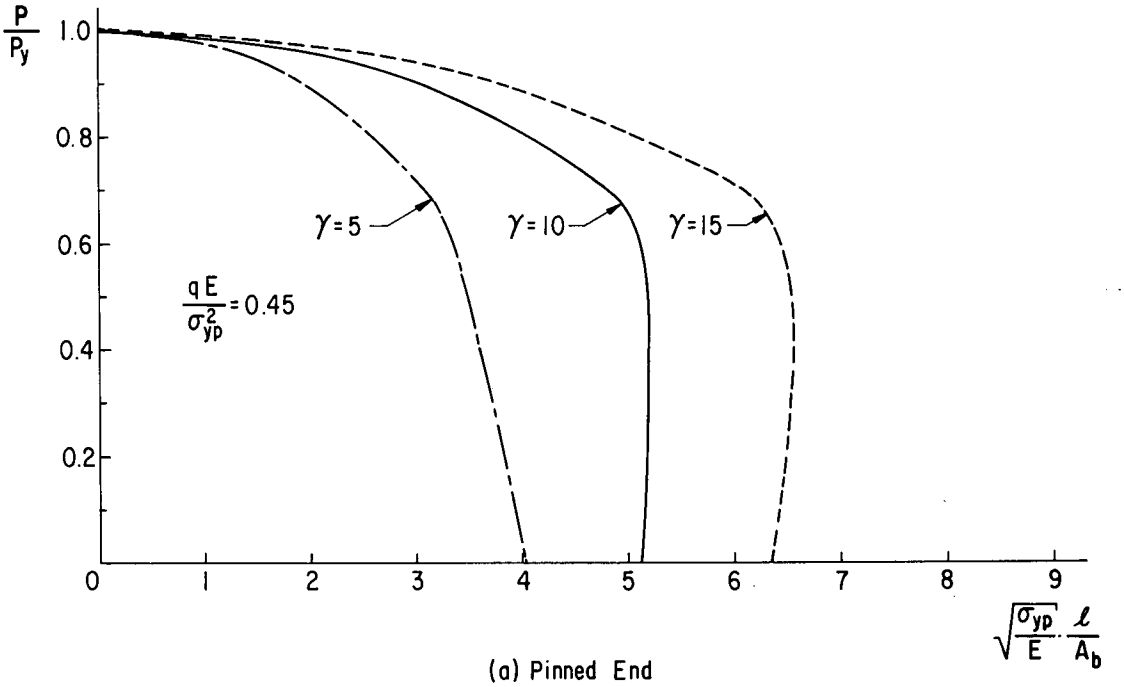

(a) Pinned End

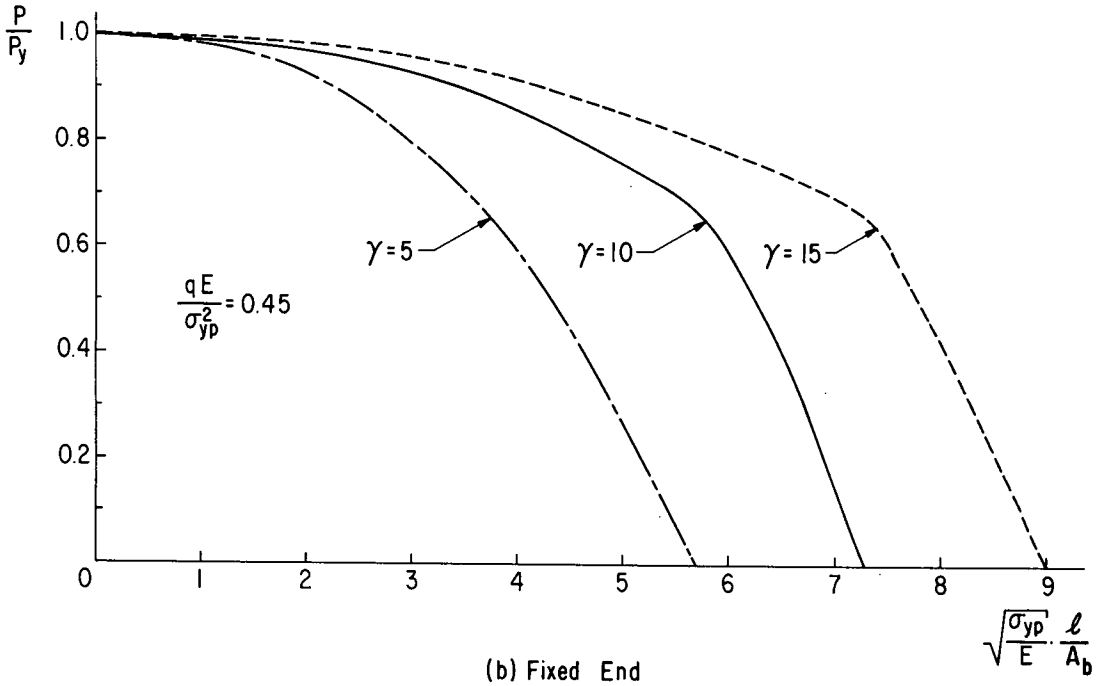

(b) Fixed End

FIG. 5.7 EFFECT OF STIFFENER DEPTH TO PLATE THICKNESS RATIO

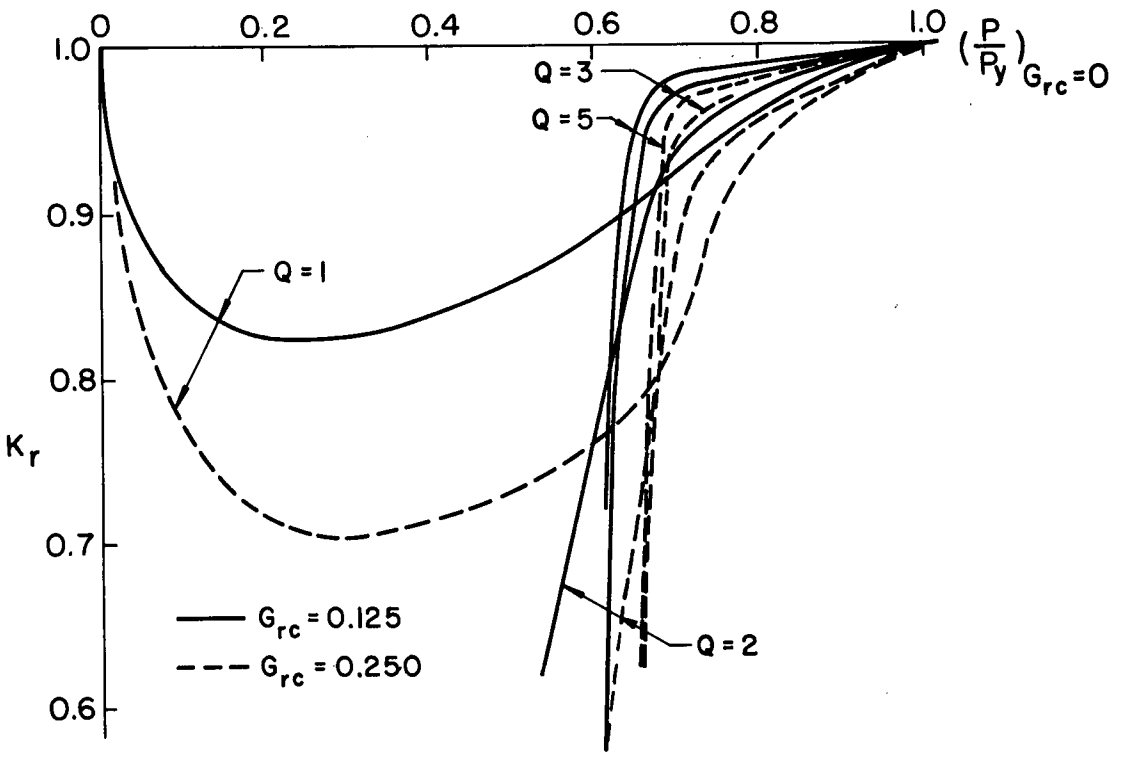

(a) Pinned Ends

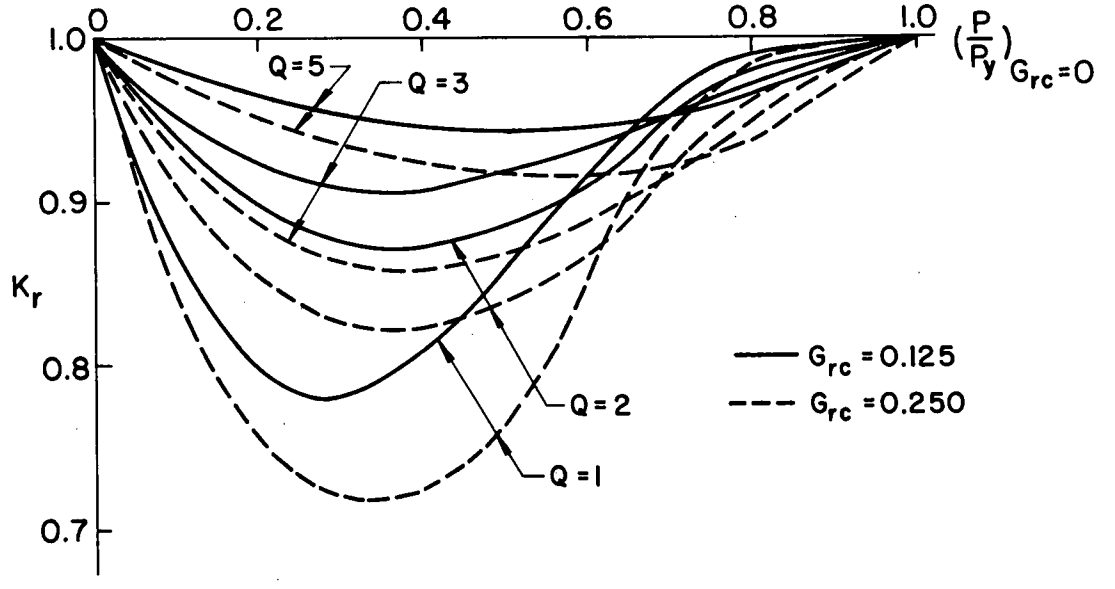

(b) Fixed Ends

FIG. 5.8 MODIFICATION FACTOR FOR RESIDUAL STRESSES

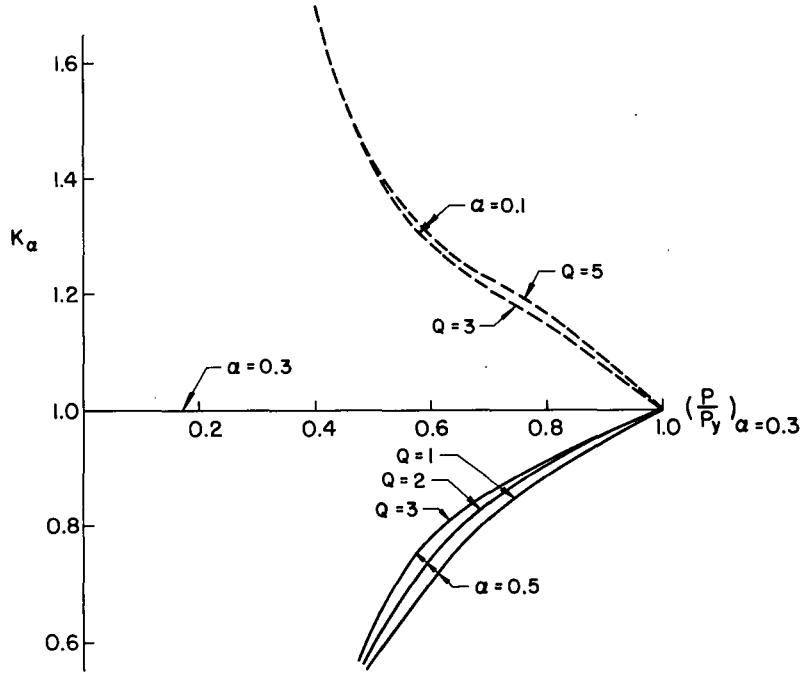

(a) Pinned Ends

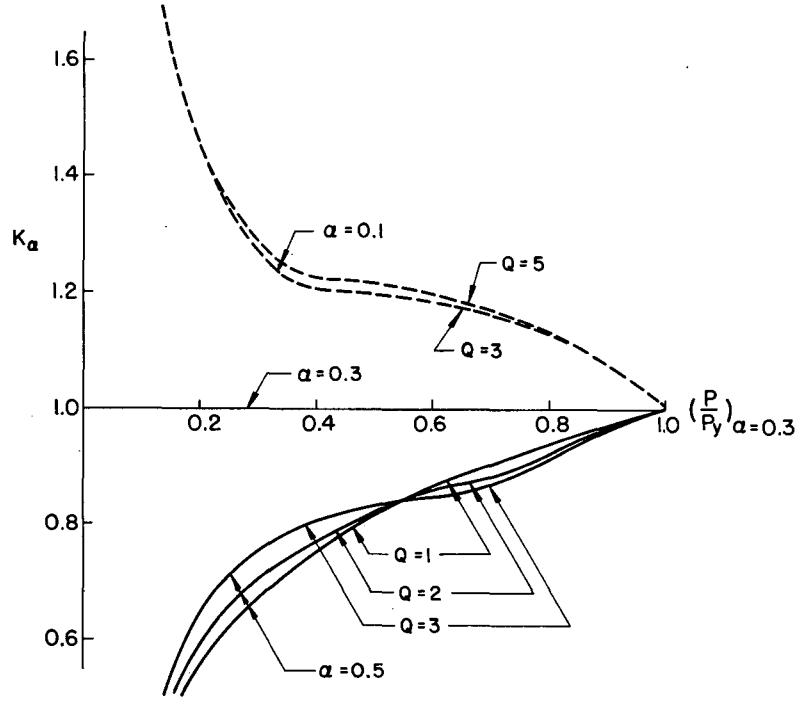

(b) Fixed Ends

FIG. 5.9 MODIFICATION FACTOR FOR STIFFENER AREA RATIO

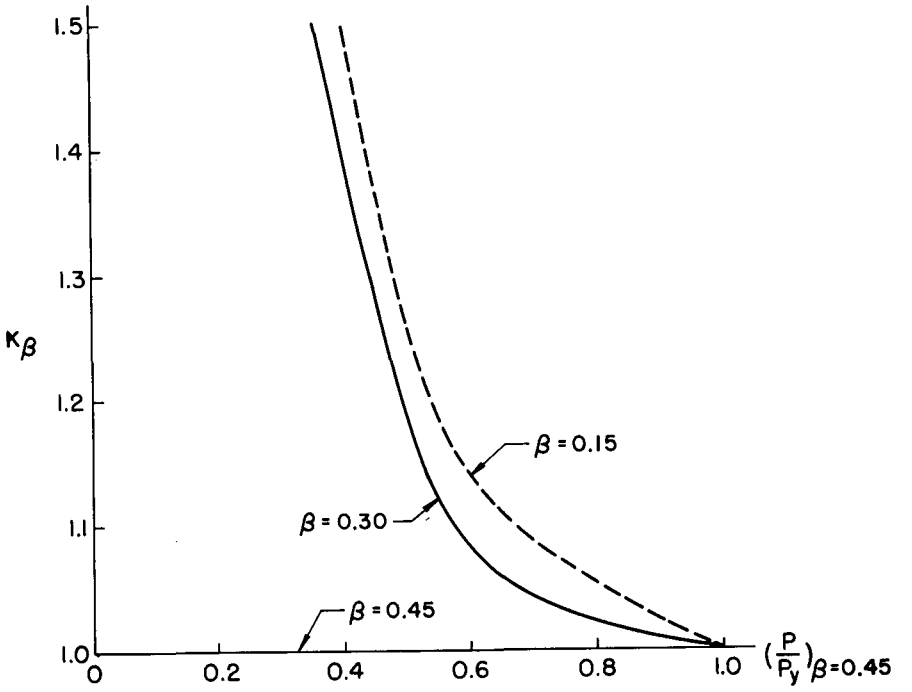

(a) Pinned Ends

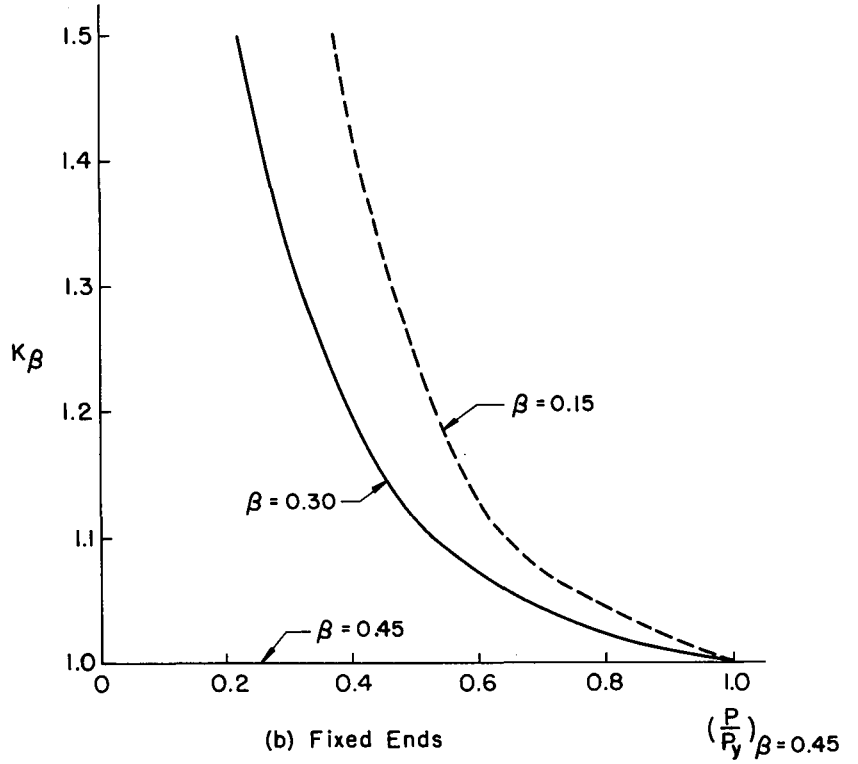

(b) Fixed Ends

FIG. 5.10 MODIFICATION FACTOR FOR STIFFENER FLANGE AREA RATIO

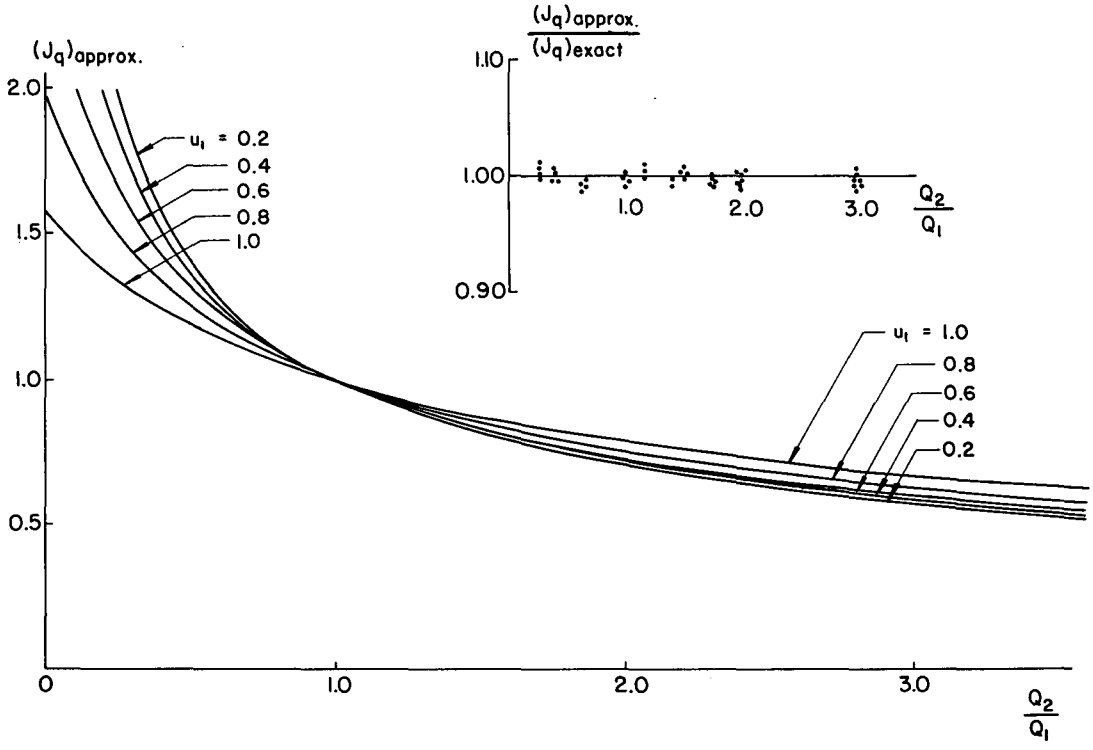

FIG. 5.11 MODIFICATION FACTOR FOR LATERAL LOAD

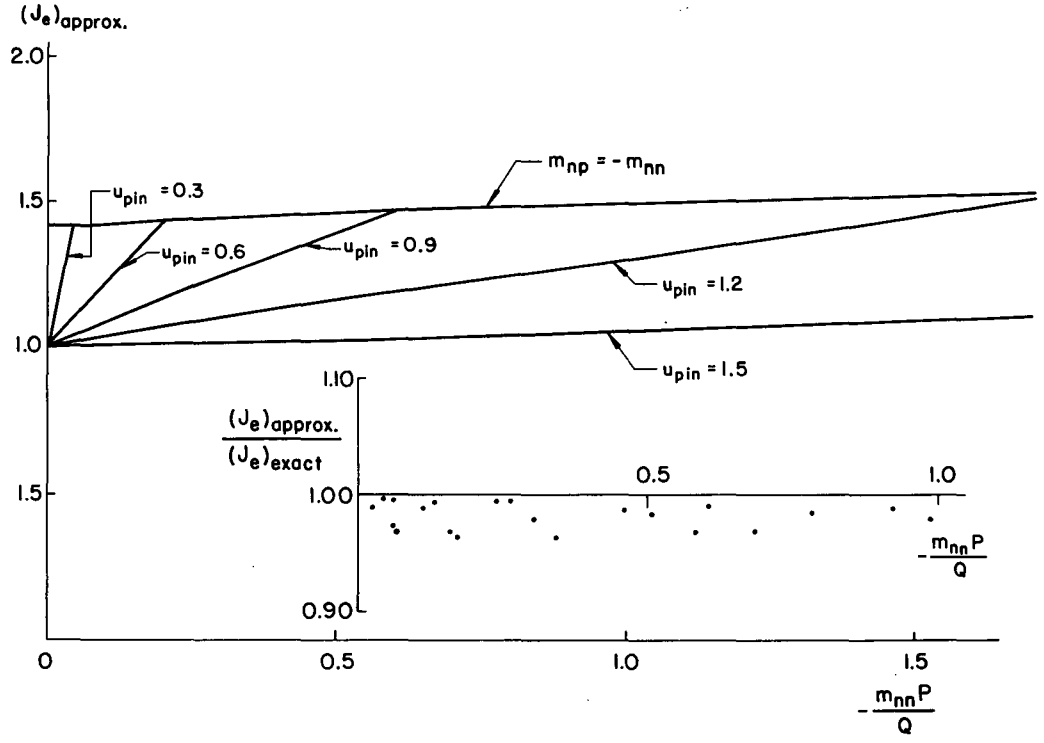

FIG. 5.12 MODIFICATION FACTOR FOR END RESTRAINT

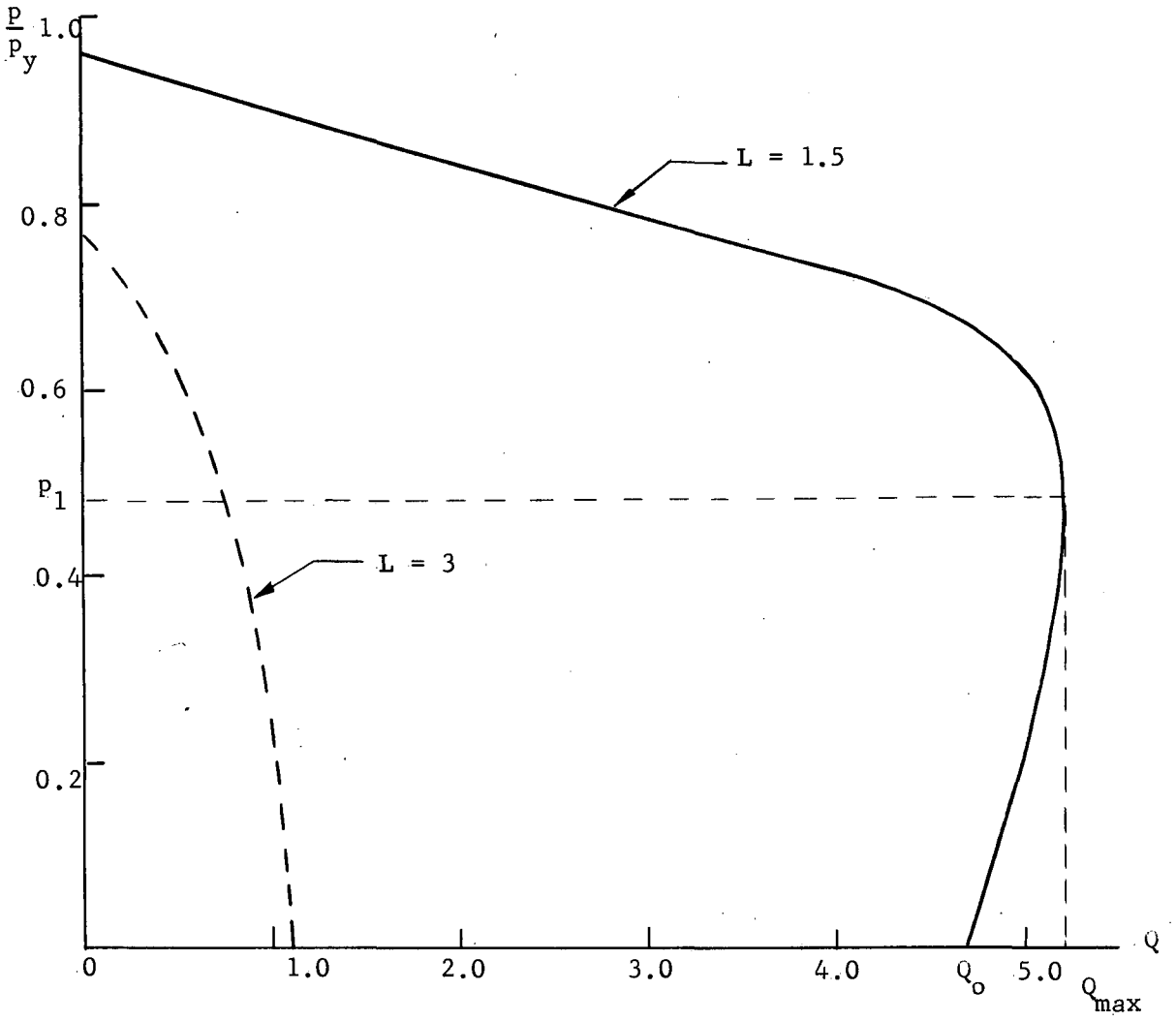

Fig. 5.13 INTERACTION CIRVES, STANDARD SECTION

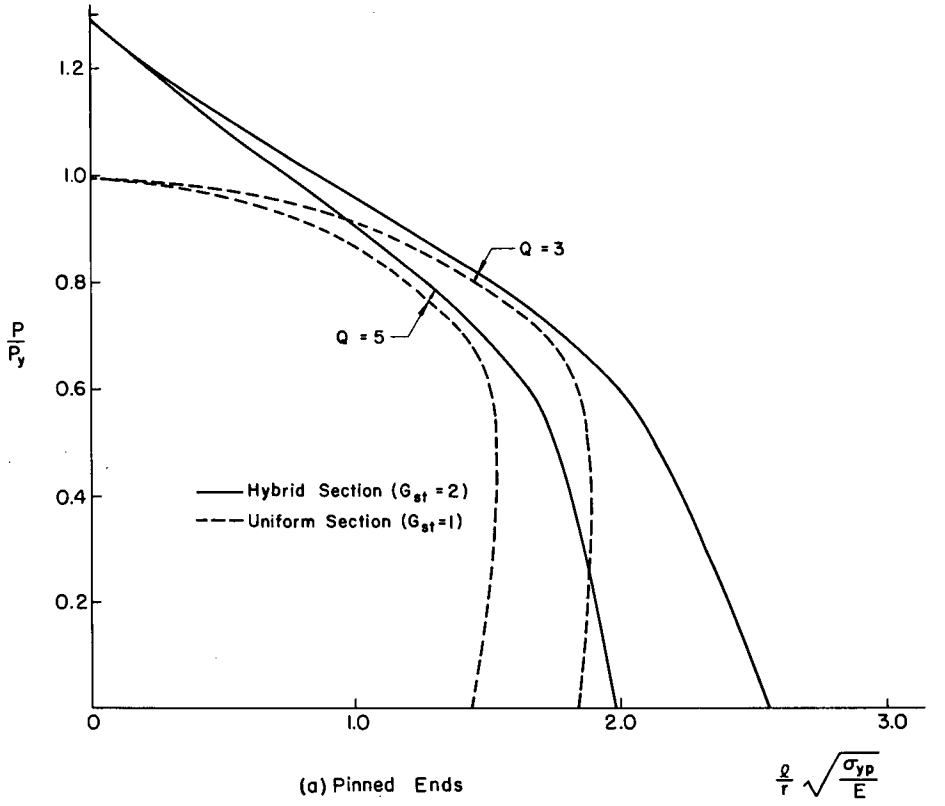

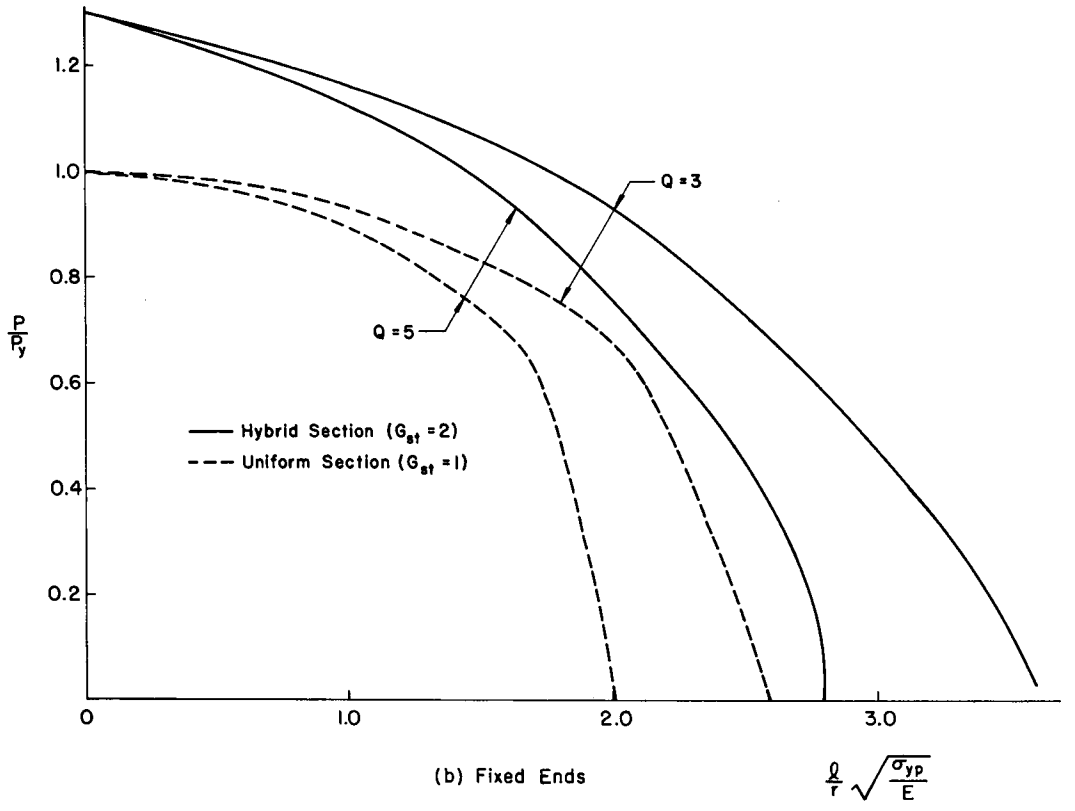

FIG. 5.14 ULTIMATE STRENGTH CURVES FOR A HYBRID SECTION

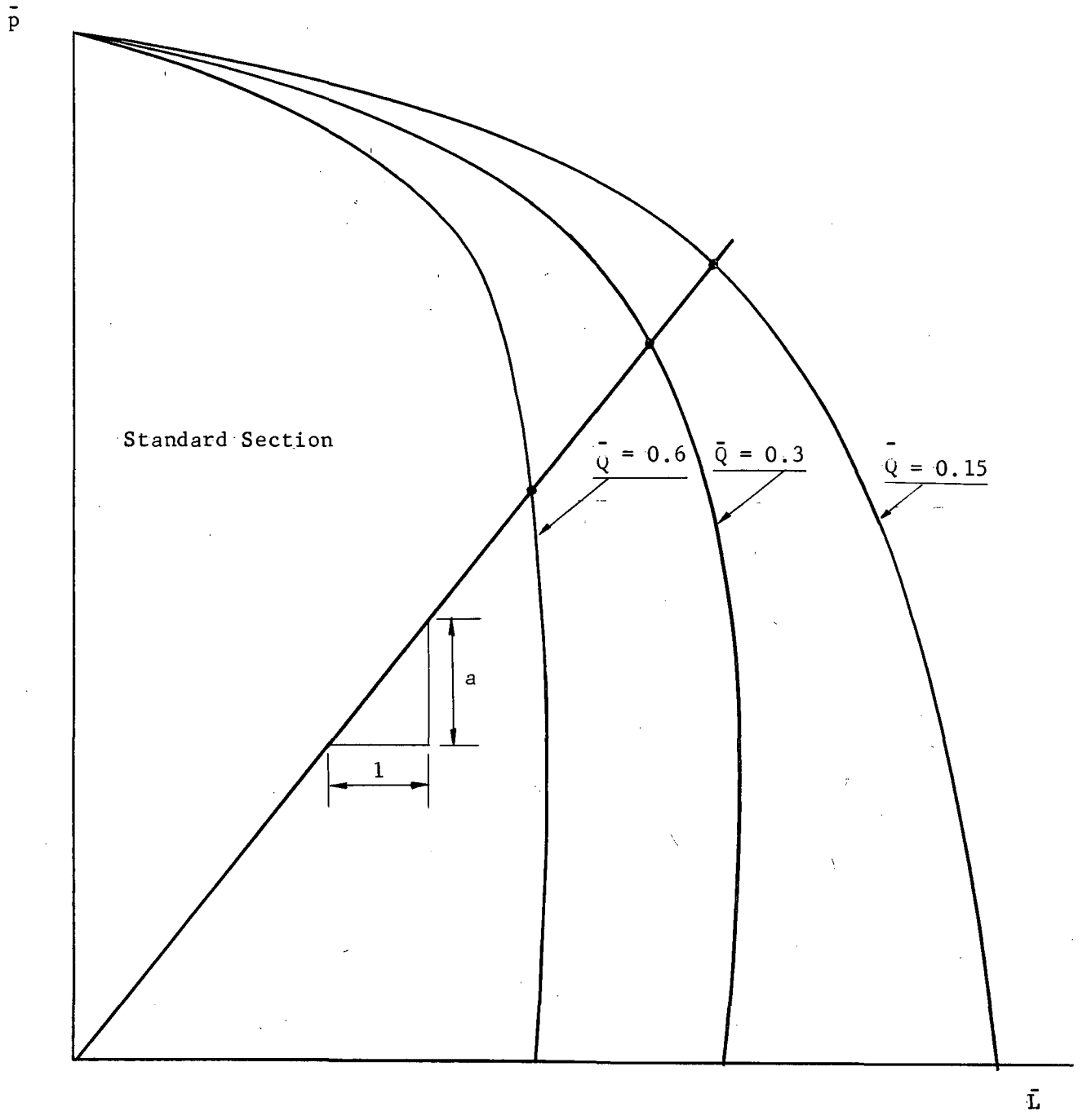

Fig. 6.1 $\bar{p}$ - $\bar{Q}$ - $\bar{L}$ Curve

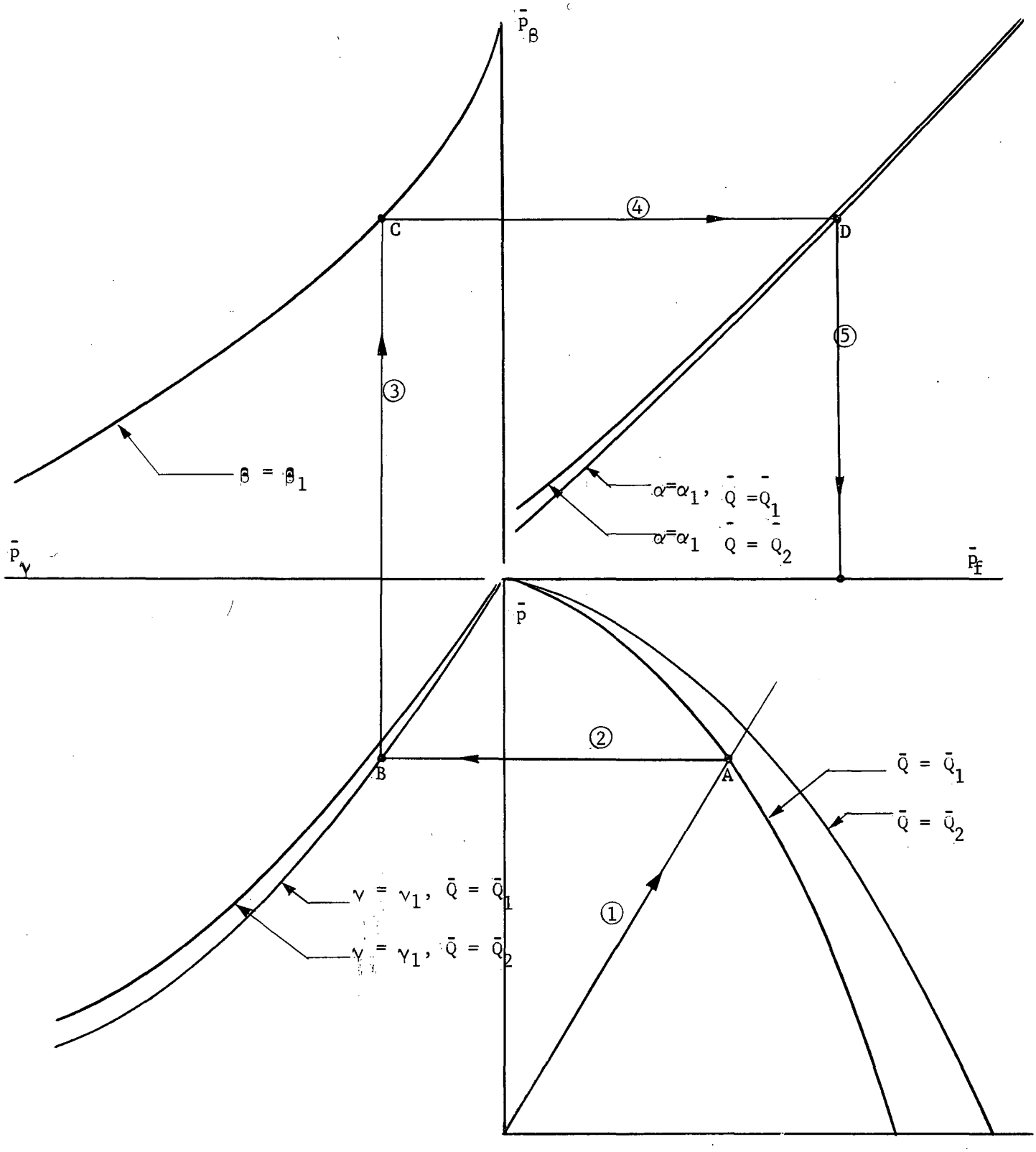

Fig. 6.2 DESIGN CHART (SCHEMATIC)

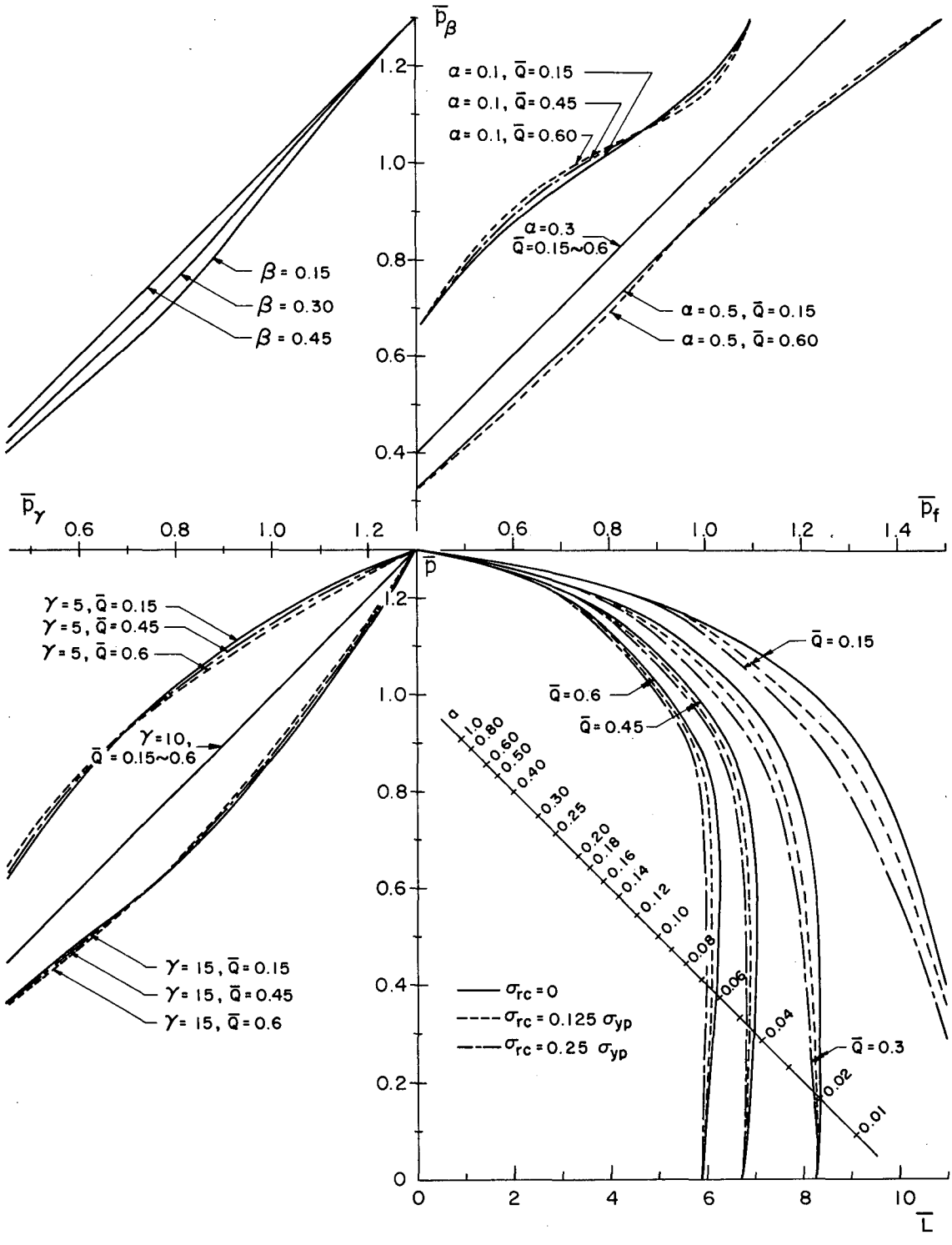

FIG. 6.3 DESIGN CHART FOR LONGITUDINALLY STIFFENED PLATE PANELS, PINNED ENDS

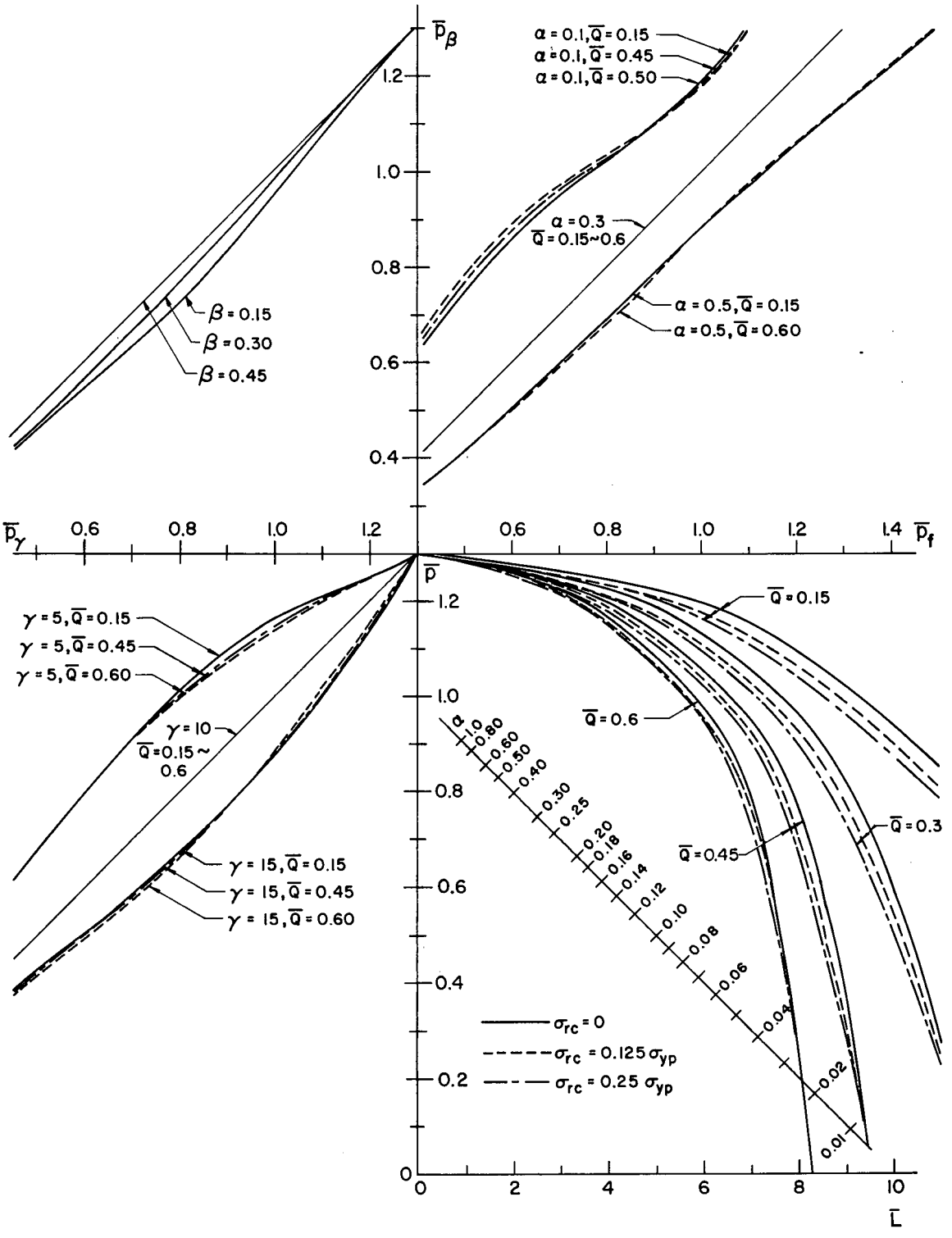

FIG. 6.4 DESIGN CHART FOR LONGITUDINALLY STIFFENED PLATE PANELS, FIXED ENDS

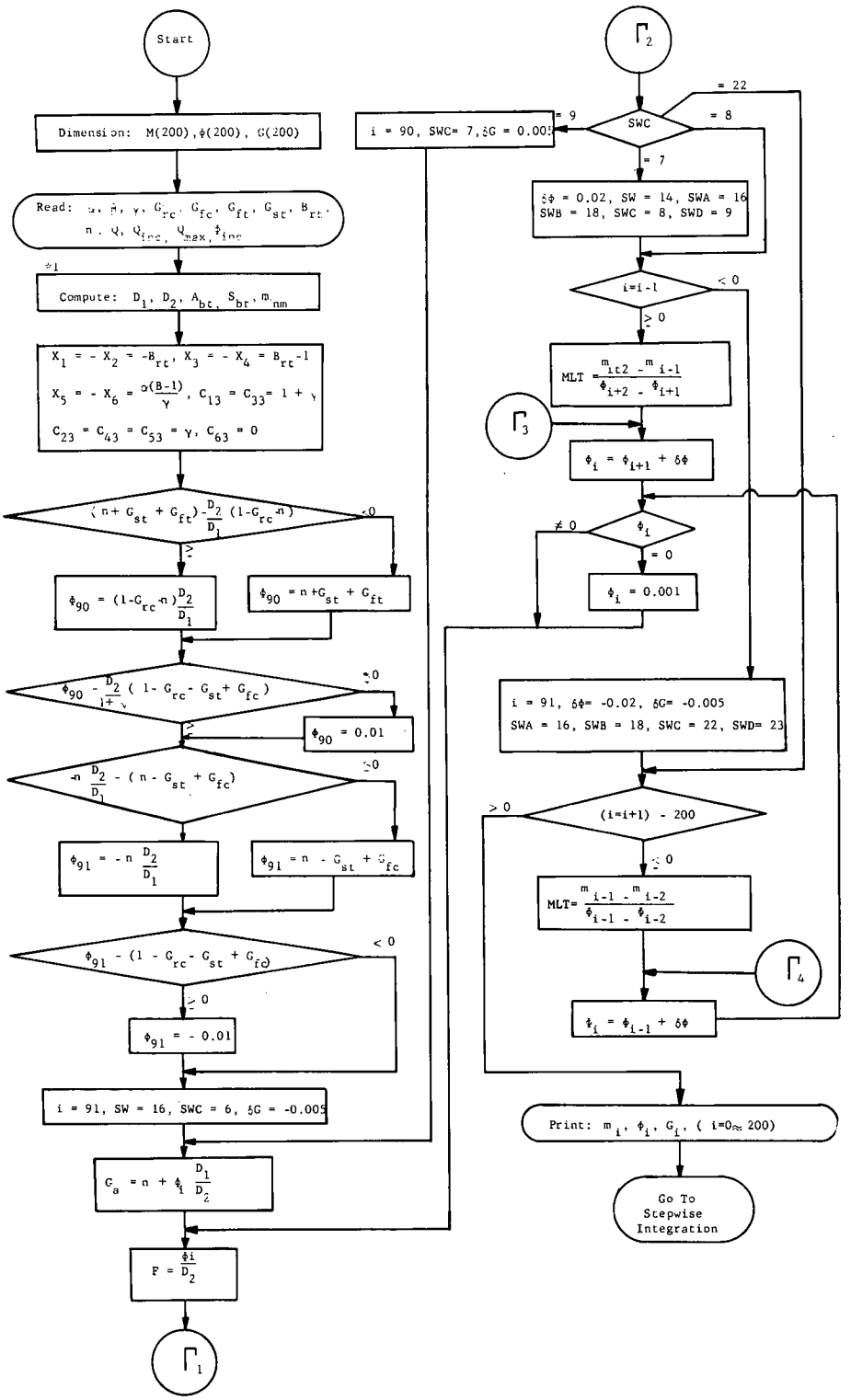

FIG. 10.1 FLOW DIAGRAM FOR MOMENT - CURVATURE - THRUST RELATIONSHIP

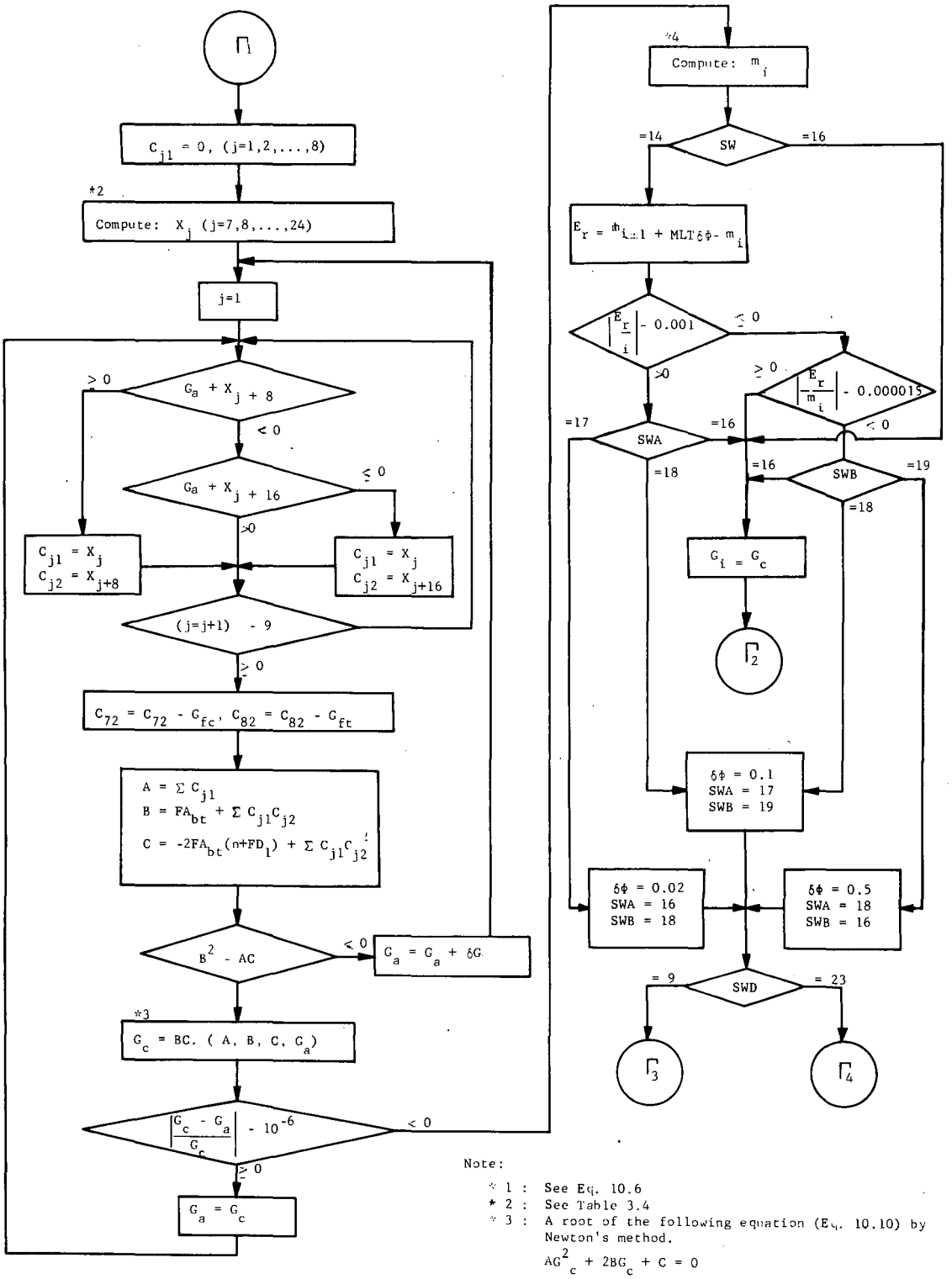

Note:

* 1 : See Eq. 10.6
* 2 : See Table 3.4
* 3 : A root of the following equation (Eq. 10.10) by Newton's method.

$$AG_c^2 + 2BG_c + C = 0$$

* 4 : See Eq. 10.9

FIG. 10.1 FLOW DIAGRAM FOR MOMENT-CURVATURE-THRUST RELATIONSHIP (Cont'd)

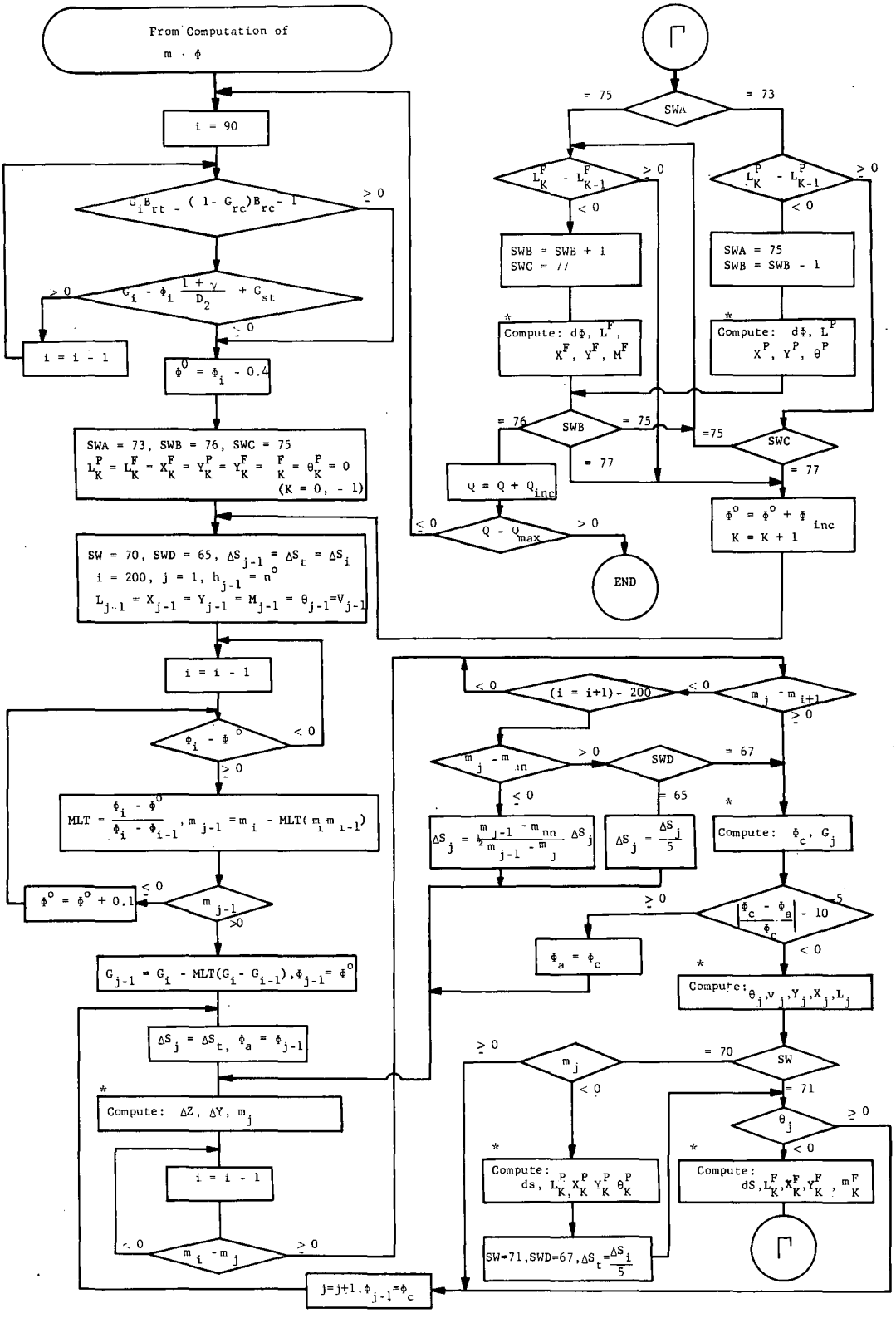

Note: Asterisked statements are described in Appendix 10.2 in detail.

FIG. 10.2 FLOW DIAGRAM FOR DETERMINATION OF ULTIMATE STRENGTH

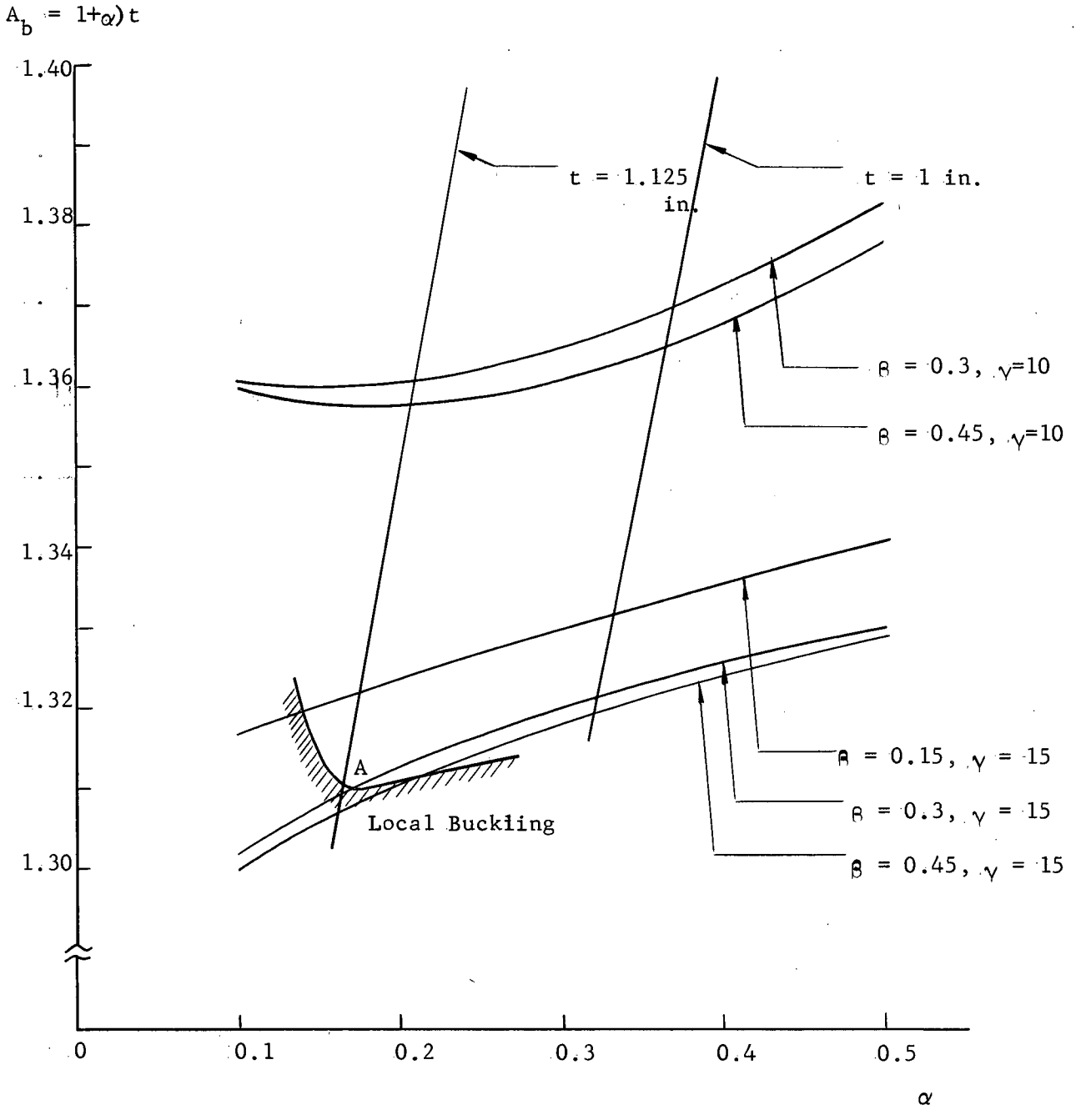

Fig. 10.3 DESIGN CHART
(TOTAL CROSS-SECTIONAL AREA CURVE)

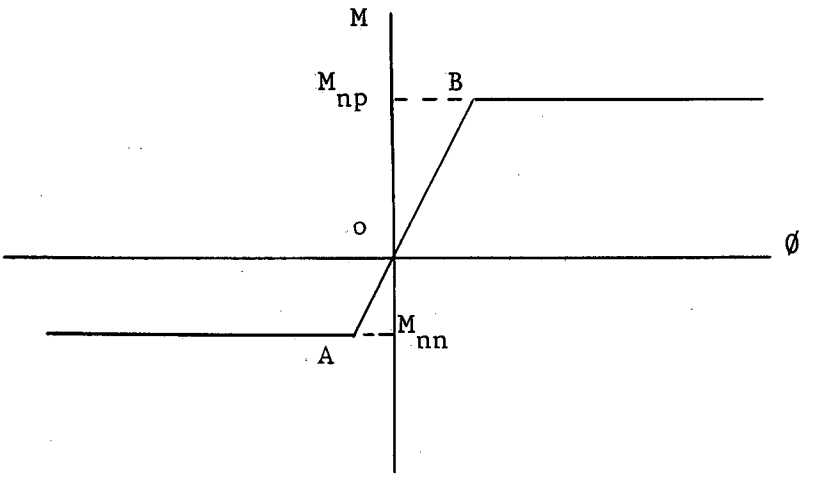

Fig. 10.4 IDEALIZED MOMENT-CURVATURE RELATIONSHIP

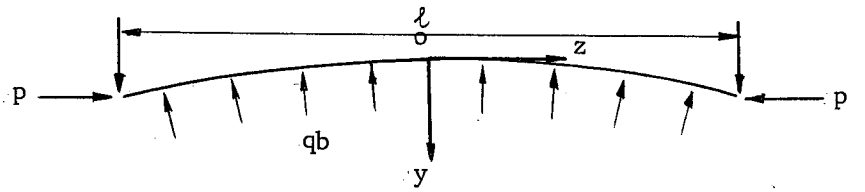

(a) Pinned Ends

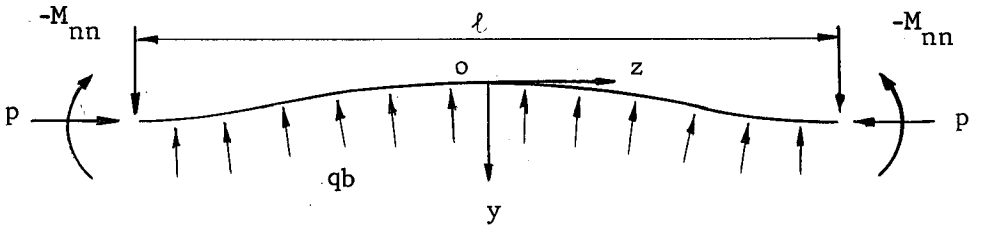

(b) Fixed Ends

Fig. 10.5 EXTERNAL LOADS ACTING ON LONGITUDINALLY STIFFENED PLATE PANELS

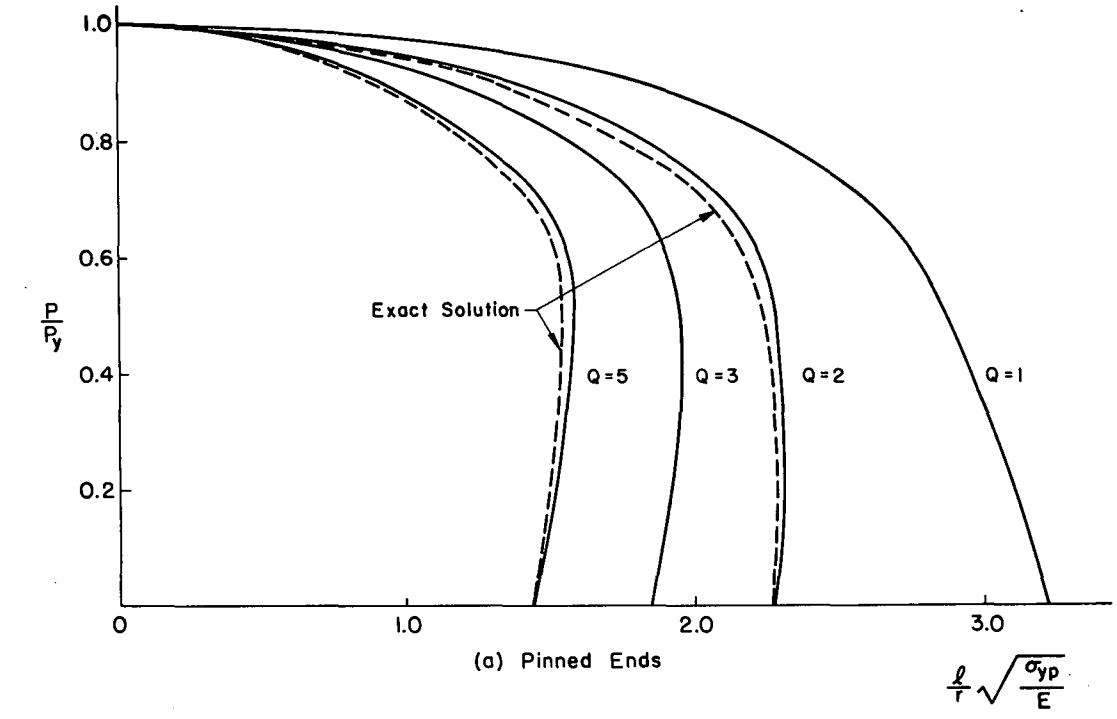

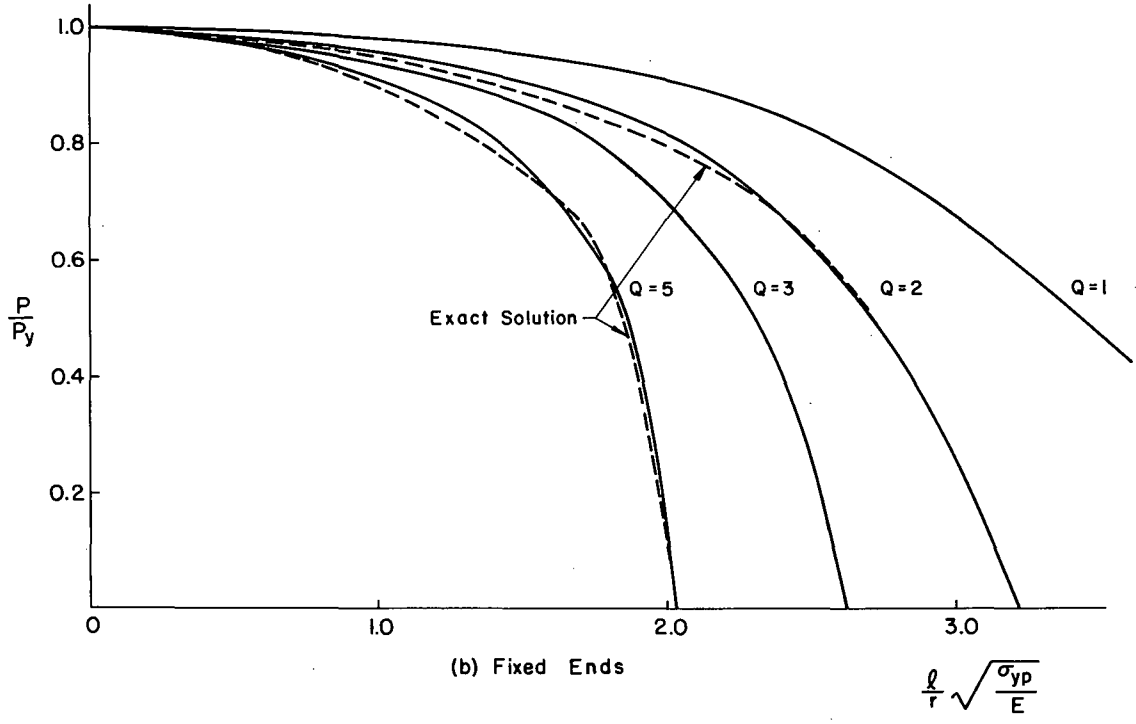

FIG. 10.6 ULTIMATE STRENGTH CURVES (APPROXIMATE SOLUTION)

13. ACKNOWLEDGEMENTS

This study is part of a research project "Built-up Members in Plastic Design" currently being carried out at Fritz Engineering Laboratory, Lehigh University, Bethlehem, Pennsylvania. Professor William J. Eney is Head of the Laboratory, and Professor Lynn S. Beedle is Director.

The research has been sponsored by the Department of the Navy under the Bureau of Ships contract No. Nobs-90041. The study was initiated by Mr. John Vasta of the Bureau of Ships. His interest in and support of the project are gratefully acknowledged.

The author is greatly indebted to Dr. Alexis Ostapenko, Director of the Project, for his encouragement, advice and suggestions. Sincere appreciation is expressed to Professor William A. Smith and Mr. James W. Muir of the Computer Laboratory, Lehigh University for their help in the use of the G.E. 225 computer.

Acknowledgement is due to Mr. H. A. Izquierdo for the preparation of drawings, and to Mrs. Brenda Herstich, who typed the report.